

The Synthesis of Chiral Perylene and Naphthalene Diimides

Süleyman Aşır

Submitted to the
Institute of Graduate Studies and Research
in partial fulfillment of the requirements for the Degree of

Doctor of Philosophy
in
Chemistry

Eastern Mediterranean University
September 2009
Gazimağusa, North Cyprus

Approval of the Institute of Graduate Studies and Research

Prof. Dr. Elvan Yılmaz
Director (a)

I certify that this thesis satisfies the requirements as a thesis for the degree of Doctor of Philosophy in Chemistry.

Prof. Dr. Mustafa Halilsoy
Chair, Department of Chemistry

We certify that we have read this thesis and that in our opinion it is fully adequate in scope and quality as a thesis for the degree of Doctor of Philosophy in Chemistry.

Prof. Dr. Huriye İcil
Supervisor

Examining Committee

1. Prof. Dr. Metin Balcı

2. Prof. Dr. Huriye İcil

3. Assist. Prof. Dr. Mustafa E. Özser

ABSTRACT

In this thesis a new naphthalene monoimide, one chiral naphthalene diimide and two chiral perylene diimides have been successfully synthesized. The synthesized products were characterized through the data from NMR, IR, MS, UV-vis, DSC, TGA, elemental analysis, cyclic voltammetry, square-wave voltammetry and circular dichroism (CD).

Naphthalene monoimide exhibits an intramolecular charge transfer complexation in its absorption spectrum in polar solvents. Excimer-like emissions were obtained in nonpolar, polar protic and aprotic solvents for naphthalene monoimide and diimide. The specific optical rotation values of unsymmetrical chiral naphthalene and perylene diimides were measured as -221.6, -24 and +200, respectively at 20 °C. All of the synthesized compounds showed high thermal and electrochemical stability. Chiral naphthalene diimide showed prominent negative Cotton effects centred at 362 and 382 nm in CH₃CN.

The results could lead to further development of sterically and stereochemically controlled conductive unsymmetrical diimides which could guide to design important optoelectronic devices.

ÖZET

Bu tezde yeni bir naftalen monoimid, kiral bir naftalen diimid ve iki kiral perilen diimid başarılı bir şekilde sentezlenmiştir. Sentezlenmiş olan maddeler NMR, IR, MS, UV-vis, DSC, TGA, elementel analiz, dönüşümlü voltametri, kare-dalga voltametri ve dairesel dikroizm (CD) yöntemleri ile karakterize edilmiştir.

Naftalin monoimidin polar çözümlerdeki UV ve görünür alan absorpsiyon spektrumunda molekül içi yük transfer kompleksleşmesi görülmektedir. Naftalin monoimid ve diimid molekülleri için apolar, polar protik ve aprotik çözümlerde ekzimer-benzeri emisyon gözlemlenmektedir. Asimetrik kiral naftalin ve perilen diimidlerin 20 °C'deki spesifik çevirme açıları sırası ile -221.6, -24 ve +200 olarak ölçülmüştür. Sentezlenen tüm bileşikler yüksek termal ve elektrokimyasal kararlılık göstermektedir. Kiral naftalin diimid asetonitril çözümlerinde 362 ve 382 nm dalgalarda belirgin olarak negatif Cotton etkisi göstermektedir.

Elde edilen sonuçlar önemli optoelektronik cihazların geliştirilmesinde sterik ve stereokimyasal kontrollü asimetrik diimidlerin geliştirilebilmesi için umut vaat etmektedir.

ACKNOWLEDGEMENTS

I would like to gratefully acknowledge the enthusiastic supervision of Prof. Dr. Huriye İcil during this work. This thesis would not appear in its present form without the valuable guidance, professional advice, constructive criticism and suggestions of Prof. Dr. Huriye İcil.

I would like to thank Prof. Dr. Ayhan S. Demir for co-supervision and providing some measurements at Middle East Technical University in Ankara. I gratefully acknowledge the financial support from the Scientific and Technical Research Council of Turkey (TUBITAK).

Also very special thanks to İcil's Organic Group at Eastern Mediterranean University, Abimbola Ololade Aleshinloye, Devrim Özdal, Duygu Uzun, Hürmüş Refiker, İlke Yücekan, Jagadeesh Babu Bodapati, Nur Paşaoğulları Aydınlık and Sayeh Shahmohammadi.

Finally, I am grateful to my wife and my family for their endless encouragements and abundant love during my studies.

To my wife, to my one and only!

TABLE OF CONTENTS

ABSTRACT	iii
ÖZET.....	iv
ACKNOWLEDGEMENTS	v
LIST OF TABLES	xi
LIST OF FIGURES	xiii
LIST OF SCHEMES.....	xxi
ABBREVIATIONS	xxii
CHAPTER 1	1
INTRODUCTION	1
CHAPTER 2	6
THEORETICAL	6
2.1 The Concept of Chirality.....	6
2.1.1 Circularly Polarized Light, ORD and CD.....	7
2.2 Molecular Chiral Recognition	10
2.3 Chiral Photochemistry	12
2.4 Chiroptical Molecular Switches	13
2.5 Properties of Naphthalene and Perylene Diimides.....	19
2.5.1 Potential Applications of Naphthalene and Perylene Diimides.....	20

CHAPTER 3	26
EXPERIMENTAL	26
3.1 Materials	26
3.2 Instruments	26
3.3 Methods of Syntheses.....	28
3.3.1 Synthesis of N-(4-hydroxyphenyl)-1,4,5,8-naphthalenetetracarboxylic-1,8-anhydride-4,5-imide (1a)	31
3.3.2 Synthesis of N-(4-hydroxyphenyl)-N'-[(S)-1-phenylethyl]-1,4,5,8-naphthalenetetracarboxydiimide (2a)	32
3.3.3 Synthesis of N-(4-hydroxyphenyl)-N'-[(S)-1-phenylethyl]-3,4,9,10-perylenetetracarboxydiimide (5a)	34
3.3.4 Synthesis of N-(2-aminohexanoic acid)-3,4,9,10 perylenetetracarboxylic-3,4-anhydride-9,10-imide (4b).....	35
3.3.5 Synthesis of N-(2-aminohexanoic acid)-N'-[(1-dehydroabietyl)-3,4,9,10 perylenetetracarboxydiimide (5b).....	36
CHAPTER 4	38
DATA AND CALCULATIONS	38
4.1 Optical Properties	38
4.1.1 Maximum Extinction Coefficients (ϵ_{\max}).....	38
4.1.2 Fluorescence Quantum Yields (Φ_f)	40
4.1.3 Singlet Energies (E_s).....	42

4.1.4 Oscillator Strengths (f).....	43
4.1.5 Theoretical Radiative Lifetimes (τ_0).....	44
4.1.6 Theoretical Fluorescence Lifetimes (τ_f).....	45
4.1.7 Fluorescence Rate Constants (k_f).....	46
4.1.8 Rate Constants of Radiationless Deactivation (k_d).....	47
4.2 Chiroptical Properties.....	48
4.3 Thermal Properties	49
4.4 Electrochemical Properties.....	49
4.4.1 Redox Potentials ($E_{1/2}$).....	49
4.4.2 Lowest Unoccupied Molecular Orbital (LUMO).....	51
4.4.3 Band Gap Energy (E_g).....	52
4.4.4 Highest Occupied Molecular Orbital (HOMO).....	53
4.4.5 Diffusion Coefficients (D).....	54
CHAPTER 5	111
RESULTS AND DISCUSSION	111
5.1 Synthesis and Characterization	111
5.2 Absorption and Fluorescence Properties.....	114
5.3 Thermal Stability.....	120
5.4 Electrochemistry.....	121

CHAPTER 6	131
CONCLUSION.....	131
REFERENCES.....	133
CURRICULUM VITAE.....	150

LIST OF TABLES

Table 4.1: Extinction coefficients ^a of compounds 1a, 2a, 5a and 5b.	39
Table 4.2: Fluorescence quantum yield data of compounds 1a, 2a, 5a and 5b.	42
Table 4.3: Singlet energies of compounds 1a, 2a, 5a and 5b.	42
Table 4.4: Oscillator strengths of compounds 1a, 2a, 5a and 5b.....	44
Table 4.5: Theoretical radiative lifetimes of compounds 1a, 2a, 5a and 5b.....	45
Table 4.6: Theoretical fluorescence lifetimes of compounds 1a, 2a, 5a and 5b.	45
Table 4.7: Fluorescence rate constants of compounds 1a, 2a, 5a and 5b.....	46
Table 4.8: Rate constants of radiationless deactivation of compounds 1a, 2a, 5a and 5b.....	47
Table 4.9: Cyclic ^a voltammetry data of compounds 1a, 2a and 5a.	50
Table 4.10: LUMO values of compounds 1a, 2a and 5a.	51
Table 4.11: The optical band gap values of compounds 1a, 2a and 5a.	52
Table 4.12: HOMO values of compounds 1a, 2a and 5a.....	53
Table 4.13: Cyclic voltammetry data of compound 1a in CH ₃ CN at different scan rates.	55
Table 4.14: Cyclic voltammetry data of compound 1a in CH ₂ Cl ₂ at different scan rates.	55

Table 4.15: Cyclic voltammetry data of compound 2a at different scan rates.	56
Table 4.16: Cyclic ^a voltammetry data of compound 5a in CHCl ₃ at different scan rates.	56
Table 4.17: Solid state cyclic ^a voltammetry data of compound 5a at different scan rates.	57
Table 4.18: Diffusion coefficients ^a of compounds 1a, 2a and 5a.	57
Table 5.1: Solubility of compounds 1a, 2a, 4a, 4b, 5a and 5b.	113
Table 5.2: Stokes shifts of 1a, 2a, 5a and 5b.	116
Table 5.3: Maximum absorption wavelengths λ_{max} (nm), extinction coefficients ϵ_{max} ($\text{l mol}^{-1} \text{cm}^{-1}$), oscillator strengths f , fluorescence quantum yields Φ_f ($\lambda_{\text{excit.}} = 360 \text{ nm}$ for 1a and 2a, $\lambda_{\text{excit.}} = 485 \text{ nm}$ for 5a and 5b), radiative lifetimes τ_0 (ns), fluorescence lifetimes τ_f (ns), fluorescence rate constants k_f (10^8 s^{-1}), rate constants of radiationless deactivation k_d (10^8 s^{-1}), optical activities $[\alpha]_D^{20}$, and singlet energies E_s (kcal mol^{-1}) data of 1a, 2a, 5a in DMF and 5b in CHCl ₃	118
Table 5.4: Cyclic ^a voltammetry data and optical band gap energy E_g , HOMO, LUMO values of compounds 1a, 2a and 5a.	122

LIST OF FIGURES

Figure 1.1: Structures of compounds 1a, 2a, 5a and 5b.....	5
Figure 2.1: Left circularly polarized light.....	8
Figure 2.2: Schematic representation of a molecular switch.....	15
Figure 4.1: A representative absorption spectrum for half-width calculation.....	43
Figure 4.2: FT-IR spectrum of N-(4-hydroxyphenyl)-1,4,5,8-naphthalenetetracarboxylic-1,8-anhydride-4,5-imide (1a).....	58
Figure 4.3: FT-IR spectrum of N-(4-hydroxyphenyl)-N'-[(S)-1-phenylethyl]-1,4,5,8-naphthalenetetracarboxydiimide (2a).....	59
Figure 4.4: FT-IR spectrum of N-(4-hydroxyphenyl)-N'-[(S)-1-phenylethyl]-3,4,9,10-perylenetetracarboxydiimide (5a).....	60
Figure 4.5: FT-IR spectrum of N-(2-aminohexanoic acid)-N'-[(1-dehydroabietyl)-3,4,9,10 perylenetetracarboxydiimide (5b).....	61
Figure 4.6: Mass spectrum of N-(4-hydroxyphenyl)-1,4,5,8-naphthalenetetracarboxylic-1,8-anhydride-4,5-imide (1a).....	62
Figure 4.7: Mass spectrum of N-(4-hydroxyphenyl)-N'-[(S)-1-phenylethyl]-1,4,5,8-naphthalenetetracarboxydiimide (2a).....	63

Figure 4.8: Mass spectrum of N-(4-hydroxyphenyl)-N'-[(S)-1-phenylethyl]-3,4,9,10-perylenetetracarboxydiimide (5a).	64
Figure 4.9: ¹ H-NMR spectrum of N-(4-hydroxyphenyl)-1,4,5,8-naphthalenetetracarboxylic-1,8-anhydride-4,5-imide (1a).....	65
Figure 4.10: ¹³ C-NMR spectrum of N-(4-hydroxyphenyl)-1,4,5,8-naphthalenetetracarboxylic-1,8-anhydride-4,5-imide (1a).....	66
Figure 4.11: ¹ H-NMR spectrum of N-(2-aminohexanoic acid)-N'-(1-dehydroabietyl)-3,4,9,10 perylenetetracarboxydiimide (5b).	67
Figure 4.12: ¹³ C-NMR spectrum of N-(2-aminohexanoic acid)-N'-(1-dehydroabietyl)-3,4,9,10 perylenetetracarboxydiimide (5b).	68
Figure 4.13: Absorption spectra of N-(4-hydroxyphenyl)-1,4,5,8-naphthalenetetracarboxylic-1,8-anhydride-4,5-imide (1a) in different solvents.	69
Figure 4.14: Absorption spectra of N-(4-hydroxyphenyl)-1,4,5,8-naphthalenetetracarboxylic-1,8-anhydride-4,5-imide (1a) in different solvents after filtration with 0.2 μm microfilter.	70
Figure 4.15: Absorption spectra of N-(4-hydroxyphenyl)-N'-[(S)-1-phenylethyl]-1,4,5,8-naphthalenetetracarboxydiimide (2a) in different solvents.	71
Figure 4.16: Absorption spectra of N-(4-hydroxyphenyl)-N'-[(S)-1-phenylethyl]-1,4,5,8-naphthalenetetracarboxydiimide (2a) in different solvents after filtration with 0.2 μm microfilter.	72

Figure 4.17: Absorption spectra of N-(4-hydroxyphenyl)-N'-[(S)-1-phenylethyl]-3,4,9,10-perylenetetracarboxydiimide (5a) in different solvents.	73
Figure 4.18: Absorption spectra of N-(4-hydroxyphenyl)-N'-[(S)-1-phenylethyl]-3,4,9,10-perylenetetracarboxydiimide (5a) in different solvents after filtration with 0.2 μm microfilter.	74
Figure 4.19: Absorption spectra of N-(2-aminohexanoic acid)-N'-(1-dehydroabietyl)-3,4,9,10 perylenetetracarboxydiimide (5b) in different solvents.	75
Figure 4.20: Absorption spectra of N-(2-aminohexanoic acid)-N'-(1-dehydroabietyl)-3,4,9,10 perylenetetracarboxydiimide (5b) in different solvents after filtration with 0.2 μm microfilter.	76
Figure 4.21: Solid-state absorption spectra of N-(4-hydroxyphenyl)-1,4,5,8-naphthalenetetracarboxylic-1,8-anhydride-4,5-imide (1a).....	77
Figure 4.22: Solid-state absorption spectra of N-(4-hydroxyphenyl)-N'-[(S)-1-phenylethyl]-1,4,5,8-naphthalenetetracarboxydiimide (2a).....	78
Figure 4.23: Solid-state absorption spectra of N-(4-hydroxyphenyl)-N'-[(S)-1-phenylethyl]-3,4,9,10-perylenetetracarboxydiimide (5a).	79
Figure 4.24: Solid-state absorption spectra of N-(2-aminohexanoic acid)-N'-(1-dehydroabietyl)-3,4,9,10 perylenetetracarboxydiimide (5b).	80
Figure 4.25: Emission spectra of N-(4-hydroxyphenyl)-1,4,5,8-naphthalenetetracarboxylic-1,8-anhydride-4,5-imide (1a) in different solvents.	81

Figure 4.26: Emission spectra of N-(4-hydroxyphenyl)-1,4,5,8-naphthalenetetracarboxylic-1,8-anhydride-4,5-imide (1a) in different solvents after filtration with 0.2 μm microfilter.	82
Figure 4.27: Emission spectra of N-(4-hydroxyphenyl)-N'-[(S)-1-phenylethyl]-1,4,5,8-naphthalenetetracarboxydiimide (2a) in different solvents.	83
Figure 4.28: Emission spectra of N-(4-hydroxyphenyl)-N'-[(S)-1-phenylethyl]-1,4,5,8-naphthalenetetracarboxydiimide (2a) in different solvents after filtration with 0.2 μm microfilter.	84
Figure 4.29: Emission spectra of N-(4-hydroxyphenyl)-N'-[(S)-1-phenylethyl]-3,4,9,10-perylenetetracarboxydiimide (5a) in different solvents.	85
Figure 4.30: Emission spectra of N-(4-hydroxyphenyl)-N'-[(S)-1-phenylethyl]-3,4,9,10-perylenetetracarboxydiimide (5a) in different solvents after filtration with 0.2 μm microfilter.	86
Figure 4.31: Emission spectra of N-(2-aminohexanoic acid)-N'-(1-dehydroabietyl)-3,4,9,10 perylenetetracarboxydiimide (5b) in different solvents.	87
Figure 4.32: Emission spectra of N-(2-aminohexanoic acid)-N'-(1-dehydroabietyl)-3,4,9,10 perylenetetracarboxydiimide (5b) in different solvents after filtration with 0.2 μm microfilter.	88
Figure 4.33: Fluorescence decay curve of 10 ⁻⁵ M N-(4-hydroxyphenyl)-N'-[(S)-1-phenylethyl]-3,4,9,10-perylenetetracarboxydiimide (5a) ($\lambda_{\text{excit.}}$ =530 nm and λ_{em} =580 nm) in DMF.	89

Figure 4.34: CD spectrum of N-(4-hydroxyphenyl)-N'-[(S)-1-phenylethyl]-1,4,5,8-naphthalenetetracarboxydiimide (2a) in acetonitrile.....	90
Figure 4.35: CD spectrum of N-(4-hydroxyphenyl)-N'-[(S)-1-phenylethyl]-1,4,5,8-naphthalenetetracarboxydiimide (2a) in ethanol.....	91
Figure 4.36: DSC thermogram of compound N-(4-hydroxyphenyl)-1,4,5,8-naphthalenetetracarboxylic-1,8-anhydride-4,5-imide (1a) (heating rate 10 K min ⁻¹).	92
Figure 4.37: DSC thermogram of compound N-(4-hydroxyphenyl)-N'-[(S)-1-phenylethyl]-1,4,5,8-naphthalenetetracarboxydiimide (2a) (heating rate 10 K min ⁻¹).	93
Figure 4.38: DSC thermogram of compound N-(4-hydroxyphenyl)-N'-[(S)-1-phenylethyl]-3,4,9,10-perylenetetracarboxydiimide (5a) (heating rate 10 K min ⁻¹).	94
Figure 4.39: DSC thermogram of compound N-(2-aminohexanoic acid)-N'-(1-dehydroabietyl)-3,4,9,10 perylenetetracarboxydiimide (5b) (heating rate 10 K min ⁻¹).	95
Figure 4.40: Thermal gravimetric analysis (TGA) of compound N-(4-hydroxyphenyl)-1,4,5,8-naphthalenetetracarboxylic-1,8-anhydride-4,5-imide (1a) (heating rate 5 K min ⁻¹).	96

Figure 4.41: Thermal gravimetric analysis (TGA) of compound N-(4-hydroxyphenyl)-N'-[(S)-1-phenylethyl]-1,4,5,8-naphthalenetetracarboxydiimide (2a) (heating rate 5 K min ⁻¹).....	97
Figure 4.42: Thermal gravimetric analysis (TGA) of compound N-(4-hydroxyphenyl)-N'-[(S)-1-phenylethyl]-3,4,9,10-perylenetetracarboxydiimide (5a) (heating rate 5 K min ⁻¹).....	98
Figure 4.43: Thermal gravimetric analysis (TGA) of compound N-(2-aminohexanoic acid)-N'-(1-dehydroabietyl)-3,4,9,10 perylenetetracarboxydiimide (5b) (heating rate 5 K min ⁻¹).....	99
Figure 4.44: Cyclic voltammograms of compound N-(4-hydroxyphenyl)-1,4,5,8-naphthalenetetracarboxylic-1,8-anhydride-4,5-imide (1a) in dichloromethane; supporting electrolyte: TBAPF ₆ , scan rates (mVs ⁻¹): 1 (50), 2 (100), 3 (200), 4 (300) at 25 °C.....	100
Figure 4.45: Cyclic voltammograms of compound N-(4-hydroxyphenyl)-1,4,5,8-naphthalenetetracarboxylic-1,8-anhydride-4,5-imide (1a) in acetonitrille; supporting electrolyte: TBAPF ₆ , scan rates (mVs ⁻¹): 1 (50), 2 (100), 3 (200), 4 (300) at 25 °C.	101
Figure 4.46: Cyclic voltammograms of compound N-(4-hydroxyphenyl)-N'-[(S)-1-phenylethyl]-1,4,5,8-naphthalenetetracarboxydiimide (2a) in chloroform; supporting electrolyte: TBAPF ₆ , scan rates (mVs ⁻¹): 1 (50), 2 (100), 3 (200) at 25 °C.....	102

Figure 4.47: Cyclic voltammogram of compound N-(4-hydroxyphenyl)-N'-[(S)-1-phenylethyl]-1,4,5,8-naphthalenetetracarboxydiimide (2a) in DMSO; supporting electrolyte: TBAPF6, scan rate (mVs-1): 50 at 25 °C.	103
Figure 4.48: Cyclic voltammograms of compound N-(4-hydroxyphenyl)-N'-[(S)-1-phenylethyl]-3,4,9,10-perylenetetracarboxydiimide (5a) in chloroform; supporting electrolyte: TBAPF6, scan rates (mVs-1): 1 (50), 2 (100), 3 (300), 4 (600), 5 (800), 6 (1000) at 25 °C.....	104
Figure 4.49: Square-wave voltammograms of compound N-(4-hydroxyphenyl)-N'-[(S)-1-phenylethyl]-3,4,9,10-perylenetetracarboxydiimide (5a) in chloroform; supporting electrolyte:TBAPF6, v (Hz): 1 (60), 2 (100), 3 (150) at 25 °C.....	105
Figure 4.50: Solid state cyclic voltammograms of compound N-(4-hydroxyphenyl)-N'-[(S)-1-phenylethyl]-3,4,9,10-perylenetetracarboxydiimide (5a); supporting electrolyte: HCl, scan rates (mVs-1): 1 (25), 2 (50), 3 (100), 4 (200), 5 (400), 6 (600) at 25 °C.....	106
Figure 4.51: Solid state square-wave voltammograms of compound N-(4-hydroxyphenyl)-N'-[(S)-1-phenylethyl]-3,4,9,10-perylenetetracarboxydiimide (5a); supporting electrolyte: HCl, v (Hz): 1 (50), 2 (100), 3 (200), 4 (300) at 25 °C.....	107
Figure 4.52: Effect of variation of scan rates on the cathodic peak currents of compound N-(4-hydroxyphenyl)-1,4,5,8-naphthalenetetracarboxylic-1,8-anhydride-4,5-imide (1a).....	108

Figure 4.53: Effect of variation of scan rates on the cathodic peak currents of compound N-(4-hydroxyphenyl)-N'-[(S)-1-phenylethyl]-1,4,5,8-naphthalenetetracarboxydiimide (2a)..... 109

Figure 4.54: Effect of variation of scan rates on the cathodic peak currents of compound N-(4-hydroxyphenyl)-N'-[(S)-1-phenylethyl]-3,4,9,10-perylenetetracarboxydiimide (5a). 110

LIST OF SCHEMES

Scheme 2.1: Potential applications of a chiral optical (chiroptical) molecular switch.	14
Scheme 2.2: Chiral Switches: A enantiomers, B diastereomers (X^* = chiral auxiliary), C functional chiral switches (FU = Functional Unit), D macromolecular switch and switching of matrix organization (Feringa, 2001).	16
Scheme 3.1: Synthesis of naphthalene monoimide and unsymmetrical chiral naphthalene diimide.	28
Scheme 3.2: Synthesis of perylene-3,4,9,10-tetracarboxylic acid monoanhydride monopotassium carboxylate, perylene monoimide and unsymmetrical chiral perylene diimide.	30
Scheme 5.1: Proposed two-step reduction mechanism for (a) 1a; (b) 2a; and (c) 5a.	123
Scheme 5.2: Schematic energy diagram of 1a, 2a and 5a.	129

ABBREVIATIONS

- 1a** : N-(4-hydroxyphenyl)-1,4,5,8-naphthalenetetracarboxylic-1,8-anhydride-4,5-imide
- 2a** : N-(4-hydroxyphenyl)-N'-[(S)-1-phenylethyl]-1,4,5,8-naphthalenetetracarboxydiimide
- 4a** : N-(4-hydroxyphenyl)-3,4,9,10-perylenetetracarboxylic-3,4-anhydride-9,10-imide
- 4b** : N-(2-aminohexanoic acid)-3,4,9,10 perylenetetracarboxylic-3,4-anhydride-9,10-imide
- 5a** : N-(4-hydroxyphenyl)-N'-[(S)-1-phenylethyl]-3,4,9,10-perylenetetracarboxydiimide
- 5b** : N-(2-aminohexanoic acid)-N'-(1-dehydroabietyl)-3,4,9,10 perylenetetracarboxydiimide
- A** : Absorbance
- Å** : Armstrong
- Anal.** : Analytical
- c** : Concentration
- Calcd.** : Calculated

CD	: Circular dichroism
CPL	: Circularly polarized light
CV	: Cyclic voltammetry
D	: Diffusion coefficient
DMF	: N,N'-dimethylformamide
DMSO	: Dimethyl sulfoxide
DNA	: Deoxyribonucleic acid
DSC	: Differential scanning calorimetry
E	: Electric field
E_{1/2}	: Half-wave potential
E_g	: Band gap energy
EI	: Electron ionization
E_{pa}	: Anodic peak potential
E_{pc}	: Cathodic peak potential
E_{red}	: Reduction potential
E_s	: Singlet energy
eV	: Electronvolt

f	: Oscillator strength
Fc	: Ferrocene
Fig.	: Figure
FT-IR	: Fourier transform infrared spectroscopy
FU	: Functional unit
h	: hour
H	: Magnetic field
HOMO	: Highest occupied molecular orbital
Hz	: Hertz
i_p	: peak current
K	: Kelvin
kcal	: kilocalorie
k_d	: Rate constant of radiationless deactivation
k_f	: Fluorescence rate constant
l	: Pathlength
LCPL	: Left circularly polarized light
LUMO	: Lowest Unoccupied Molecular Orbital

M	: Molar concentration
max	: Maximum
mdeg	: millidegrees
mg	: milligram
min	: Minute
mL	: milliliter
mmol	: millimol
MS	: Mass spectroscopy
mV	: millivolt
M_w	: Molecular weight
n	: Refractive index
NDI	: Naphthalene diimide
nm	: Nanometer
NMP	: N-Methylpyrrolidone
NMR	: Nuclear magnetic resonance spectroscopy
ORD	: Optical rotatory dispersion
PDI	: Perylene diimide

PIGE	: Paraffin impregnated graphite electrode
RCPL	: Right circularly polarized light
Red	: Reduction
RNA	: Ribonucleic acid
Std.	: Standard
SWV	: Square wave voltammetry
TBAPF₆	: Tetrabutylammoniumhexafluorophosphate
TGA	: Thermogravimetric analysis
T_d	: Decomposition temperature
u	: Unknown
UV/VIS	: Ultra violet visible spectroscopy
V	: Volt
vs.	: Versus
ΔE_p	: Separation between the peak potentials
ε	: Extinction coefficient
Θ	: Ellipticity
λ	: Wavelength

λ_{exc}	:	Excitation wavelength
ν	:	Wavenumber
τ_0	:	Radiative lifetime
τ_f	:	Fluorescence lifetime
Φ_f	:	Fluorescence Quantum Yield
$\Delta\bar{\nu}_{1/2}$:	Half-width
$\bar{\nu}_{\text{max}}$:	Mean frequency
$[\Theta]$:	Molar ellipticity
μm	:	micrometer
$[\alpha]_D^{20}$:	Specific optical rotation

CHAPTER 1

INTRODUCTION

Scientists have been fascinated by handedness in the structure of matter ever since the concept first arose as a result of the discovery, in the early years of the last century, of natural optical activity in refracting media. This concept inspired major advances in physics, chemistry and the life sciences and continues to catalyse scientific and technological progress even today.

Perylene diimides, due to their outstanding chemical, thermal and photochemical stability, are highly promising materials for applications in organic solar cells, photovoltaic devices, and for dye lasers (Icil, 1995; Icli, 1996; Icil, 2001a; Icil, 2001b; Langhals, 1995a; Pösch, 1999; Gregg, 1996; Rudiono, 1999; Tian, 2000). On the other hand, 1,4,5,8-naphthalene diimides are heteroaromatic compounds with numerous applications. Applications of this kind of heteroatomic compounds include use as acceptors for rigid electron-transfer model systems (Sessler, 1998; Osuka, 1995; Wiederrecht, 1996; Nagata, 1991), as linkers in electron donor-acceptor molecules (Zsom, 1978; Wiederrecht, 1995; Hunter, 1989), as constituents of threading intercalators

for DNA (Takenaka, 1998a), rigid molecular clefts (Shimizu, 1994), macrocyclic receptor molecules (Jazwinski, 1987), electrically conducting dendrimers (Duan, 1997; Miller, 1997), as well as UV absorbing agents in polymers (Hirahara, 1993). The main reason of the increasing interest for these dyes originates from their electron acceptor properties and photochemical stability.

Although significant advances in the synthesis of chiral naphthalaene and perylene diimides have been made, the synthesis of macromolecules with inherently strong chiral properties remains as a challenge. Optical property of helically chiral compounds depends strongly to the helical structure (conjugation and dihedral angle). Consequently, there has been growing interest in the development of new chiral molecular switches (Todd, 2005; Zhou, 2005; Zhang, 2005). Moreover, the area using molecular chirality to engineer useful properties in nanoscience materials is fruitful and exciting, and represents an exceptionally strong promise for future development. Many types of achiral perylene and naphthalene diimides synthesis and their attractive properties for photonic materials, molecular devices and biological applications have been well reported in literature (Uzun, 2003; Dou, 2006; Figueiredo, 2005; Nagao, 1997; Shchepinov, 2000; Langhals, 2000; Tomizaki, 2002; Pasaogullari, 2006). Chiral perylene and naphthalene diimides are particularly very promising classes of dyes for chiral molecular switches due to their excellent photochemical and electrochemical properties, and good thermal stabilities as well.

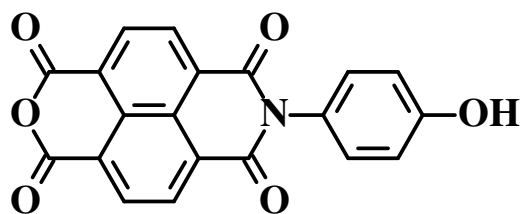
Introduction of chirality into naphthalene and perylene diimides remains a challenge and may lead to materials with optimized optical properties that can emit circularly polarized

light. Several helical naphthalene and perylene diimides with strong CD (circular dichroism) effects have been prepared with optimized properties (Gawroński, 2000; Sterzel, 2003; Langhals, 1997; Langhals, 2006b; Sun, 2007; Amiralaei, 2008; Osswald, 2007; Xue, 2008; Dehm, 2007). Unsymmetric chiral perylene diimides have been synthesized with the same method used for achiral unsymmetric perylene dyes synthesis. By substituent tuning the face-to-face π - π interaction of perylene dyes can be tailored in order to achieve a balance between good solubility and the ability to form stacks with extensive intermolecular π orbital overlap, which is very important for applications envisaged in the area of photonics (Sun, 2007; Amiralaei, 2008). Importantly, enhancement of structural stability should be taken into account when tailoring the structures in order to provide efficient chiroptical switching. Recently, the first solution-processable nonracemic chiral main-chain perylene polymers has been prepared which emerged as a promising helical polymer for use in optoelectronic devices (Xue, 2008).

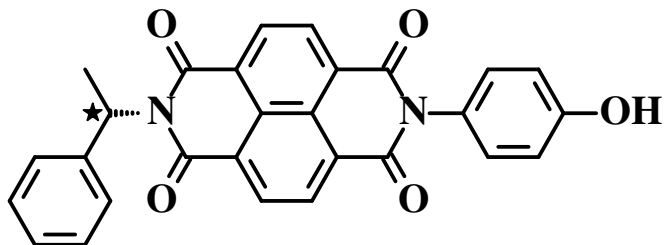
NDI (naphthalene diimide) and PDI (perylene diimide) derivatives are able to intercalate inside DNA (Hopkins, 1986; Lokey, 1997; Gianolio, 2000; Asseline, 2001; Rahe, 2003; Lewis, 2007; Haga, 2006; Zandonella, 1996). Additionally, it is possible to increase their binding property via conjugation to other binding species, nucleic acids (Gianolio, 2000; Asseline, 2001; Rahe, 2003; Lewis, 2007; Haga, 2006; Zandonella, 1996). The facile reduction of these compounds has allowed them to be used as electrochemical DNA biosensors for the detection of specific genes (Asseline, 2001). Naphthalene modified cyclic D,L-peptide nanotubes with interesting optical and electronic properties have been well documented (Thalacker, 2002; Schenning, 2002). On the other hand, molecular recognition dyads self-assembles in solvents to form helically stacking

structures. Notably, the chirality in the tails is crucial to control the chiroptical responses of the self-assembled structures (Herrikhuyzen, 2004; Würthner, 2004; Horne, 2005; Ashkenasy, 2006; Masu, 2006; Franke, 2006). Remarkably, use of chiral, self-assembled, donor and acceptor chromophores substituting fibers in optoelectronic devices, and prototypes and models for new nanoscale devices would lead to very exciting near future applications. Transfer of chirality from low molecular chiral tectons to supramolecular assemblies has been presented (Franke, 2006). Donor and acceptor chromophores on naphthalene and perylene diimide molecules revealed electron mobility via intra or intermolecular charge transfer interactions and electron transfer reactions (Lukas, 2000; Andric, 2004; Wilson, 2007). Furthermore, results of similar studies on fluorophores conjugated DNA could be extremely important for environmental and biotechnological applications (Wilson, 2007).

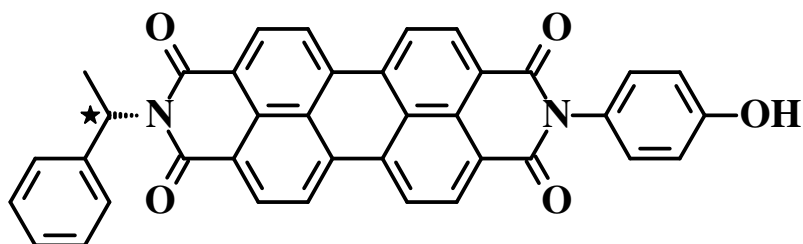
In this thesis a new naphthalene monoimide N-(4-hydroxyphenyl)-1,4,5,8-naphthalenetetracarboxylic-1,8-anhydride-4,5-imide (**1a**), one chiral naphthalene diimide N-(4-hydroxyphenyl)-N'-[(S)-1-phenylethyl]-1,4,5,8-naphthalenetetracarboxy-diimide (**2a**) and two chiral perylene diimides, N-(4-hydroxyphenyl)-N'-[(S)-1-phenylethyl]-3,4,9,10-perylenetetracarboxydiimide (**5a**) and N-(2-aminohexanoic acid)-N'-(1-dehydroabietyl)-3,4,9,10 perylenetetracarboxydiimide (**5b**) (Figure 1.1) have been successfully synthesized, for exploring photophysical, electrochemical, chiroptical and intramolecular charge transfer properties. Further, their solid state properties were analysed and discussed. The synthesized products were characterized through the data from NMR, IR, MS, UV-vis, DSC, TGA, elemental analysis, cyclic voltammetry, square-wave voltammetry and circular dichroism (CD).



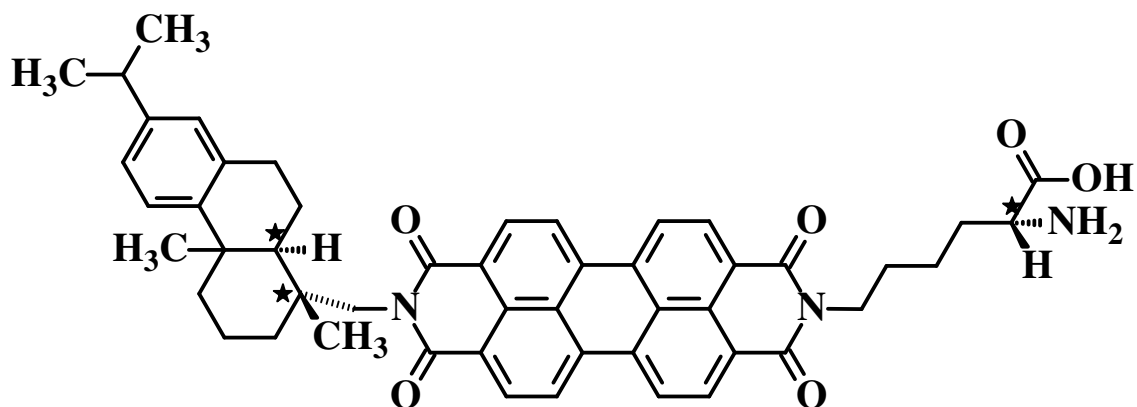
N-(4-hydroxyphenyl)-1,4,5,8-naphthalenetetracarboxylic-1,8-anhydride-4,5-imide (**1a**)



N-(4-hydroxyphenyl)-N'-(*S*)-1-phenylethyl-1,4,5,8-naphthalenetetracarboxydiimide (**2a**)



N-(4-hydroxyphenyl)-N'-(*S*)-1-phenylethyl-3,4,9,10-perylenetetracarboxydiimide (**5a**)



N-(2-aminohexanoic acid)-N'-(1-dehydroabietyl)-3,4,9,10-perylenetetracarboxydiimide (**5b**)

Figure 1.1: Structures of compounds **1a**, **2a**, **5a** and **5b**.

CHAPTER 2

THEORETICAL

2.1 The Concept of Chirality

Asymmetry in chemistry is realized by chiral molecules. Chirality (or handedness) is a symmetry property: chiral structures lack a center of inversion and a mirror plane. In group theory they belong to the nonaxial point group C_1 or the purely rotational groups C_n and D_n . Chiral molecules always exist in two forms: the structures of the two enantiomers (the old term optical antipodes is considered obsolete (Mislow, 2002)) are like left and right hands or differ by a left or right screw sense in their structure. The labeling of the individual enantiomers follows different nomenclatures. The enantiomers of most organic molecules, especially those with an asymmetric C atom, are identified by the affixes R and S (Cahn, 1966), helicenes by P and M, and octahedral bidentate complexes by Δ and Λ .

The bond lengths and bond angles of enantiomers have the same magnitude, but at least some bond angles have identical positive values in one and negative values in the other enantiomer. Thus the nonvectorial properties, as e.g. energies of formation and activation, reaction rates, or excited state lifetimes, are identical for both enantiomers. Therefore in nonasymmetric chemistry both enantiomers are produced in equal

quantities, and such a mixture is called a racemic mixture, or more loosely a racemate. The individual enantiomer of a chiral molecule can be identified only by its interaction with a chiral probe. The interactions between one enantiomer of the object and the two of the chiral probing system leads to states or complexes of different energies, reaction rates, or lifetimes, which can be discriminated by normal analytical tools. This is the important principle of diastereomerism. In all asymmetric reactions, an element of diastereomerism, i.e., a combination of, for example, R/R and R/S, or S/ Λ and S/ Δ , is apparent or hidden. Important probing systems are circularly polarized light (cpl) or chromatography at chiral phases.

Control of molecular chirality is central to contemporary chemistry- and biology related areas, such as pharmaceutical, medicinal, agricultural, environmental, and materials science and technology. Thus, a wide variety of sophisticated chiral reagents, auxiliary, catalysts, hosts, and methodologies have been developed particularly in recent years as tools for controlling chiral reactions, equilibria, and recognition in both chemistry and biology.

2.1.1 Circularly Polarized Light, ORD and CD

Chirality is the origin of the spectroscopic property optical activity. The interaction of light and matter is characterized by the refractive index and the absorption coefficient. For chiral molecules, both the refractive index and the absorbance coefficient of one enantiomer differ for right and left circularly polarized light (r-cpl and l-cpl).

Light is a transversal electromagnetic wave, i.e., the electric and magnetic field vectors (\mathbf{E} and \mathbf{H} , respectively) are perpendicular to the direction of propagation \mathbf{z} (and perpendicular to one another). In polarized radiation there are spatial and temporal restrictions for these vectors. Linear polarization requires a constant direction of the vectors, the point of the electric field vector \mathbf{E} moves up and down on a line if a spectator observes it in the direction of propagation. If two coherent perpendicularly linearly polarized light beams are superimposed, the \mathbf{E} vector point leaves the line and may in general create an elliptic figure. With equal amplitude and a $+\pi$ and $-\pi$ phase shift, the vector point rotates on a circle in a right or left handed sense. Light is addressed as l-cpl if the point of the \mathbf{E} vector rotates counterclockwise when the light approaches the observer (Fig 2.1). On the other hand, the superposition of r-cpl and l-cpl of equal phase and amplitude realizes linearly polarized light. Thus r-cpl and l-cpl on one side and two perpendicularly linearly polarized beams are both bases to describe polarization phenomena. If the amplitudes are not equal, the degree of circular polarization γ is less than unity.

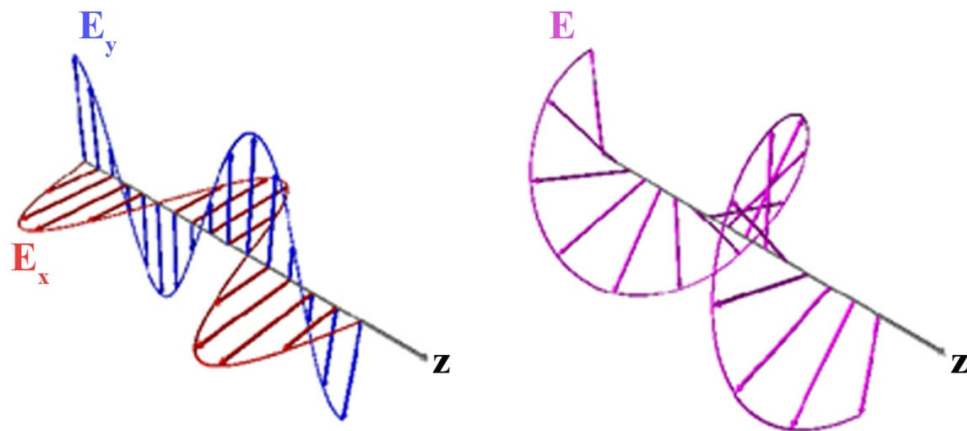


Figure 2.1: Left circularly polarized light.

Experimentally optical activity becomes manifest in the phenomena of optical rotatory dispersion (ORD) and of circular dichroism (CD), both being wavelength dependent. ORD is related to the differential refractive indices $\Delta n_\lambda = (n_{l\text{-cpl}} - n_{r\text{-cpl}})_\lambda$, CD to the differential absorption coefficients $\Delta \epsilon_\lambda = (\epsilon_{l\text{-cpl}} - \epsilon_{r\text{-cpl}})_\lambda$; Δn and $\Delta \epsilon$ generally are small differences of large numbers. However, ORD is measured by the rotation of the polarization plane of linearly polarized light that is tied directly to the difference $(n_{l\text{-cpl}} - n_{r\text{-cpl}})_\lambda$ and does not require the subtraction of two separate measurements of $n_{l\text{-cpl}}$ and $n_{r\text{-cpl}}$. So high precision is possible, and very small effects can be detected. For the determination of CD, the two absorbances of one enantiomer versus l-cpl and r-cpl have to be measured separately. By symmetry the different absorption of one kind of light by the two enantiomers is also $\Delta \epsilon_\lambda = \epsilon_{S,\lambda} - \epsilon_{R,\lambda}$. The same holds for the refractive indices. CD is mostly quantified by the molar ellipticity $[\theta]_\lambda$. The units of the chiroptical properties are, owing to the historic background, somewhat odd:

$$[\theta]_\lambda = \frac{100\theta_\lambda}{dc} = 3300\Delta\epsilon_\lambda \quad (2.1)$$

is expressed in $\text{deg cm}^2/\text{dmol}$, where θ_λ is the ellipticity instrument reading at wavelength λ in degrees, d the path length in cm, and c the concentration in mol/L. The factor 3300 adjusts also the units.

The magnitude of CD should be seen in relation to the magnitude of absorption. Kuhn has introduced a wavelength-dependent anisotropy factor g_λ defined by

$$\alpha_D = \frac{\epsilon_1 - \epsilon_2}{\epsilon} = \frac{\Delta\epsilon}{\epsilon} = \frac{\Delta\epsilon}{(\epsilon_R + \epsilon_S)/2} = \frac{\epsilon_S - \epsilon_R}{\epsilon} = \frac{\Delta\epsilon}{(\epsilon_R + \epsilon_S)/2} \quad (2.2)$$

which ranges between 0 and 2. For symmetry reasons, $\epsilon_S = \epsilon + \Delta\epsilon/2$ and $\epsilon_R = \epsilon - \Delta\epsilon/2$ (Kuhn, 1930).

2.2 Molecular Chiral Recognition

In 1848, Louis Pasteur used a hand lens and a pair of tweezers to separate the sodium ammonium salt of paratartaric acid into two piles, one of left-handed crystals and the other of right-handed crystals, thereby accomplishing the enantioselective resolution of racemic tartaric acid (Pasteur, 1948). Thus, the first reported mechanism for the recognition and differentiation of enantiomeric molecules was visual recognition of crystal structures.

Pasteur also accomplished the first chemical resolution of a racemic compound through the formation of diastereomeric salts (Pasteur, 1948; Drayer, 1993). In 1853 he neutralized a solution of the optically pure alkaloid L-cinchonine with racemic tartaric acid. The solution was left to crystallize and the first crop of crystals comprised entirely the L-tartrate- L-cinchonine salt.

With this experiment, Pasteur demonstrated that the transformation of enantiomers into diastereomers converted molecules with the same physicochemical properties (enantiomers) into compounds with different physicochemical properties (diastereomers). Thus, while the solubilities of D- and L-tartaric acid were identical, those of the diastereomeric D- and L-tartaric acid-L-cinchonine salts were not. The

resolution of enantiomers through their conversion into diastereomeric salts or covalent diastereomeric derivatives is now a routine chemical procedure.

In biological systems, the differentiation between enantiomeric compounds is conceptually similar to the chemical process, *i.e.* based upon conversion of enantiomers into diastereomers. In this case, however, instead of diastereomeric compounds, the key step is the formation of transient diastereomeric complexes. This mechanism is based upon the capacity of one chiral molecule (the selector) to interact with the enantiomers of a second (the selectand). Differentiation or molecular chiral recognition is the result of energy differences between the diastereomeric selector-selectand complexes.

The chiral selectors in biological systems are most often biopolymers which derive their chirality from L-amino acid backbones and the resulting secondary and tertiary structures. The most prominent are enzymes, receptors and carrier proteins such as serum albumin. In addition to amino acid-based biopolymers, carbohydrates such as amylose and cellulose (Yashima & Okamoto, 1997) and cyclodextrins (Francotte, 1997) also have the capacity for chiral recognition. Native and derivatized forms of these biopolymers have been utilized in *in vitro* systems for the analytical and preparative chromatographic separations of chiral compounds (Wainer, 1993; Francotte, 1997; Yashima & Okamoto, 1997).

The recognition of three-dimensional structure during enzyme-substrate or ligand-receptor interactions is a complicated but basic aspect of biological and pharmacological processes. Yet within the very complexity of this process lies the simplicity of nature

and a key to understanding many basic pharmacological processes. This realization can also be attributed to Pasteur who, in 1858, reported that the *dextro* form of ammonium tartrate was more rapidly destroyed by the mould *Penicillium glaucum* than the *laevo* isomer (Pasteur, 1901; Drayer, 1993). This was the first report of molecular chiral recognition.

2.3 Chiral Photochemistry

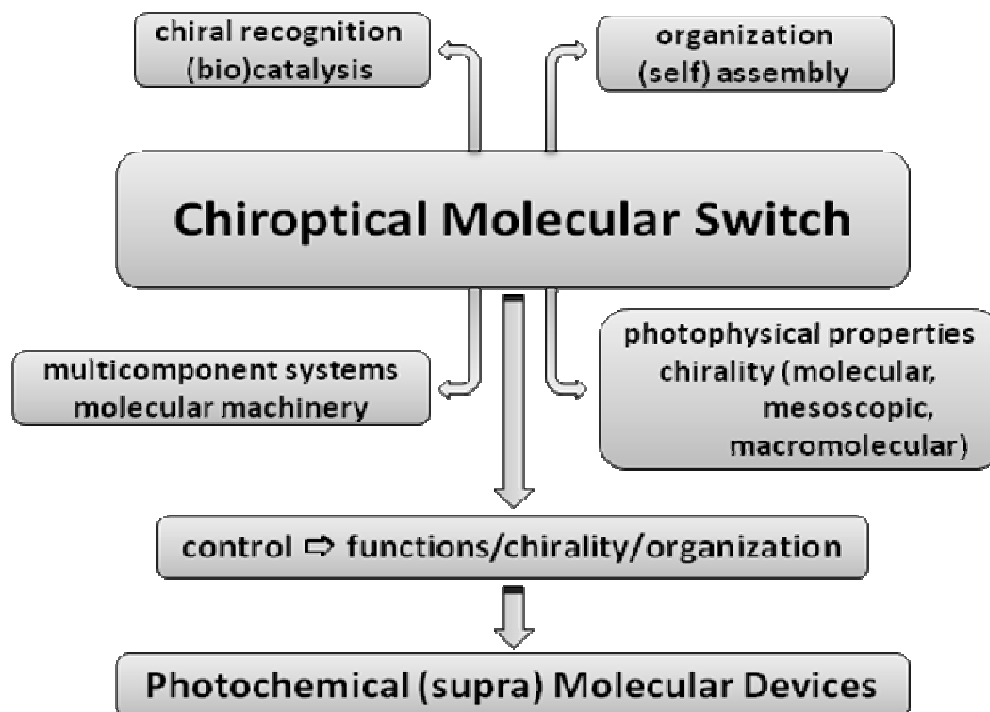
Traditionally, chirality control has been achieved predominantly through the ground-state interactions of substrate/guest with chiral reagent/auxiliary/catalyst/host/receptor/enzyme, which are structurally and energetically well defined and characterized in considerable detail. In sharp contrast, the possibility of chirality control in the electronically excited state has not been extensively explored experimentally or theoretically, until recently. This is simply because of the long held belief that in the excited states chiral interactions, particularly the intermolecular ones, are too weak and short-lived in general to achieve high stereochemical recognition and differentiation. However, this has turned out not to be true, and several recent works have clearly demonstrated that chirality control in the excited state is not a difficult but rather a fascinating subject to study, displaying various novel phenomena which are unexpected and unprecedented in the conventional *thermal* chiral chemistry occurring in the ground electronic state. The origin of chiral photochemistry, or photochirogenesis, dates back to the late 19th Century, when le Bel (1875) and van't Hoff (1894) suggested the use of circularly polarized light for so-called "absolute asymmetric synthesis (AAS)." The first successful AAS was achieved by Kuhn in 1929, immediately after the discovery of circular dichroism by Cotton. Modern chiral organic photochemistry may be traced back

to the work of Hammond and Cole reported in 1965; they demonstrated for the first time that chiral information could be transferred from an optically active sensitizer to a substrate upon photosensitization. In the 1970s, considerable effort was devoted to the AAS of helicene precursors by Kagan's and Calvin's groups, while more recently, and particularly in the last decade, molecular and supramolecular chiral photochemistry has attracted growing interest as a unique methodology for inducing molecular chirality in the photoproducts.

2.4 Chiroptical Molecular Switches

Chiral photobistable molecules comprise a particular attractive class of photochromic compounds, as the reversible photochemical transformation between two forms can lead simultaneously to a chirality change in the system (Brown, 1971; Dürr, 1990; El'tsov, 1990; Feringa, 1993, Feringa, 1996). In addition to the conventional absorption spectrum change associated with photochromic materials, and the possibility of modulating other physicochemical properties such as dipole moment or redox potential, it is also possible to exploit the unique properties associated with the different stereoisomers of such chiral photoresponsive molecules (Balzani, 1991; Irie, 1994; Willner, 1996; Gómez-López, 1997). It is important to realize that an intrinsic feature of living organisms is the precise control, in many essential components, of chirality at the molecular, supramolecular, and macromolecular levels (Gardner, 1974). In biosystems, molecular recognition, transport, information storage and processing, structure and assembly of materials, catalysis, and replication are all intimately controlled by chirality (Crick, 1981).

Chiral optical (chiroptical) switches might therefore offer intriguing prospects in the design of trigger elements and new photonic materials (Feringa, 2000). The use of light to control chirality in a reversible manner can be applied in molecular memory elements, which are essential for the development of materials for optical data storage and processing (Balzani, 1991; Irie, 1994; Willner, 1996; Gómez-López, 1997). Furthermore, nanoscale devices and machinery, for “bottom up” construction of complex systems, require integration of control and trigger elements at the molecular level (Feynman, 1960; Drexler, 1991; Hoch 1996). A chiroptical switch provides a powerful means for the control of functions, chirality, and organization, as the physical properties and geometries of such molecules can be modulated by light, and this principle has been exploited in triggering more complex systems (Scheme 2.1).



Scheme 2.1: Potential applications of a chiral optical (chiroptical) molecular switch.

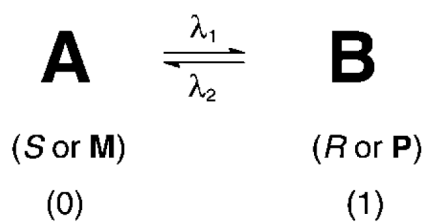
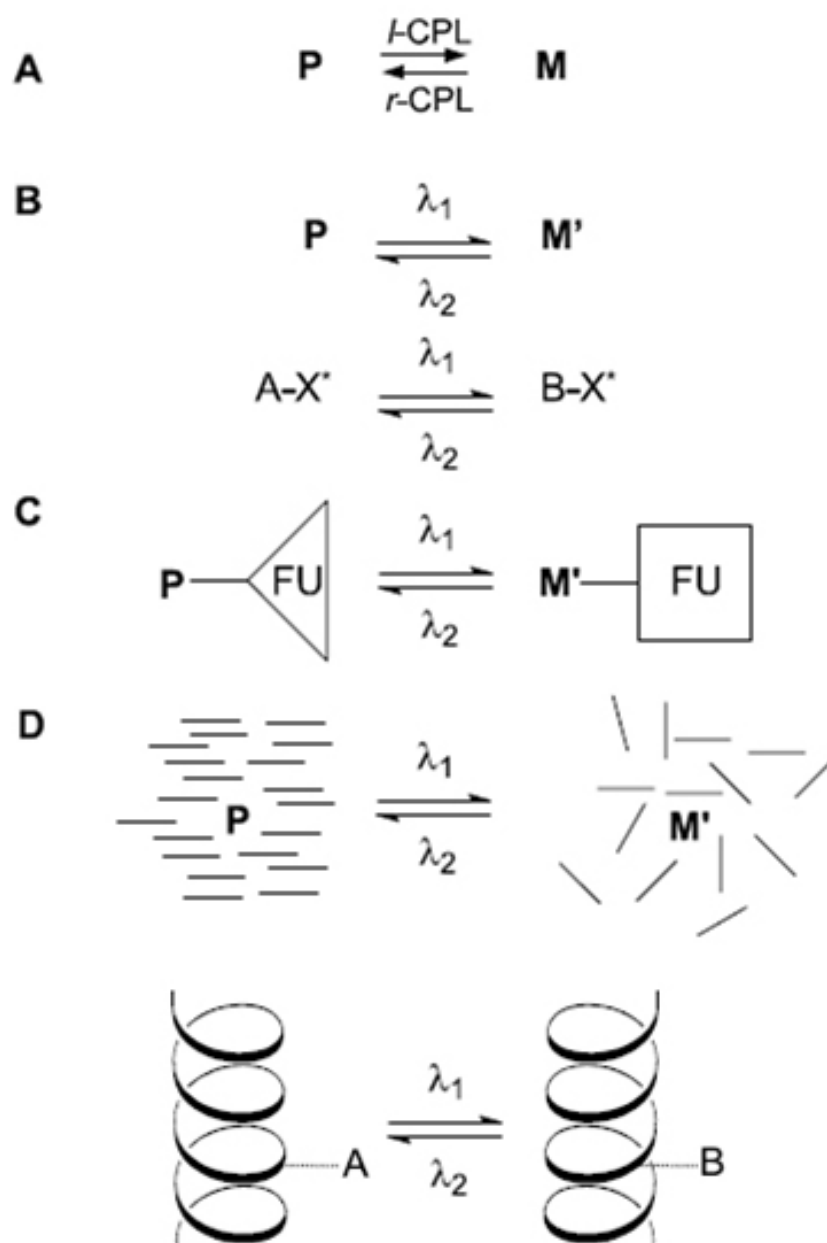


Figure 2.2: Schematic representation of a molecular switch.

In a chiral photochromic system (Figure 2.2), A and B represent two different chiral forms of a bistable molecule, and a reversible change in chirality occurs upon light irradiation. The left-handed (S or M) and right-handed (R or P) forms of a chiral compound represent two distinct states in a molecular binary logic element.



Scheme 2.2: Chiral Switches: A enantiomers, B diastereomers (X^* = chiral auxiliary), C functional chiral switches (FU = Functional Unit), D macromolecular switch and switching of matrix organization (Feringa, 2001).

Various types of chiral switches based on photochromic molecules are schematically summarized in Scheme 2.2.

A) Switching of enantiomers:

Unless chiral light is used, irradiation of either enantiomer of a chiral photochromic molecule (R/S or P/M) will, irrespective of the wavelength used, always lead to a racemic mixture, due to the identical absorption characteristics of the two enantiomers. In these systems, therefore, the enantiomers are interconverted at a single wavelength by employing left or right circularly polarized light (l- or r- CPL). Enantioselective switching in either direction is in principle possible.

B) Switching of diastereomers:

The compound consists of two diastereomeric photobistable forms: for instance, P (right-handed) and M' (left-handed) helices, which can undergo photoisomerization at two different wavelengths: λ_1 and λ_2 . Alternatively, a chiral auxiliary (X*) and a photochromic unit (A) (either chiral or achiral) may be present in systems A-X*, with the auxiliary X* controlling the change in chirality during the switching event.

C) Functional chiral switches:

Because of the multifunctional nature of these photochromic systems, the change in chirality simultaneously triggers the modulation of some particular function, such as fluorescence, molecular recognition, or motion. In most cases, this is the result of a change in the geometry or the electronic properties of the system.

D) Switching of macromolecules or supramolecular organization:

Photobistable molecules (chiral or achiral) may be covalently attached to, for example, a polymer or be part of a host-guest system. The photoisomerization process induces changes in some property such as the helical structure of a chiral polymer or the organization of the surrounding matrix: the chiral phase of a liquid crystalline material or a gel, for example. The photochemical event is recorded by means of the chiral response of the structure, organization, or other property of the macromolecule or the larger ensemble.

Photochemical bistability is an inalienable condition, but a number of other requirements are essential for application of chiral switches in photonic materials or optical devices (Feringa, 2001):

- Thermal stability; there should be a large temperature range in which no interconversion of the isomers takes place. This includes stability towards racemization.
- Low fatigue; numerous cycles should be possible without any change in performance.
- Fast response times, high sensitivity, and detectability; switching should be fast and easy, both forms should be readily detectable.
- Nondestructive read-out; the detection method should not erase the stored information.

- The photochemical and other properties must be retained when the chiral molecular switch is incorporated in a polymer or acts as a part of a multicomponent assembly.

In most photochromic systems, absorption or emission spectroscopy, monitoring near the switching wavelengths, is used for read-out. This often leads to partial reversal of the photochemical process used to store information (Dürr, 1989). Chiroptical techniques allow the change in chirality of the photochromic system to be measured, and so a major advantage of chiroptical switches, compared to other photochromic systems, is the possibility of non-destructive read-out by monitoring the optical rotation at wavelengths remote from the wavelengths used for switching (information storage). The sensitivity towards changes in organization and chirality in larger ensembles such as gels and liquid crystals, together with the conformational changes in polymers, and concomitant change in physical properties associated with these events, offer other attractive possibilities for avoiding destructive read-out (Feringa, 1996).

2.5 Properties of Naphthalene and Perylene Diimides

Carboxylic imides are stabilized by their very high resonance energy which exceeds even that of carboxylic amides. A further stabilization is achieved by their incorporation into heterocyclic rings.

Naphthalenediimides preparatively easily accessible from the dianhydride and are formally the lower analogues of the well-known perylene dyes. Perylene dye has been known as highly photostable pigments or vat dyes. Perylene tetracarboxylic diimide

derivatives have been studied because of their brilliant colour, strong absorption and fluorescence and good thermal, chemical, photochemical and electrochemical stability (Shim, 2001; Langhals and Blanke, 2003; Schlichting, 1997; Langhals, 1995b; Submeier and Langhals, 2001). However, the light absorption of the naphthalenediimides is so hypsochromically shifted that they are colourless; they are only weakly fluorescent and having low fluorescence quantum yields (Uzun, 2003; Langhals, 2006a).

2.5.1 Potential Applications of Naphthalene and Perylene Diimides

Many derivatives of perylene and naphthalene diimides have been synthesized and their attractive properties for optical and photonic materials, molecular devices and biotechnological applications have been well reported in the literature.

2.5.1.1 Optical and Photonic Materials

Optical and Photonic Materials will play a key role in the future miniaturization of electronic and telecommunication devices and systems. Photonics is the science of generating, controlling, and detecting photons, particularly in the visible and near infrared spectrum, but also extending to the ultraviolet (0.2–0.35 μm wavelength), long-wave infrared (8–12 μm wavelength), and far-infrared/THz portion of the spectrum. Photonic devices include optoelectronic devices such as lasers and photodetectors, as well as optical fiber and planar waveguides, and waveguide-based passive devices.

Perylene and naphthalene diimides potentially can be used as organic photorefractive media for optical signal processing, electron transporting components in organic light-

emitting diodes, semiconducting materials for solar energy conversion, fluorescent dyes and near-IR dyes.

Perylene pigments cover the whole range of the visible spectrum and find applications in the fields of paints and lacquers, namely for the car industry. Beside these conventional uses, perylenes are key chromophores for high-tech application. Perylene diimide based electroluminescent display devices typically undergo emission in the red spectral region believed to arise from excimer formation, which in turn depends in the orientation and organization of the chromophore (Menikh and Bounaovi, 1997).

Perylene diimides are used as charge-generating materials, independently or along with other photoconductive pigments, electrophotographic photoreceptors. Perylene derivatives have also been used in heterojunctions with phthalocyanines in all organic photovoltaic and photoelectrochemical cells. Most of reports suggest that perylene derivatives generally behave like n-type semiconductor (Tamizhmani and Dodelet, 1991; Greeg, 2002; Ebeid and El-Daly, 1988; Kudo et al., 1998; Williams and Murray, 1998; Lu et al., 1999; Thelakkat et al., 2001; Mackinnon and Wong, 2000)

2.5.1.2 Molecular Devices

A molecular-level device can be defined as an assembly of a discrete number of molecular components (i.e., a supramolecular structure) designed to perform a specific function. Each molecular component performs a single act, while the entire supramolecular assembly performs a more complex function, which results from the cooperation of the various components. A molecular-level machine is a particular type of molecular-level device in which the relative positions of the component parts can change as a result of some external stimulus. Molecular-level devices and machines operate via electronic and/or nuclear rearrangements and, like macroscopic devices and machines, need energy to operate and signals to communicate with the operator (Balzani, 2003).

The linear triad consisting of a 4-aminonaphthalene monoimide electron-donor and naphthalene-1,8:4,5-diimide and a pyromellitimide electron acceptors show that it is possible to control the movement of electrons within a multisite donor–acceptor array on a femtosecond time scale (Debrecezy, 1996). In a triad which consists of two free-base triphenylporphyrin electron donors linked to a perylene-(3,4:9,10-tetracarboxylic)diimide electron acceptor, photoinduced electronic switching can be achieved by modulating the intensity of a laser (O’Neil, 1992). In another triad consisting of a zinc porphyrin, a perylene-3,4-dicarboximide, and a naphthalene-1,8:4,5-diimide viewed as a molecular switch in which it can be rapidly turned on and off by use of different laser pulses (Hayes, 2000).

Hierarchically assembled chiral dye superstructures exhibit photoinduced electron transfer on subpicosecond time scale, and thus, these supramolecular entities might serve as valuable nanoscopic functional units (Würthner, 2004). Use of chiral, self-assembled, donor and acceptor chromophores substituting fibers in optoelectronic devices, and prototypes and models for new nanoscale devices would lead to very exciting near future applications.

2.5.1.3 Biotechnological Applications

Biotechnology is often used to refer to genetic engineering technology of the 21st century, however the term encompasses a wider range and history of procedures for modifying biological organisms according to the needs of humanity, going back to the initial modifications of native plants into improved food crops through artificial selection and hybridization.

Perylene and naphthalene diimides have found uses in a wide variety of biotechnological applications. They are excellent electron acceptors and the photophysics of these species has been well-studied (Rogers, 2000; Uzun, 2003). Selected perylene and naphthalene diimide derivatives are examples of molecules that undergo spontaneous organization in solution (Tomasulo, 2005; Gabriel, 2005; Yang et al., 2008).

Photolysis of naphthalene diimides has been used to reduce heme proteins; photoactivation of hydroperoxy derivatives has been used to oxidize both proteins and DNA (Figueiredo, 2005; Matsugo, 1995; Nakajima, 2002). Naphthalene diimide derivatives have been known for many years to intercalate in duplex DNA. Binding to

bulged duplexes (Takenaka, 1997), triplexes (Bever, 2000; Gianolio, 2001), quadruplexes (Fedoroff, 1998; Han, 2000; Sato, 2005), hairpins (Bever, 2000), and DNA-RNA heteroduplexes (Sato, 2001) has been studied. Molecules with the naphthalene diimide moiety have been shown to thread into DNA, with the diimide groups intercalating and the side chains or conjugating moieties lying in the grooves (Murr, 2001; Guelev, 2001; Guelev, 2002; Lee, 2004; Chu, 2007). The NDIs can carry reactive groups to the DNA including metal centers (Steullet, 1999; Dixon, 1999) and alkylating agents (Okamoto, 2000). Naphthalene diimides have been used to conjugate other nucleic acid binding species, thus increasing their binding (Tok, 2001; Mokhir, 2003) and have been employed to stabilize DNA hairpins (Michel, 2002). Diimides intercalated into or covalently bound to DNA have been used extensively in studies of photoinduced charge separation and charge recombination processes (Vicic, 2000; Nunez, 2000; Lewis, 2001; Lewis, 2004; Nakajima 2007). The facile reduction of NDI bound to DNA has allowed these species to be used in the electrochemical detection of DNA (Takenaka, 1998b; Tansil, 2005; Komatsu, 2006).

In general, studies of NDI with nucleic acids involve cationic substituents on the NDI side chains to favor electrostatic interactions between these side chains and the phosphate groups of the nucleic acid. Side chains with a methylene group adjacent to the imide nitrogen are necessary to prevent a steric clash between the side chain of the NDI and the DNA. A cationic center no further than three atoms away from the central core prevents self-stacking in aqueous solution, which can complicate DNA binding measurements (Steullet, 1999).

Perylene diimide derivatives have an unusual propensity to form self-assembled dimers and aggregates and thus have been widely used as building blocks for supramolecular architectures (Li, 2003; Würthner, 2004; Shaller, 2008). Conjugates of oligonucleotides with photostable perylene diimide dyes were extensively studied because of their interesting ability to selfassemble. Bis(oligonucleotide) conjugates possessing PDI linkers have been reported to form a variety of structures, including duplexes, triplexes, and capped hairpins, as well as novel structures possessing several PDI chromophores connected by disordered oligonucleotides (Bever, 2000; Rahe, 2003; Wang, 2003). The perylene diimide moiety located in the middle of an oligonucleotide strand is known to increase its propensity to triplex formation (Bever, 1998; Bever, 2002). The combination of PDI's favorable optical properties with molecular recognition capabilities have been enabled attractive applications of these dyes as biological probes (Qu, 2004; Abdalla, 2004; Franceschin, 2004; Krauß, 2005).

CHAPTER 3

EXPERIMENTAL

3.1 Materials

1,4,5,8-naphthalenetetracarboxylic dianhydride, perylene-3,4,9,10-tetracarboxylic dianhydride, 4-aminophenol, potassium hydroxide, phosphoric acid and isoquinoline were obtained from Aldrich. (*S*)-(-)- α -methylbenzylamine, tetrabutylammonium hexafluorophosphate (TBAPF₆) and ferrocene were purchased from Fluka. All organic solvents employed were of spectroscopic grade.

3.2 Instruments

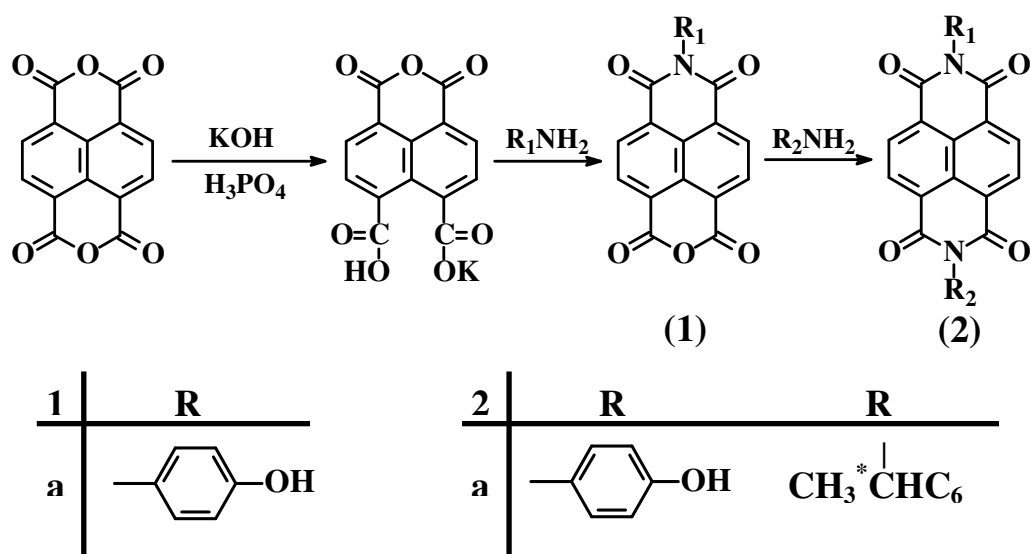
IR spectra were measured as KBr pellets using a Mattson Sattelite FTIR spectrometer. UV-vis spectra in solutions were recorded with a Varian-Cary 100 spectrometer. UV-vis spectra of solid state were measured in thin films using a Perkin-Elmer UV/VIS/NIR Lambda 19 spectrometer, equipped with solid accessories. Mass spectra were recorded with a Finnigan MAT 311A instrument at 70 eV ionization energy. Data were presented in m/z (%) values. Emission spectra were measured using a Varian Cary Eclipse Fluorescence spectrometer. Optical rotations were measured with a Dr. Kernchen

Sucromat digital automatic polarimeter, at 589 nm and 20 °C. CD spectra were measured on a JASCO 810 spectropolarimeter. Elemental analyses were obtained from a Carlo-Erba-1106 C, H, N analyzer. ^1H and ^{13}C NMR spectra were measured with a Bruker AVANCE-500 spectrometer. TGA thermograms were recorded with a TG-MS: Simultane TG-DTA/DSC apparatus STA 449 Jupiter from Netzsch, equipped with Balzers Quadstar 422 V. The samples were heated at 5 K/min in oxygen. Thermal analyses were recorded using a DSC 820 Mettler Toledo instrument. The samples were heated at 5 K/min in nitrogen. Cyclic and square-wave voltammetries in solvents were performed using a three-electrode cell with a polished 2 mm glassy carbon as working and Pt as counter electrode; solutions were 10^{-4} M in electroactive material and 0.1 M in supporting electrolyte, TBAPF₆. Data were recorded on an EG&G PAR 273A computer-controlled potentiostat. Ferrocene was used as internal reference. The scan rate of 50-1000 mVs⁻¹ and the frequency 60-150 Hz were employed for cyclic and square-wave voltammetries, respectively. Cyclic and square-wave voltammetries in solid state were performed using an AUTOLAB system (Eco-Chemie, Utrecht, The Netherlands). The reference electrode was an Ag/AgCl electrode (saturated NaCl) with a potential of 0.200 V vs. SHE at 25 °C. A platinum wire served as an auxiliary electrode. A graphite rod (diameter: 0.5 cm) was used as working electrode. Compound was immobilized at the surface of the paraffin impregnated graphite electrodes (PIGEs) with a diameter of 5 mm. The solid compound was attached to the surface of PIGE by scratching. The supporting electrolyte was 1 M HCl. The scan rate of 25-600 mVs⁻¹ and the frequency 50-300 Hz were employed for solid state cyclic and square-wave voltammetries, respectively. Fluorescence lifetime measurement was performed by time correlated single photon counting technique (FLS920, from Edinburgh Instruments).

3.3 Methods of Syntheses

Unsymmetrically substituted chiral naphthalene and perylene diimides were prepared according to the synthetic routes shown in Scheme 3.1 and Scheme 3.2, respectively.

The unsymmetrical chiral naphthalene diimide has been prepared by a two-step reaction process starting from 1,4,5,8-naphthalenetetracarboxylic dianhydride. At the first step a N-alkyl-1,4,5,8-naphthalenetetracarboxylic-1,8-anhydride-4,5-imide (1) was synthesized according to literature (Horne and Ghadiri et al., 2005). At the last step, the chiral unsymmetrical naphthalene diimide was synthesized via condensation of N-alkyl-1,4,5,8-naphthalenetetracarboxylic-1,8-anhydride-4,5-imide (1) with corresponding amine using m-cresol and isoquinoline as solvent mixture.

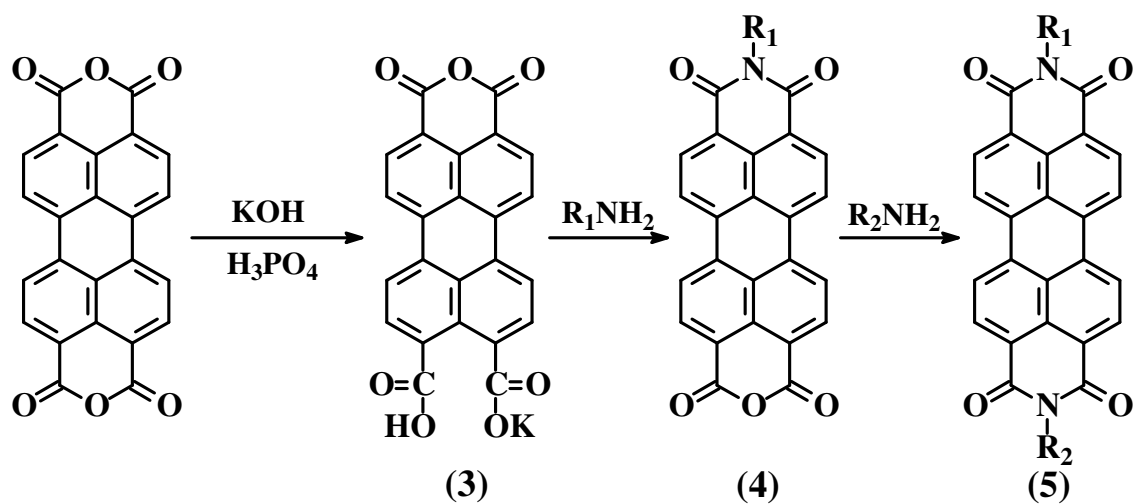


Scheme 3.1: Synthesis of naphthalene monoimide and unsymmetrical chiral naphthalene diimide.

The unsymmetrical chiral perylene diimides have been synthesized from perylene-3,4,9,10-tetracarboxylic dianhydride by a three-step reaction with corresponding amines. At the first and second steps, perylene-3,4,9,10-tetracarboxylic acid monoanhydride

monopotassium carboxylate (3) and N-alkyl-3,4,9,10-perylenetetracarboxylic-3,4-anhydride-9,10-imide (4) were synthesized and purified according to literature (Pasaogullari, 2006), respectively. Finally, the unsymmetrical chiral perylene diimide (5) was synthesized via condensation of corresponding amine with N-alkyl-3,4,9,10-perylenetetracarboxylic-3,4-anhydride-9,10-imide using m-cresol and isoquinoline as solvent mixture.

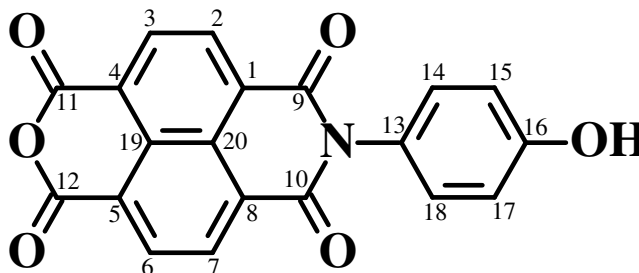
The structures of the compounds were characterized by ^1H NMR, ^{13}C NMR, MS, IR, and elemental analysis. The optical, photochemical, thermal, electrochemical and chiroptical properties of unsymmetrically substituted chiral naphthalene and perylene diimides have been investigated in detail.



4	R_1	
a		
b	$-\text{CH}_2(\text{CH}_2)_3^* \text{CH}(\text{NH}_2)\text{COOH}$	
5	R_1	R_2
a		$\text{CH}_3^* \text{CHC}_6\text{H}_5$
b	$-\text{CH}_2(\text{CH}_2)_3^* \text{CH}(\text{NH}_2)\text{COOH}$	

Scheme 3.2: Synthesis of perylene-3,4,9,10-tetracarboxylic acid monoanhydride monopotassium carboxylate, perylene monoimide and unsymmetrical chiral perylene diimide.

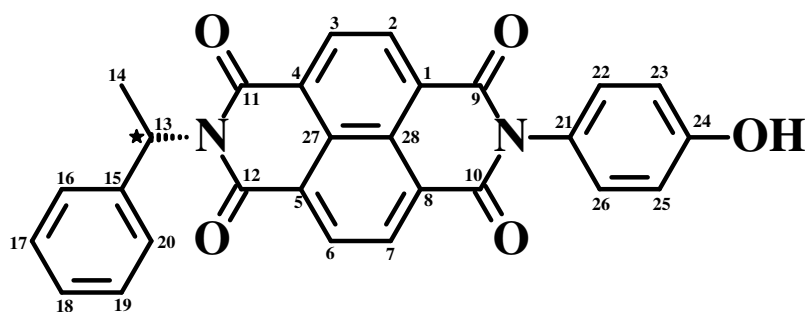
3.3.1 Synthesis of N-(4-hydroxyphenyl)-1,4,5,8-naphthalenetetracarboxylic-1,8-anhydride-4,5-imide (1a)



Following the procedure of Ghadiri (Horne and Ghadiri et al., 2005) 1,4,5,8-naphthalenetetracarboxylic dianhydride (2.0 g, 7.5 mmol), water (350 mL) and KOH (1.0 M, 65 mL) were stirred for 2h. After the starting material had dissolved, the pH of the solution was adjusted to pH 6.4 with H₃PO₄ (1.0 M). 4-Aminophenol (0.8 g, 7.5 mmol) was added and the solution was refluxed at 110 °C for 10h. The solution was filtered, and the filtrate acidified with acetic acid (10%). The precipitate was collected by vacuum filtration, washed with water and dried in vacuum at 100 °C. The crude product was extracted with acetone in a Soxhlet apparatus during one day, in order to remove unreacted reactants. Yield (2.10 g, 78%); light-brown powder. FT-IR(KBr , cm⁻¹): $\nu = 3430, 1783, 1709, 1660, 1609, 1591, 1516, 1439, 1382, 1351, 1243, 1163, 1102, 956, 861, 824, 770, 646, 582, 535, 431$. ¹HNMR, δ_{H} (ppm) (500MHz, DMSO-d₆): 8.51-8.49 (d, $J = 6.8$ Hz, 2 Ar-H, H-C(3), H-C(6)), 8.12-8.11(d, $J = 6.8$ Hz, 2 Ar-H, H-C(2), H-C(7)), 7.15-7.14 (app d, $J = 7.7$ Hz, 2 Ar-H, H-C(14), H-C(18)), 6.88-6.86 (app d, $J = 7.7$ Hz, 2 Ar-H, H-C(15), H-C(17)). ¹³CNMR, δ_{C} (ppm) (100MHz, DMSO-d₆): 169.5 (2 C=O, C(9), C(10)), 163.5 (2 C=O, C(11), C(12)), 157.3 (1(C), C(16)), 139.5 (1(C), C(13)), 130.2 (2 Ar-CH, C(2), C(7)), 129.9 (2 Ar-CH, C(3), C(6)), 128.9 (1(C), C(19)),

128.4 (2 Ar-CH, C(14), C(18)), 126.7 (2(C), C(1), C(8)), 125.7 (1(C), C(20)), 124.3 (2(C), C(4), C(5)), 115.5 (2 Ar-CH, C(15), C(17)). UV/Vis (DMF): λ_{max} (nm) (ϵ) = 356 (11732). Fluorescence (DMF): λ_{max} (nm) = 407. Fluorescence quantum yield (MeOH, reference Anthracene with $\Phi_f = 27\%$, $\lambda_{\text{excit.}} = 360$ nm) = 0.2%. MS (EI): m/z : 359 [M]⁺. Anal. Calcd. for C₂₀H₉NO₆ (M_w, 359.3); C, 66.86; H, 2.52; N, 3.90. Found: C, 66.36; H, 2.54; N, 3.94.

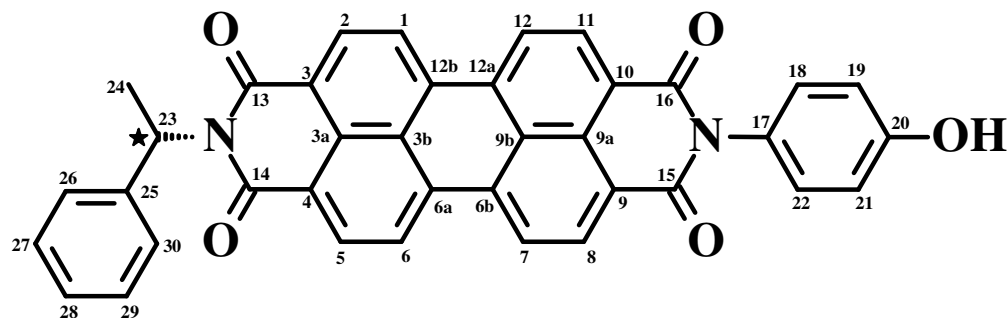
3.3.2 Synthesis of N-(4-hydroxyphenyl)-N'-[(S)-1-phenylethyl]-1,4,5,8-naphthalenetetracarboxydiimide (2a)



N-(4-hydroxyphenyl)-1,4,5,8-naphthalenetetracarboxylic-1,8-anhydride-4,5-imide (**1a**) (1.0 g, 2.8 mmol), (S)-(-)- α -methylbenzylamine (1.1 mL, 8.4 mmol), m-cresol (40 mL) and isoquinoline (8 mL) were stirred under argon at 80 °C for 3h, at 120 °C for 6h, at 160 °C for 8h and at 190 °C for 5h. The warm solution was poured into methanol (350 mL) and filtered. Hydrochloric acid (1.0 M) was added to the filtrate, and a brown solid precipitated from the solution. The product was further purified by crystallization from chloroform. The solid was collected by vacuum filtration, washed with water and dried in vacuum at 100 °C. Yield (1.10 g, 85%); brown powder. R_f (silica gel, CHCl₃) = 0.54. $[\alpha]_D^{20}$: -221.6 (c 0.0194, CHCl₃), FT-IR(KBr, cm⁻¹): ν = 3430, 3053, 3026, 2976, 1708,

1600, 1611, 1590, 1513, 1450, 1350, 1326, 1250, 1195, 1102, 1066, 1030, 974, 876, 829, 769, 697, 568, 405. ^1H NMR, δ_{H} (ppm) (500MHz, CDCl_3): 8.71-8.68 (d, 4 Ar-H, H-C(2), H-C(3), H-C(6), H-C(7)), 7.65-7.48 (m, 2 Ar-H, H-C(16), H-C(20)), 7.41-7.21 (m, 5 Ar-H, H-C(17), H-C(18), H-C(19), H-C(22), H-C(26)), 7.13-6.85 (m, 2 Ar-H, H-C(23), H-C(25)), 6.54-6.50 (q, $J = 7.0$, 1 C-H, H-C(13)), 2.00-1.99 (d, $J = 7.4$, 1 CH_3 , $\text{H}_3\text{-C}(14)$). ^{13}C NMR, δ_{C} (ppm) (100MHz, CDCl_3): 163.3 (2 C=O, C(11), C(12)), 162.84 (2 C=O, C(9), C(10)), 157 (1(C), C(24)), 140.0 (1(C), C(15)), 139.9 (1(C), C(21)), 131.4 (2 Ar-CH, C(3), C(6)), 131.1 (2 Ar-CH, C(2), C(7)), 129.4 (1 Ar-CH, C(18)), 128.3 (2 Ar-CH, C(22), C(26)), 127.3 (2 Ar-CH, C(17), C(19)), 127.2 (2 Ar-CH, C(16), C(20)), 127.1 (1(C), C(27)), 126.9 (1(C), C(28)), 126.8 (2(C), C(4), C(5)), 126.5 (2(C), C(1), C(8)). UV/Vis (DMF): λ_{max} (nm) (ϵ) = 345 (13714), 360 (17918), 381 (18318). Fluorescence (DMF): λ_{max} (nm) = 410, 458, 500. Fluorescence quantum yield (DMF, reference Anthracene with $\Phi_{\text{f}} = 27\%$, $\lambda_{\text{excit.}} = 360$ nm) = 0.8%. MS (EI): m/z : 463.5 $[\text{M}+1]^+$. Anal. Calcd. for $\text{C}_{28}\text{H}_{18}\text{N}_2\text{O}_5$ (M_{w} , 462.5); C, 72.72; H, 3.92; N, 6.06. Found: C, 73.08 ; H, 4.02; N, 6.24.

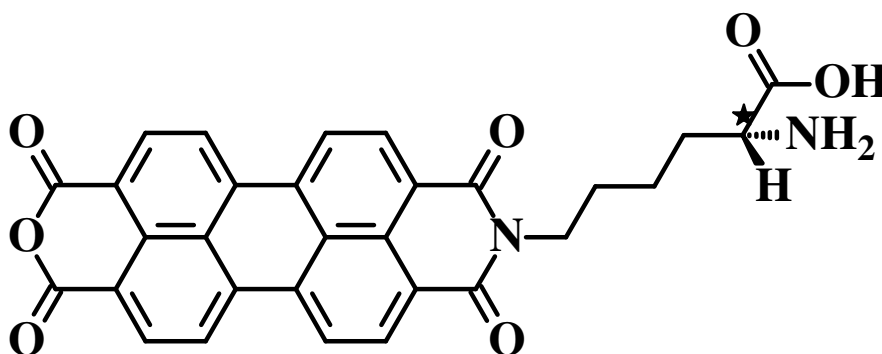
3.3.3 Synthesis of N-(4-hydroxyphenyl)-N'-[(S)-1-phenylethyl]-3,4,9,10-perylenetetracarboxydiimide (5a)



N-(4-hydroxyphenyl)-3,4,9,10-perylenetetracarboxylic-3,4-anhydride-9,10-imide (4a) (0.4 g, 0.8 mmol), (*S*)-(-)- α -methylbenzylamine (0.2 mL, 1.8 mmol) and isoquinoline (40 mL) were stirred under argon at 60 °C for 2h, at 80 °C for 3h, at 120 °C for 8h, at 160 °C for 10h, at 180 °C for 8h and at 200 °C for 18h. The warm solution was poured into methanol (300 mL). The precipitate was collected by vacuum filtration, washed with water and dried in vacuum at 100 °C. The crude product was extracted for 24h with methanol then ethanol in order to remove high boiling solvents and the unreacted reactants using a Soxhlet apparatus. Yield (0.45 g, 92%); black-brownish powder. R_f (silica gel, CHCl_3) = 0.25. $[\alpha]_D^{20}$: -24 (c 0.052, DMSO). FT-IR(KBr, cm^{-1}): ν = 3370, 3063, 3025, 2966, 2926, 1698, 1659, 1594, 1577, 1513, 1449, 1403, 1354, 1256, 1179, 1124, 960, 837, 810, 746, 697, 601, 531, 490, 430. ^1H NMR, δ_{H} (ppm) (400MHz, Pyridine- d_5) = 8.92-8.48 (m, 8 Ar-H, H-C(1), H-C(2), H-C(5), H-C(6), H-C(7), H-C(8), H-C(11), H-C(12)), 7.79-7.69 (m, 4 Ar-H, H-C(18), H-C(19), H-C(21), H-C(22)), 7.43-7.25 (m, 5 Ar-H, H-C(26), H-C(27), H-C(28), H-C(29), H-C(30)), 6.98 (s, 1 OH, HO-

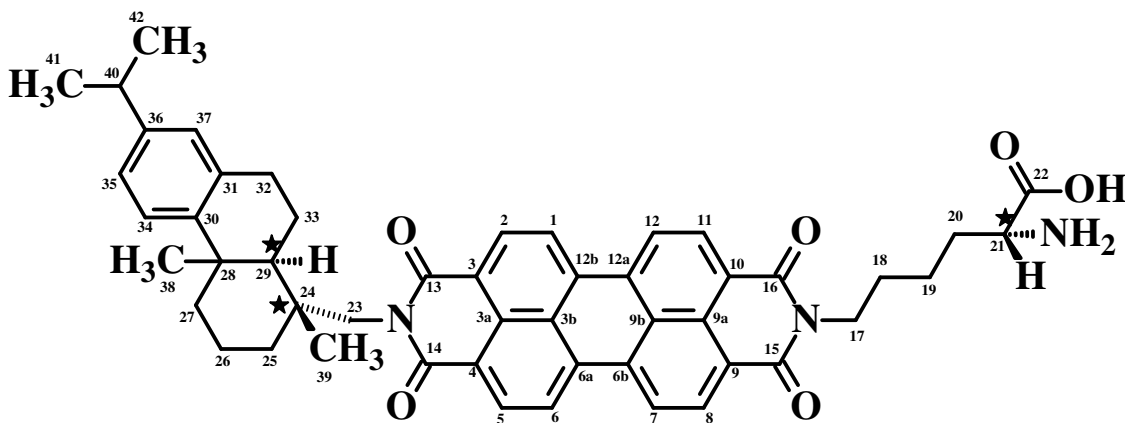
C(20)), 6.85-6.80 (q, $J = 7.1$, 1 CH, H-C(23)), 2.18-2.16 (d, $J = 6.8$, 1CH₃, H₃-C(24)). UV/Vis (DMF): λ_{max} (nm) (ϵ) = 459(40 606), 490 (58 465), 526 (70 000). Fluorescence (DMF): λ_{max} (nm) = 539, 580. Fluorescence quantum yield (DMF, reference N, N'-didodecy-3,4,9,10-perylenebis(dicarboxiimide) with $\Phi_f = 100\%$, $\lambda_{\text{excit.}} = 485$ nm) = 80%. MS (EI): m/z : 587.5 [M+1]⁺. Anal. Calcd. for C₃₈H₂₂N₂O₅ (M_w, 586.6); C, 77.81; H, 3.78; N, 4.78. Found: C, 77.52; H, 3.64; N, 4.43.

3.3.4 Synthesis of N-(2-aminohexanoic acid)-3,4,9,10 perylenetetracarboxylic-3,4-anhydride-9,10-imide (4b)



N-(2-aminohexanoic acid)-3,4,9,10 perylenetetracarboxylic-3,4-anhydride-9,10-imide was synthesized and purified according to the unpublished procedure (Refiker, unpublished article), and used for the synthesis of N-(2-aminohexanoic acid)-N'-(1-dehydroabietyl)-3,4,9,10 perylenetetracarboxydiimide.

3.3.5 Synthesis of N-(2-aminohexanoic acid)-N'-(1-dehydroabietyl)-3,4,9,10 perylenetetracarboxydiimide (5b)



N-(2-aminohexanoic acid)-3,4,9,10 perylenetetracarboxylic-3,4-anhydride-9,10-imide (1 g, 1.9 mmol), (+)-dehydroabietylamine (1.1 g, 3.8 mmol) and isoquinoline (40 mL) were stirred under argon at 60 °C for 6h, at 90 °C for 6h, at 125 °C for 9h, at 150 °C for 3h, at 180 °C for 12h and at 200 °C for 3h. The warm solution was poured into methanol (300 mL) and the precipitate was collected by vacuum filtration. The crude product was purified by crystallization from chloroform. Yield (1.44 g, 95%); bordeaux-red powder. $[\alpha]_D^{20}$: +200 (c 0.012, CHCl₃). FT-IR(KBr, cm⁻¹): ν = 3480, 3083, 2955, 2930, 2867, 1698, 1658, 1595, 1578, 1483, 1403, 1340, 1252, 1163, 856, 811, 748. ¹HNMR, δ_H (ppm) (400MHz, CDCl₃) = 8.52-8.48 (m, 8 Ar-H, H-C(1), H-C(2), H-C(5), H-C(6), H-C(7), H-C(8), H-C(11), H-C(12)), 7.06-6.87 (m, 3 Ar-H, H-C(34), H-C(35), H-C(37)), 4.22-4.18 (m, 1 CH₂, H₂-C(23)), 2.96 (m, 1 CH₂, H₂-C(32)), 2.75 (m, 1 CH, H-C(40)), 2.27-1.17 (m, 2 CH, H-C(21), H-C(29)); 8CH₂, H₂-C(17), H₂-C(18), H₂-C(19), H₂-C(20),

$\text{H}_2\text{-C}(25)$, $\text{H}_2\text{-C}(26)$, $\text{H}_2\text{-C}(27)$, $\text{H}_2\text{-C}(33)$), 1.15 (d, $J = 6.8$, 2CH_3 , $\text{H}_3\text{-C}(41)$, $\text{H}_3\text{-C}(42)$),
 1.02 (s, 1CH_3 , $\text{H}_3\text{-C}(38)$) , 0.80 (m, 1CH_3 , $\text{H}_3\text{-C}(39)$) . ^{13}C NMR, δ_{C} (ppm) (100MHz,
 CDCl_3): 164.3 (4 C=O, C(13), C(14) , C(15), C(16)), 163.2 (1 C=O, C(22)), 147.0 (1(C),
 C(30)), 145.8 (1(C), C(36)), 135.3 (1(C), C(31)), 134.1 (4 (C), C(3), C(4), C(9), C(10)),
 131.3 (4 (C), C(6a), C(6b), C(12a), C(12b)), 129.0 (2 (C), C(3b), C(9b)), 127.2 (1 Ar-
 CH, C(37)), 125.9 (2 (C), C(3a), C(9a)), 124.1 (1 Ar-CH, C(35)), 123.9 (1 Ar-CH,
 C(34)), 123.3 (4 Ar-CH, C(2), C(5), C(8), C(11)), 122.9 (4 Ar-CH, C(1), C(6), C(7),
 C(12)), 50.2 (1CH, C(21)), 46.7 (1CH, C(29)), 40.2 (2CH_2 , C(17), C(23)), 38.4 (1(C),
 C(24)), 38.1 (2CH_2 , C(18), C(32)), 37.7 (1(C), C(28)), 33.7 (1CH_3 , C(39)), 32.9 (1CH_2 ,
 C(27)), 30.7 (1CH, C(40)), 26.8 (1CH_3 , C(38)), 24.2 (2CH_3 , C(41), C(42)), 20.2 (1CH_2 ,
 C(20)), 19.9 (1CH_2 , C(25)), 19.5 (1CH_2 , C(19)), 19.2 (1CH_2 , C(26)), 18.9 (1CH_2 ,
 C(33)). UV/Vis (CHCl_3): λ_{max} (nm) (ϵ) = 465 (32 866), 490 (61 533), 526 (65 695) .
 Fluorescence (CHCl_3): λ_{max} (nm) = 535, 576, 621. Fluorescence quantum yield (CHCl_3 ,
 reference N, N'-didodecyl-3,4,9,10-perylenebis(dicarboxiimide) with $\Phi_{\text{f}} = 100\%$, $\lambda_{\text{excit.}} =$
 485 nm) = 40%. Anal. Calcd. for $\text{C}_{50}\text{H}_{49}\text{N}_3\text{O}_6$ (M_{w} , 788.0); C, 76.2; H, 6.3; N, 5.3.
 Found: C, 76.1; H, 6.1; N, 5.2.

CHAPTER 4

DATA AND CALCULATIONS

4.1 Optical Properties

4.1.1 Maximum Extinction Coefficients (ϵ_{\max})

The maximum extinction coefficient is a measurement of how strongly a chemical species absorbs light at a given wavelength. It is an intrinsic property of the species; the actual absorbance, A , of a sample is dependent on the pathlength (l) and the concentration (c) of the species via the Beer-Lambert law,

$$A = \epsilon_{\max}cl \quad (4.1)$$

where,

A = absorbance

ϵ_{\max} = molar extinction coefficient at the selected absorption wavelength ($\text{L mol}^{-1} \text{cm}^{-1}$)

c = concentration (mol L^{-1})

l = pathlength (cm)

Table 4.1: Extinction coefficients^a of compounds **1a**, **2a**, **5a** and **5b**.

Compound	λ (nm)	A	ϵ_{\max} (L mol ⁻¹ cm ⁻¹)
1a	356	0.11732	11 732
2a	345	0.13714	13 714
	360	0.17918	17 918
	381	0.18318	18 318
5a	459	0.40606	40 606
	490	0.58465	58 465
	526	0.70000	70 000
5b	465	0.32866	32 866
	490	0.61533	61 533
	526	0.65695	65 695

^a $c = 1 \times 10^{-5}$, $l = 1$ cm

4.1.2 Fluorescence Quantum Yields (Φ_f)

When a fluorophore absorbs a photon of light, an energetically excited state is formed. The fate of this species is varied, depending upon the exact nature of the fluorophore and its surroundings, but the end result is deactivation (loss of energy) and return to the ground state.

The fluorescence quantum yield (Φ_f) is the ratio of photons absorbed to photons emitted through fluorescence. In other words the quantum yield gives the probability of the excited state being deactivated by fluorescence rather than by another, non-radiative mechanism.

The most reliable method for recording Φ_f is the comparative method which involves the use of well characterised standard samples with known Φ_f values. Essentially, solutions of the standard and test samples with identical absorbance at the same excitation wavelength can be assumed to be absorbing the same number of photons. Hence, a simple ratio of the integrated fluorescence intensities of the two solutions (recorded under identical conditions) will yield the ratio of the quantum yield values. Since Φ_f for the standard sample is known, it is trivial to calculate the Φ_f for the test sample.

The quantum yield of the unknown relative to the standard is the ratio of the integrated band areas under the two fluorescence spectra (plotted on a frequency scale) after they have been corrected for the detector response function. Multiplying by the known quantum yield of the standard then gives the absolute quantum yield of the unknown.

$$\Phi_u = \frac{A_s}{A_u} \times \frac{S_u}{S_s} \times \left[\frac{n_u}{n_s} \right]^2 \times \Phi_s \quad (4.2)$$

where,

Φ_u = quantum yield of the unknown

Φ_s = quantum yield of the standard

A_s = absorbance of the standard

A_u = absorbance of the unknown

S_u = integral emission area across the unknown band

S_s = integral emission area across the standard band

n_u = refractive index for the solvent of unknown

n_s = refractive index for the solvent of standard

The emission spectra of compounds **1a** and **2a** were taken at $\lambda_{exc} = 360$ nm and the relative fluorescence quantum yields were determined by using anthracene with a $\Phi_f = 27\%$ as standard in EtOH ($n_s = 1.3611$). The emission spectra of **5a** and **5b** were taken at $\lambda_{exc} = 485$ nm and the relative fluorescence quantum yields were determined by using N, N'-didodecy-3,4,9,10-perylenebis(dicarboxiimide) with a $\Phi_f = 100\%$ as standard in $CHCl_3$ ($n_s = 1.4459$).

Table 4.2: Fluorescence quantum yield data of compounds **1a**, **2a**, **5a** and **5b**.

Compound	Solvent	n_u	A_u	S_u	A_s	S_s	Φ_f
1a	DMF	1.4305	0.1065	247.65	0.1020	35368	0.002
2a	DMF	1.4305	0.1051	988.81	0.1005	35249	0.008
5a	DMF	1.4305	0.0993	10120	0.1010	12594	0.80
5b	CHCl ₃	1.4459	0.1002	4790.5	0.1073	12825	0.40

4.1.3 Singlet Energies (E_s)

Singlet energies were calculated using the equation 4.3 shown below (Turro, 1965).

$$E_s = \frac{2.86 \times 10^5}{\lambda_{\max}} \quad (4.3)$$

where,

E_s = singlet energy (kcal mol⁻¹)

λ_{\max} = maximum absorption wavelength (Å)

Table 4.3: Singlet energies of compounds **1a**, **2a**, **5a** and **5b**.

Compound	λ_{\max} (Å)	E_s (kcal mol ⁻¹)
1a	3560	80.3
2a	3810	75.1
5a	5260	54.4
5b	5260	54.4

4.1.4 Oscillator Strengths (f)

Oscillator strengths were calculated using the equation 4.4 shown below (Turro, 1965).

$$f = 4.32 \times 10^{-9} \Delta\bar{\nu}_{1/2} \epsilon_{\max} \quad (4.4)$$

where,

f = oscillator strength

$\Delta\bar{\nu}_{1/2}$ = the half-width of the selected absorption (cm^{-1})

ϵ_{\max} = molar extinction coefficient at the selected absorption wavelength ($\text{L mol}^{-1} \text{cm}^{-1}$)

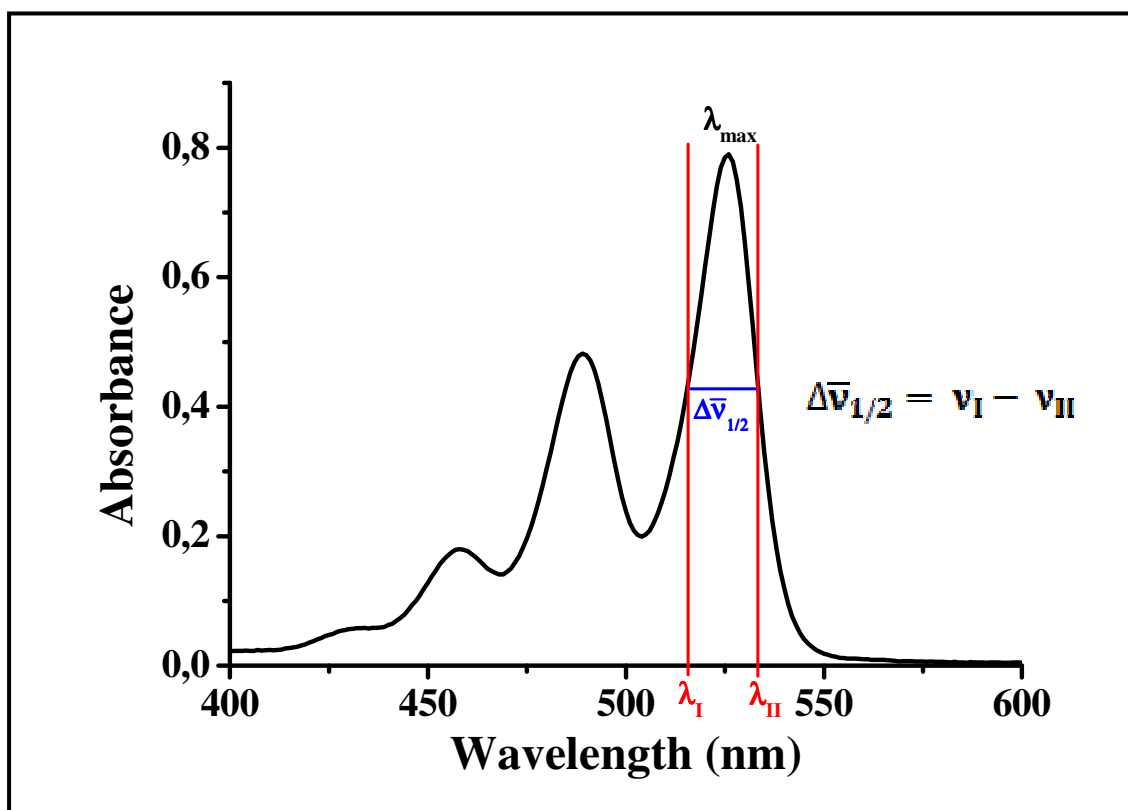


Figure 4.1: A representative absorption spectrum for half-width calculation.

Table 4.4: Oscillator strengths of compounds **1a**, **2a**, **5a** and **5b**.

Compound	$\Delta\bar{\nu}_{1/2}$ (cm ⁻¹)	ϵ_{\max} (L mol ⁻¹ cm ⁻¹)	f
1a	7180.31	11 732	0.4
2a	7649.10	18 318	0.6
5a	1302.75	70 000	0.4
5b	1356.61	65 695	0.4

4.1.5 Theoretical Radiative Lifetimes (τ_0)

Theoretical radiative lifetimes were calculated using the equation 4.5 shown below (Turro, 1965).

$$\tau_0 = \frac{3.5 \times 10^8}{\bar{\nu}_{\max}^2 \cdot \epsilon_{\max} \cdot \Delta\bar{\nu}_{1/2}} \quad (4.5)$$

where,

τ_0 = radiative lifetime (s)

ϵ_{\max} = molar extinction coefficient at the selected absorption wavelength (L mol⁻¹ cm⁻¹)

$\bar{\nu}_{\max}$ = mean frequency for the absorption band (cm⁻¹)

$\Delta\bar{\nu}_{1/2}$ = the half-width of the selected absorption (cm⁻¹)

Table 4.5: Theoretical radiative lifetimes of compounds **1a**, **2a**, **5a** and **5b**.

Compound	$\Delta\bar{\nu}_{1/2}$ (cm ⁻¹)	ϵ_{\max} (L mol ⁻¹ cm ⁻¹)	$\bar{\nu}_{\max}$ (cm ⁻¹)	τ_0 (ns)
1a	7180.31	11 732	28089.89	5.3
2a	7649.10	18 318	26246.72	3.6
5a	1302.75	70 000	19011.41	10.6
5b	1356.61	65 695	19011.41	10.9

4.1.6 Theoretical Fluorescence Lifetimes (τ_f)

Theoretical fluorescence lifetimes were calculated using the equation 4.6 shown below (Turro, 1965).

$$\tau_f = \tau_0 \times \Phi_f \quad (4.6)$$

where,

τ_f = fluorescence lifetime (ns)

τ_0 = radiative lifetime (ns)

Φ_f = fluorescence quantum yield

Table 4.6: Theoretical fluorescence lifetimes of compounds **1a**, **2a**, **5a** and **5b**.

Compound	τ_0 (ns)	Φ_f	τ_f (ns)
1a	5.3	0.002	0.01
2a	3.6	0.008	0.03
5a	10.6	0.80	8.48
5b	10.9	0.40	4.35

4.1.7 Fluorescence Rate Constants (k_f)

Fluorescence rate constants were calculated using the equation 4.7 shown below.

$$k_f = \frac{1}{\tau_0} \quad (4.7)$$

where,

k_f = fluorescence rate constant (s^{-1})

τ_0 = radiative lifetime (s)

Table 4.7: Fluorescence rate constants of compounds **1a**, **2a**, **5a** and **5b**.

Compound	τ_0 (ns)	k_f ($10^8 s^{-1}$)
1a	5.3	1.9
2a	3.6	2.8
5a	10.6	0.9
5b	10.9	0.9

4.1.8 Rate Constants of Radiationless Deactivation (k_d)

Rate constants of radiationless deactivation were calculated using the equation 4.8 shown below.

$$k_d = \left(\frac{k_f}{\Phi_f} \right) - k_f \quad (4.8)$$

where,

k_d = rate constant of radiationless deactivation (s^{-1})

k_f = fluorescence rate constant (s^{-1})

Φ_f = fluorescence quantum yield

Table 4.8: Rate constants of radiationless deactivation of compounds **1a**, **2a**, **5a** and **5b**.

Compound	$k_f (10^8 s^{-1})$	Φ_f	$k_d (10^8 s^{-1})$
1a	1.9	0.002	948
2a	2.8	0.008	341
5a	0.9	0.80	0.2
5b	0.9	0.40	1.3

4.2 Chiroptical Properties

Chiroptical properties of synthesized chiral compounds were studied using circular dichroism spectroscopy. Circular dichroism (CD) is defined as the differential absorbance of left circularly polarized light (LCPL) and right circularly polarized light (RCPL): $CD = Abs(LCPL) - Abs(RCPL)$. Current CD spectrometers measure CD in terms of ellipticity Θ , usually expressed in millidegrees and literature data are usually reported in molar ellipticity $[\Theta]$:

$$[\Theta] = \frac{(\Theta \times M)}{(c \times l \times 10000)} \quad (4.9)$$

where,

Θ = ellipticity (mdeg)

M = molecular weight (g/mole)

c = concentration (g/mL)

l = the cell path (cm)

4.3 Thermal Properties

The thermal behavior of all compounds was investigated by DSC (heating rate 10 K min⁻¹) and TGA (heating rate 5 K min⁻¹).

4.4 Electrochemical Properties

The electrochemical characterization of all compounds were studied in detail using cyclic and square-wave voltammetries in different solvents containing 0.1 M TBAPF₆ as a supporting electrolyte and in solid state.

All redox potentials, HOMO (highest occupied molecular orbital), LUMO (lowest unoccupied molecular orbital) and band gap energies (E_g) were calculated from cyclic voltammograms.

4.4.1 Redox Potentials ($E_{1/2}$)

For reversible processes, reduction potentials can be calculated from cyclic voltammograms according to internal reference by using the following equation 4.10 (Brad A. J., 1980).

$$E_{1/2} = \frac{E_{pc} + E_{pa}}{2} \quad (4.10)$$

where,

$E_{1/2}$ = half-wave potential (V)

E_{pc} = cathodic peak potential (V)

E_{pa} = anodic peak potential (V)

The separation between the peak potentials (for a reversible couple) is given by equation 4.11, where n is the number of electrons.

$$\Delta E_p = E_{pa} - E_{pc} = \frac{0.059}{n} V \quad (4.11)$$

Thus, the peak separation can be used to determine the number of electrons transferred.

Accordingly, a fast one-electron process exhibits a ΔE_p of about 59 mV.

Table 4.9: Cyclic^a voltammetry data of compounds **1a**, **2a** and **5a**.

Compound	E_{pc}/V	E_{pa}/V	$\Delta E_p/mV$	$E_{1/2}/V$ vs. Ag/AgNO ₃	E_{Fc}/V vs. Ag/AgNO ₃	$E_{1/2}/V$ vs. Fc
1a^b (CH ₂ Cl ₂)	-0.729	-0.662	67	-0.695	0.172	-0.867
	-1.157	-1.097	60	-1.127	0.172	-1.299
2a^b (CHCl ₃)	-0.825	-0.728	97	-0.776	0.234	-1.010
	-1.226	-1.127	99	-1.176	0.234	-1.411
5a^b (CHCl ₃)	-0.865	-0.789	76	-0.827	0.196	-1.023
	-1.054	-0.982	72	-1.018	0.196	-1.214
5a^c	-0.244	-0.378	134	-0.311 ^d	0.360 ^d	-0.671

(solid state)

^a Scan rate of 100 mV s⁻¹.

^b Supporting electrolyte: 0.1 M tetrabutylammonium hexafluorophosphate (TBAPF₆).

^c Supporting electrolyte: 1 M HCl.

^d vs. Ag/AgCl

4.4.2 Lowest Unoccupied Molecular Orbital (LUMO)

In order to calculate the absolute energies of LUMO level with respect to the vacuum level, the redox data are standardized to the ferrocene/ferricenium couple which has a calculated absolute energy of -4.8 eV (Bredas, 1983; Peng, 1998).

$$E_{\text{LUMO}} = - (4.8 + E_{1/2}) \quad (4.12)$$

where,

E_{LUMO} = energy of LUMO level (eV)

$E_{1/2}$ = half-wave potential (V)

Table 4.10: LUMO values of compounds **1a**, **2a** and **5a**.

Compound	$E_{1/2}$ / V vs. Fc	LUMO / eV
1a (CH ₂ Cl ₂)	-0.867	-3.93
2a (CHCl ₃)	-1.010	-3.79
5a (CHCl ₃)	-1.023	-3.78
5a (solid state)	-0.671	-4.13

4.4.3 Band Gap Energy (E_g)

The optical band gap values were calculated using the equation 4.13 shown below.

$$E_g = \frac{1240 \text{ eV nm}}{\lambda} \quad (4.13)$$

where,

E_g = band gap energy (eV)

λ = cut-off wavelength of the absorption band (nm)

Table 4.11: The optical band gap values of compounds **1a**, **2a** and **5a**.

Compound	λ (nm)	E_g / eV
1a (CH ₂ Cl ₂)	386	3.21
2a (CHCl ₃)	394	3.15
5a (CHCl ₃)	544	2.28
5a (solid state)	646	1.92

4.4.4 Highest Occupied Molecular Orbital (HOMO)

Highest occupied molecular orbital energy levels were calculated using the equation 4.14 shown below.

$$E_{\text{HOMO}} = E_{\text{LUMO}} - E_{\text{g}} \quad (4.14)$$

where,

E_{HOMO} = energy of HOMO level (eV)

E_{LUMO} = energy of LUMO level (eV)

E_{g} = band gap energy (eV)

Table 4.12: HOMO values of compounds **1a**, **2a** and **5a**.

Compound	LUMO / eV	E_{g} / eV	HOMO / eV
1a (CH ₂ Cl ₂)	-3.93	3.21	-7.14
2a (CHCl ₃)	-3.79	3.15	-6.94
5a (CHCl ₃)	-3.78	2.28	-6.06
5a (solid state)	-4.13	1.92	-6.05

4.4.5 Diffusion Coefficients (D)

The peak current for a reversible couple (at 25 °C) is given by the Randles-Sevcik equation:

$$i_p = (2.69 \times 10^5) n^{3/2} v^{1/2} D^{1/2} A C \quad (4.15)$$

where,

i_p = peak current (A)

n = number of transferred electrons

v = scan rate ($V s^{-1}$)

D = diffusion coefficient ($cm^2 s^{-1}$)

A = electrode area (cm^2)

C = concentration of the electroactive species ($mol cm^{-3}$)

Accordingly, the current is directly proportional to concentration and increases with the square root of the scan rate. Such dependence on the scan rate is indicative of electrode reaction controlled by mass transport (semiinfinite linear diffusion). The reverse-to-forward peak current ratio is unity for a simple reversible couple. Diffusion coefficients were calculated from the slope of the linear plot of i_p vs. $v^{1/2}$ using the equation 4.15 (Bard, 1980).

Table 4.13: Cyclic^a voltammetry data of compound **1a** in CH₃CN at different scan rates.

Scan Rate (mVs ⁻¹)	E _{pc} (V)	E _{pa} (V)	ΔE _p (mV)	i _{pc} (μA)	i _{pa} (μA)	i _{pa} /i _{pc}
50	-0.826	-0.749	77	0.55	0.55	1.00
	-1.242	-1.177	65			
100	-0.824	-0.756	68	0.80	0.80	1.00
	-1.239	-1.171	68			
200	-0.826	-0.754	72	1.20	1.20	1.00
	-1.240	-1.170	70			
300	-0.826	-0.754	72	1.67	1.68	1.01
	-1.240	-1.170	70			

^a supporting electrolyte: TBAPF₆Table 4.14: Cyclic^a voltammetry data of compound **1a** in CH₂Cl₂ at different scan rates.

Scan Rate (mVs ⁻¹)	E _{pc} (V)	E _{pa} (V)	ΔE _p (mV)	i _{pc} (μA)	i _{pa} (μA)	i _{pa} /i _{pc}
50	-0.736	-0.658	78	0.29	0.29	1.00
	-1.157	-1.097	60			
100	-0.729	-0.662	67	0.44	0.44	1.00
	-1.157	-1.097	60			
200	-0.729	-0.660	69	0.69	0.69	1.00
	-1.157	-1.098	59			
300	-0.730	-0.660	70	0.94	0.94	1.00
	-1.157	-1.098	59			

^a supporting electrolyte: TBAPF₆

Table 4.15: Cyclic^a voltammetry data of compound **2a** at different scan rates.

Scan Rate (mVs ⁻¹)	E _{pc} (V)	E _{pa} (V)	ΔE _p (mV)	i _{pc} (μA)	i _{pa} (μA)	i _{pa} /i _{pc}
50^b	-0.820	-0.734	86	2.46	2.45	1.00
	-1.219	-1.132	87			
100^b	-0.825	-0.728	97	3.41	3.42	1.00
	-1.226	-1.127	99			
200^b	-0.834	-0.720	114	4.90	4.82	0.98
	-1.234	-1.120	114			
50^c	-0.914	-0.839	75	2.17	2.18	1.00
	-1.369	-1.294	75			

^a supporting electrolyte: TBAPF₆^b in chloroform^c in DMSOTable 4.16: Cyclic^a voltammetry data of compound **5a** in CHCl₃ at different scan rates.

Scan Rate (mVs ⁻¹)	E _{pc} (V)	E _{pa} (V)	ΔE _p (mV)	i _{pc} (μA)	i _{pa} (μA)	i _{pa} /i _{pc}
50	-0.862	-0.792	70	2.87	2.76	0.96
	-1.053	-0.980	73			
100	-0.865	-0.789	76	4.19	4.19	1.00
	-1.054	-0.982	72			
300	-0.868	-0.786	82	8.74	8.74	1.00
	-1.058	-0.980	78			
600	-0.872	-0.781	91	14.3	14.2	0.99
	-1.065	-0.976	89			
800	-0.874	-0.777	97	17.4	17.4	1.00
	-1.070	-0.974	96			
1000	-0.877	-0.774	103	21.5	21.4	1.00
	-1.072	-0.969	103			

^a supporting electrolyte: TBAPF₆

Table 4.17: Solid state cyclic^a voltammetry data of compound **5a** at different scan rates.

Scan Rate (mVs ⁻¹)	E _{pc} (V)	E _{pa} (V)	ΔE _p (mV)	i _{pc} (μA)	i _{pa} (μA)	i _{pa} /i _{pc}
25	-0.259	-0.396	137	0.834	0.834	1.00
50	-0.253	-0.388	135	1.95	1.95	1.00
100	-0.244	-0.378	134	10.4	10.4	1.00
200	-0.236	-0.380	144	17.2	17.2	1.00
400	-0.232	-0.386	154	28.8	28.8	1.00
600	-0.224	-0.388	164	31.4	31.4	1.00

^a supporting electrolyte: HCl

Table 4.18: Diffusion coefficients^a of compounds **1a**, **2a** and **5a**.

Compound	Slope ² of i _p vs. v ^{1/2} (A ² s V ⁻¹)	D (cm ² s ⁻¹)
1a (CH ₂ Cl ₂)	3.9778 x 10 ⁻¹²	8.73 x 10 ⁻⁸
1a (CH ₃ CN)	1.1597 x 10 ⁻¹¹	2.55 x 10 ⁻⁷
2a (CHCl ₃)	1.1974 x 10 ⁻¹⁰	2.63 x 10 ⁻⁶
5a (CHCl ₃)	5.5126 x 10 ⁻¹⁰	1.21 x 10 ⁻⁵
5a (solid state)	2.8893 x 10 ⁻⁹	1.62 x 10 ⁻⁶

^a A = 0.196 cm², C = 1 x 10⁻⁷ mol cm⁻³, n = 4

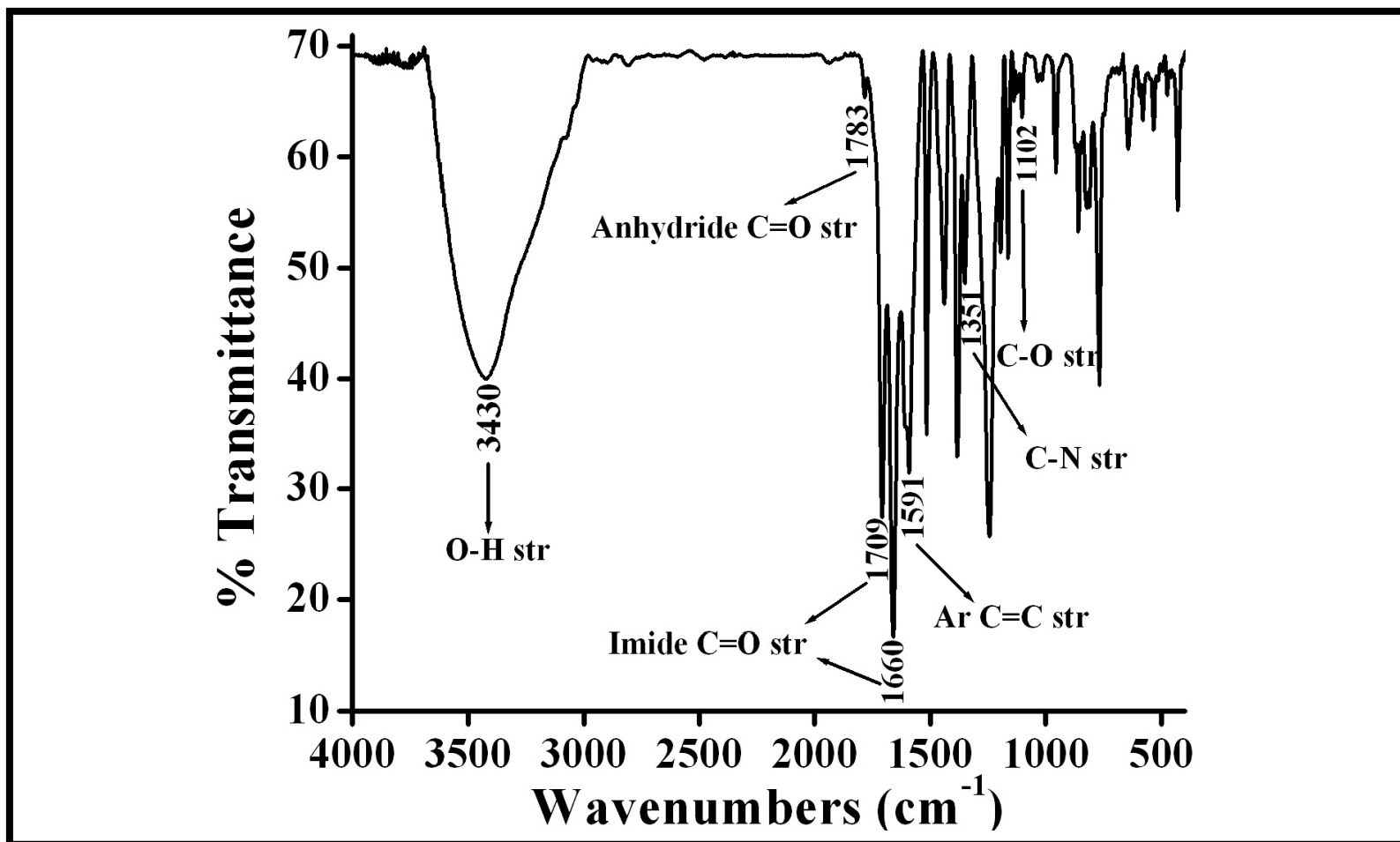


Figure 4.2: FT-IR spectrum of N-(4-hydroxyphenyl)-1,4,5,8-naphthalenetetracarboxylic-1,8-anhydride-4,5-imide (**1a**).

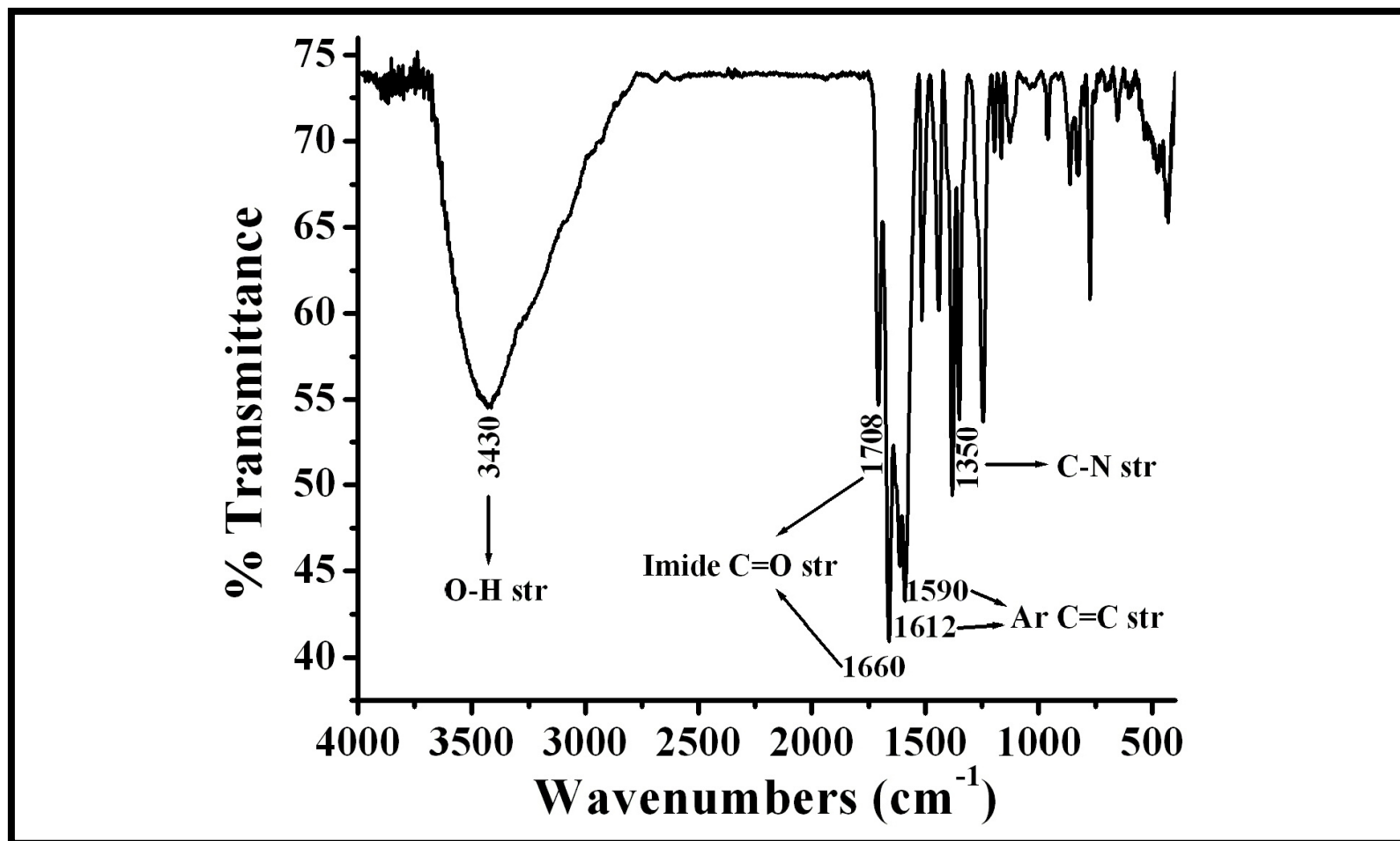


Figure 4.3: FT-IR spectrum of N-(4-hydroxyphenyl)-N'-[(S)-1-phenylethyl]-1,4,5,8-naphthalenetetracarboxydiimide (**2a**).

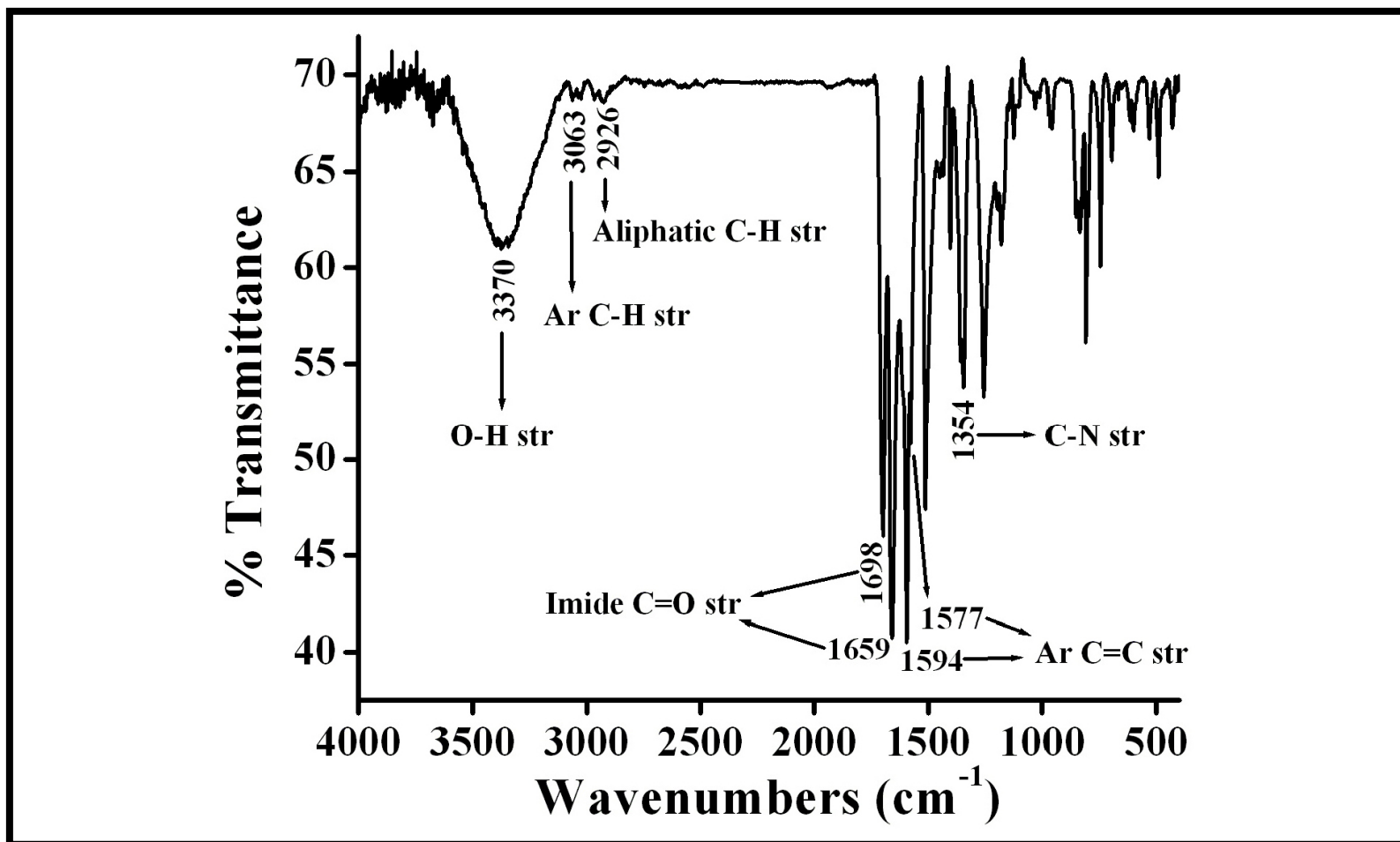


Figure 4.4: FT-IR spectrum of N-(4-hydroxyphenyl)-N'-[(S)-1-phenylethyl]-3,4,9,10-perylenetetracarboxydiimide (**5a**).

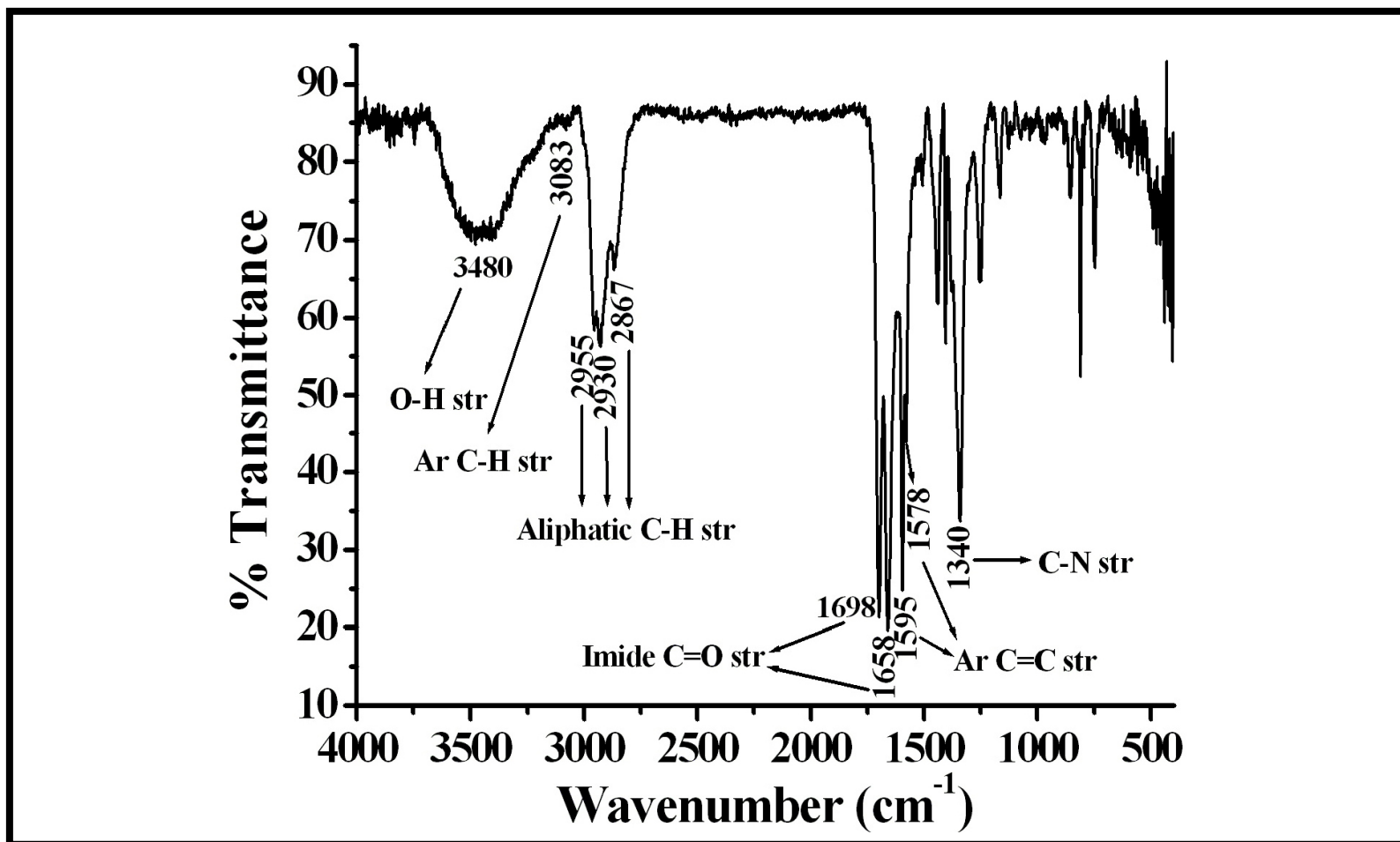


Figure 4.5: FT-IR spectrum of N-(2-aminohexanoic acid)-N'-(1-dehydroabietyl)-3,4,9,10 perylenetetracarboxydiimide (5b).

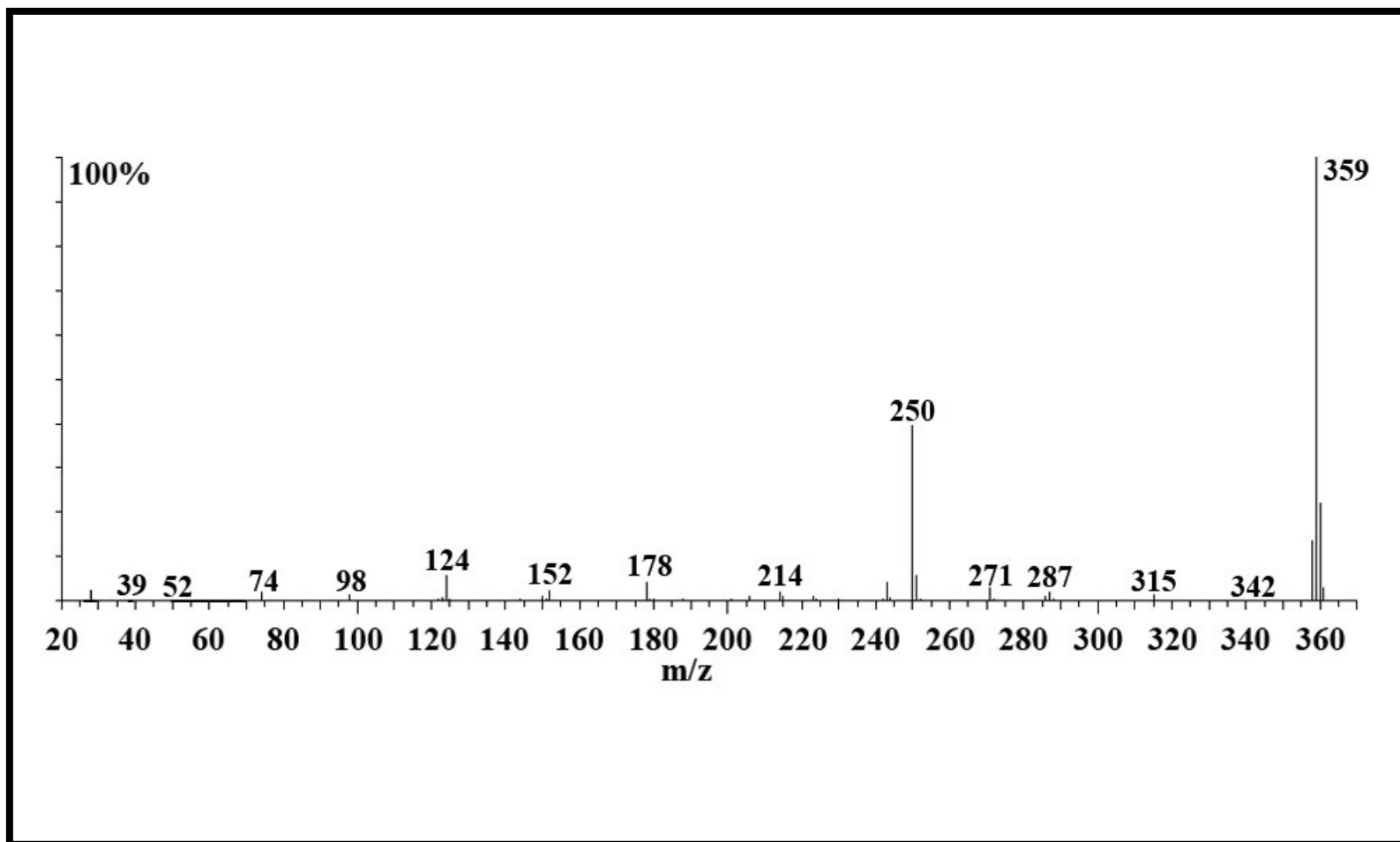


Figure 4.6: Mass spectrum of N-(4-hydroxyphenyl)-1,4,5,8-naphthalenetetracarboxylic-1,8-anhydride-4,5-imide (**1a**).

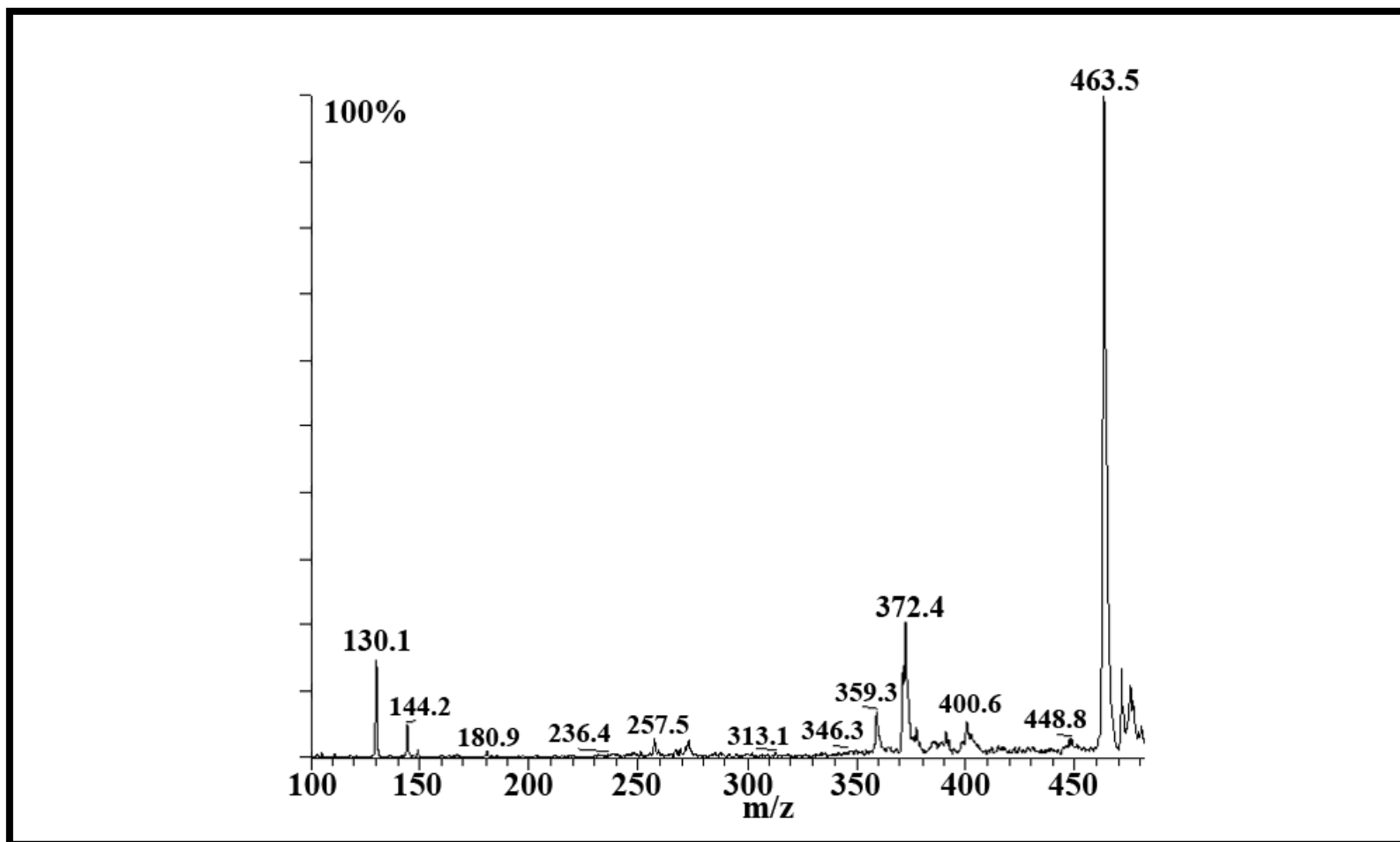


Figure 4.7: Mass spectrum of N-(4-hydroxyphenyl)-N'-[(S)-1-phenylethyl]-1,4,5,8-naphthalenetetracarboxydiimide (**2a**).

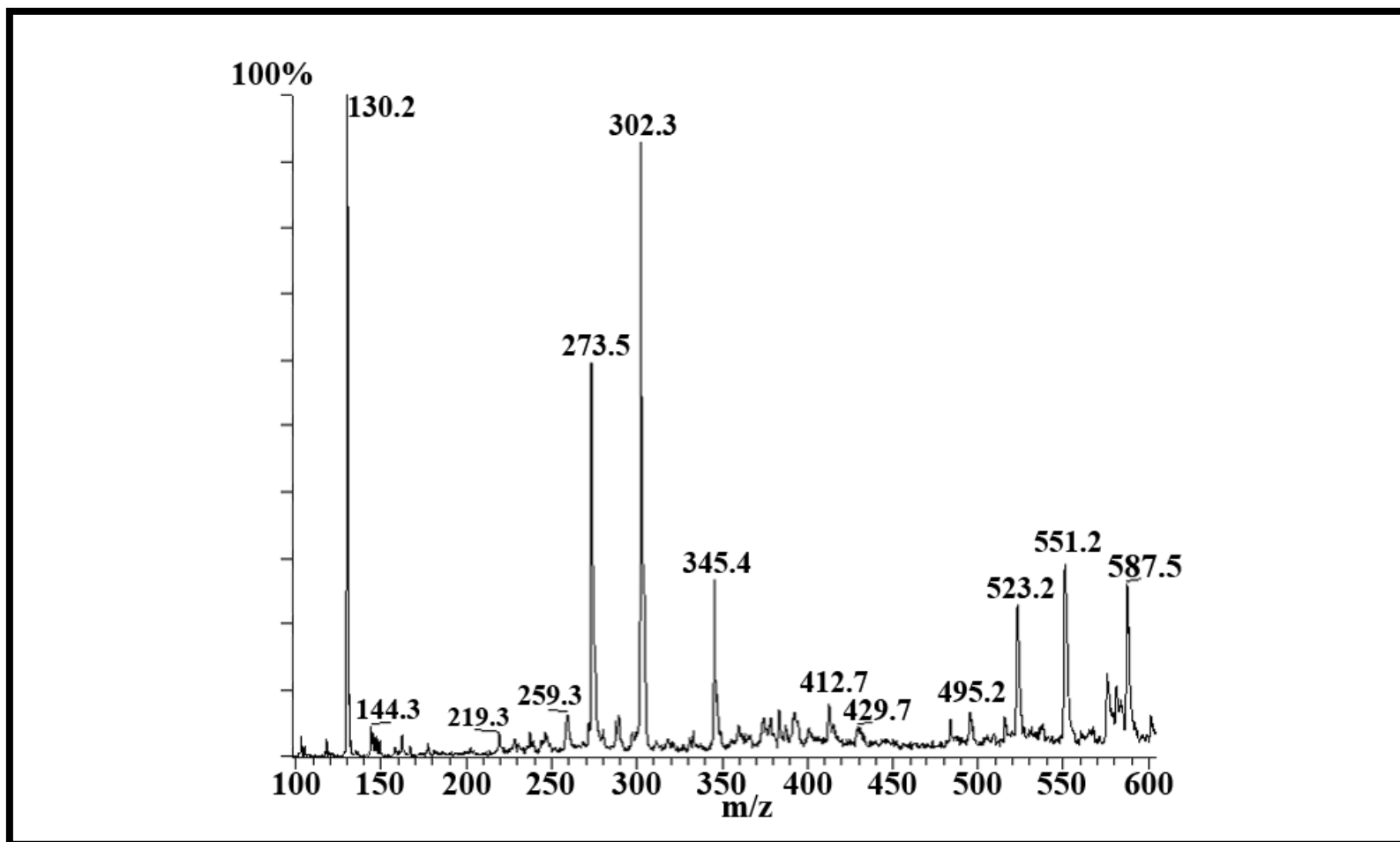


Figure 4.8: Mass spectrum of N-(4-hydroxyphenyl)-N'-[(S)-1-phenylethyl]-3,4,9,10-perylenetetracarboxydiimide (**5a**).

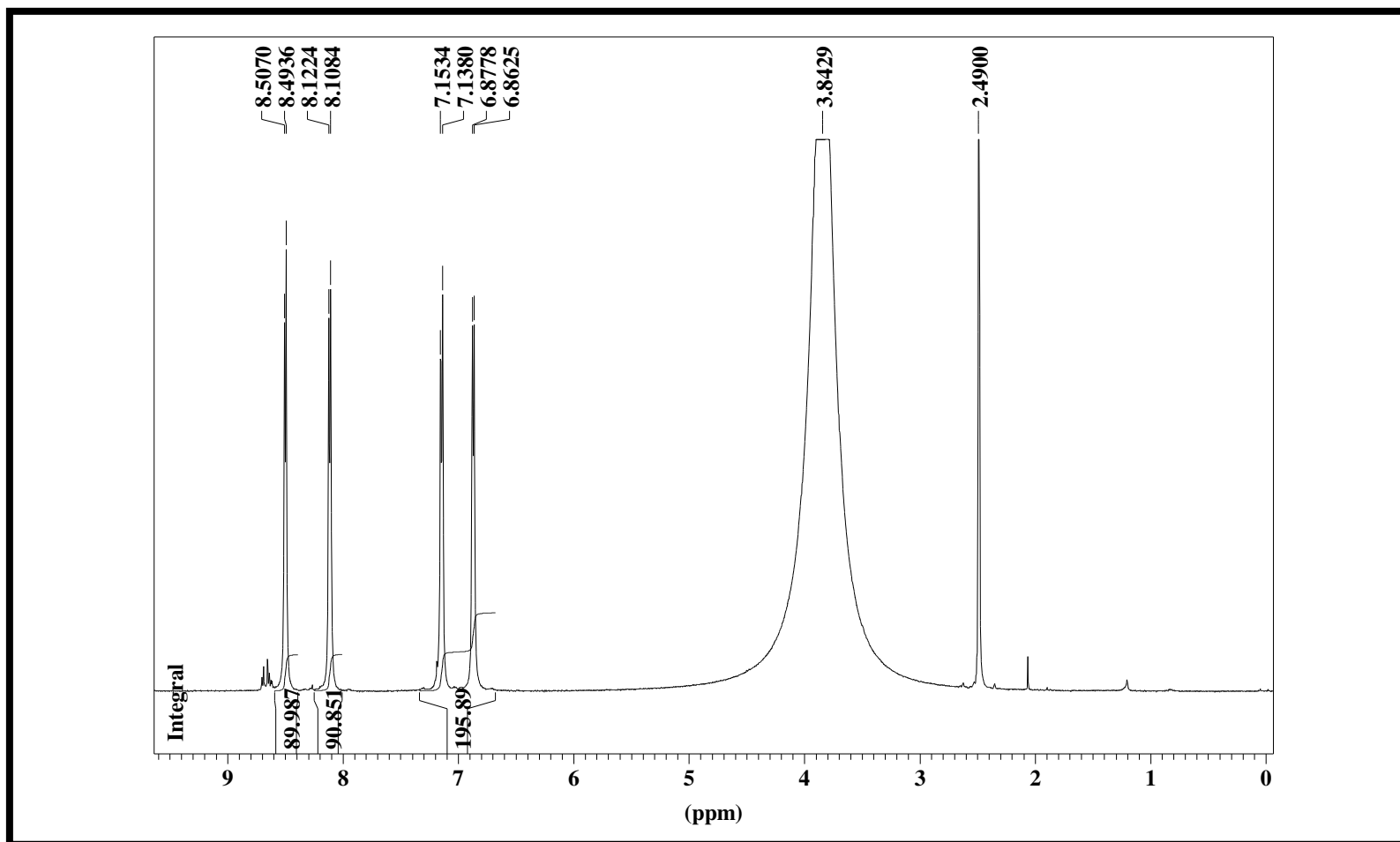


Figure 4.9: ¹H-NMR spectrum of N-(4-hydroxyphenyl)-1,4,5,8-naphthalenetetracarboxylic-1,8-anhydride-4,5-imide (**1a**).

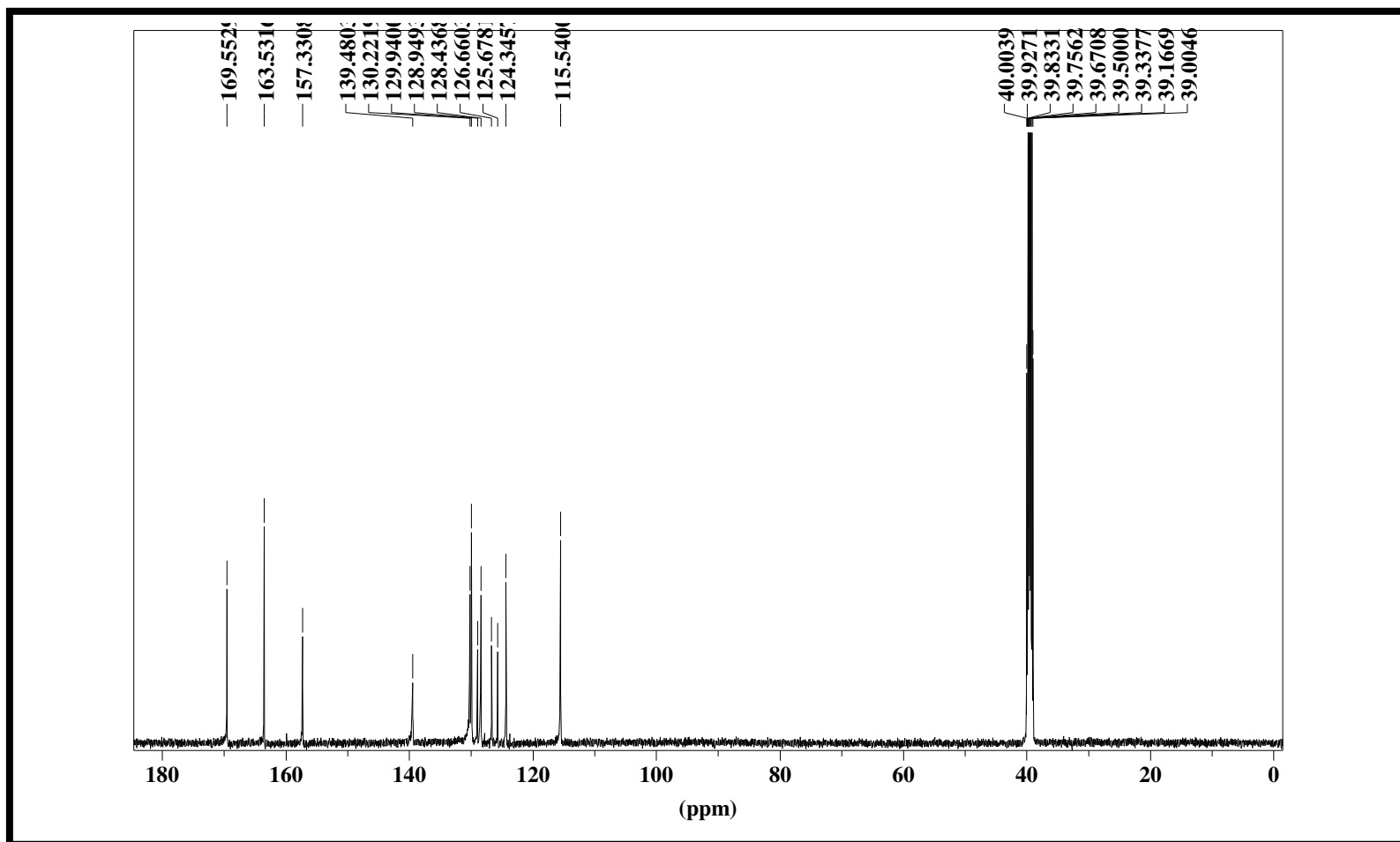


Figure 4.10: ^{13}C -NMR spectrum of N-(4-hydroxyphenyl)-1,4,5,8-naphthalenetetracarboxylic-1,8-anhydride-4,5-imide (**1a**).

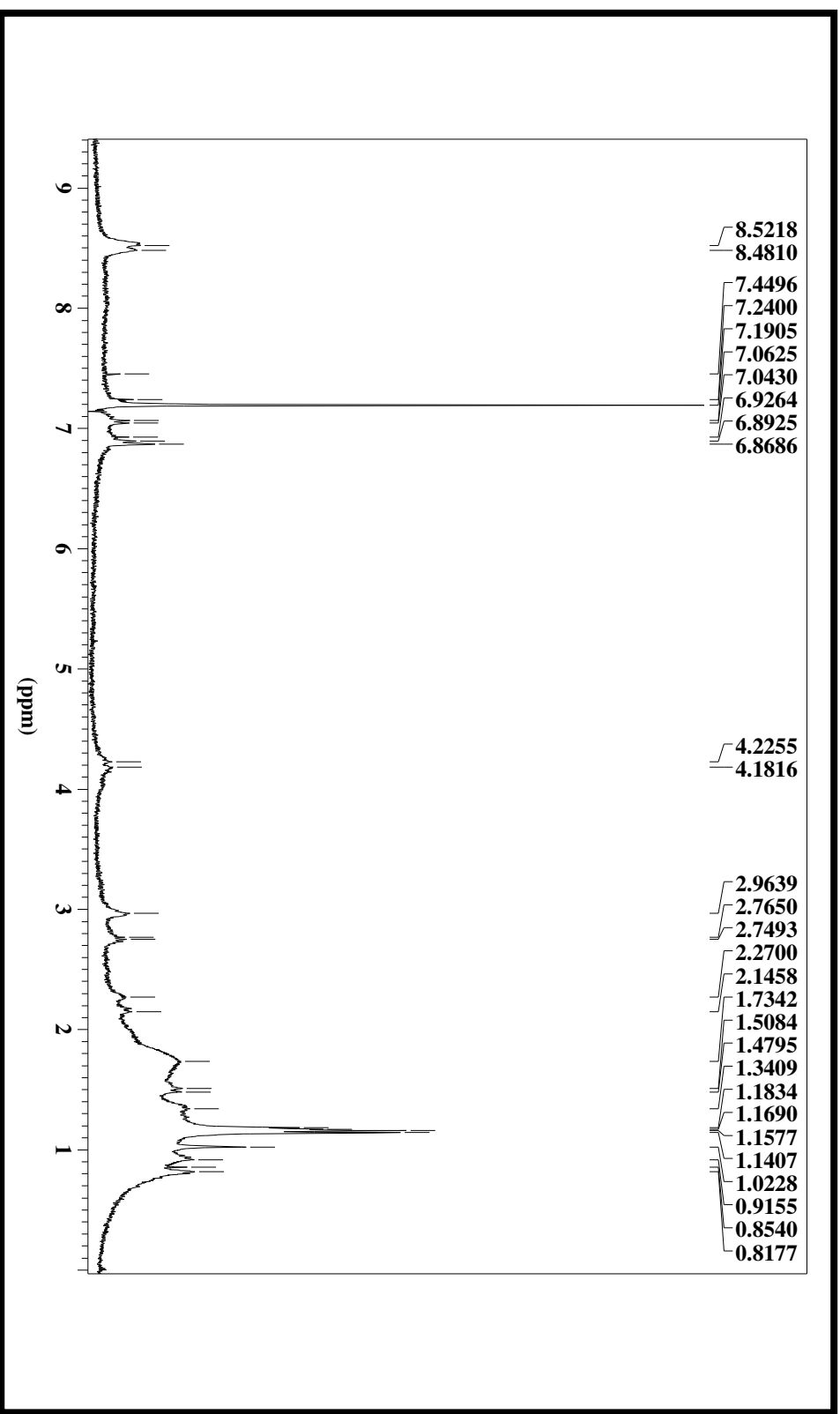


Figure 4.11: ¹H-NMR spectrum of N-(2-aminohexanoic acid)-N'-(1-dehydroabietyl)-3,4,9,10-perylene-tetracarboxydiimide (5b).

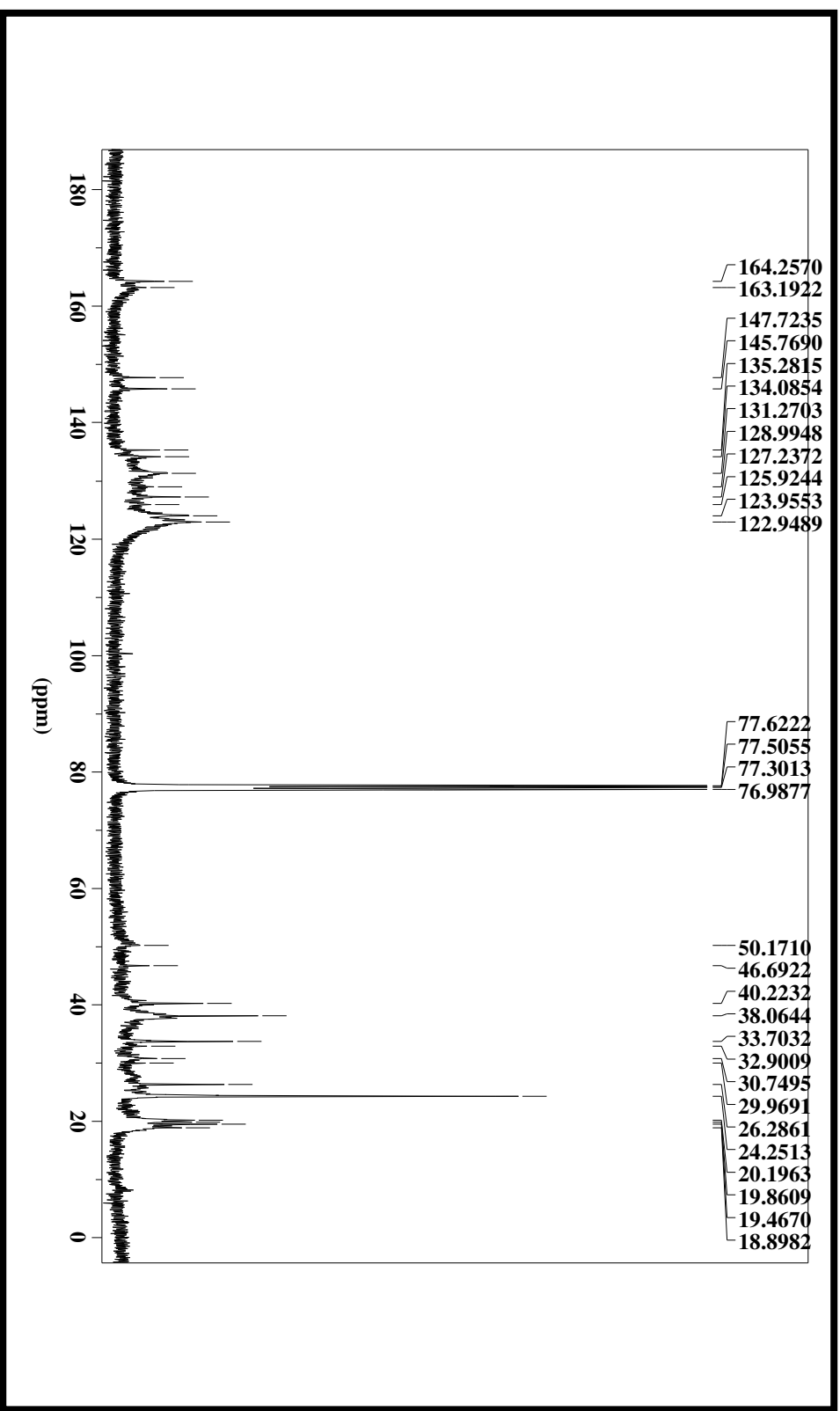


Figure 4.12: ^{13}C -NMR spectrum of N-(2-aminohexanoic acid)-N'-(1-dehydroabietyl)-3,4,9,10 perylenetetracarboxyldiimide (5b).

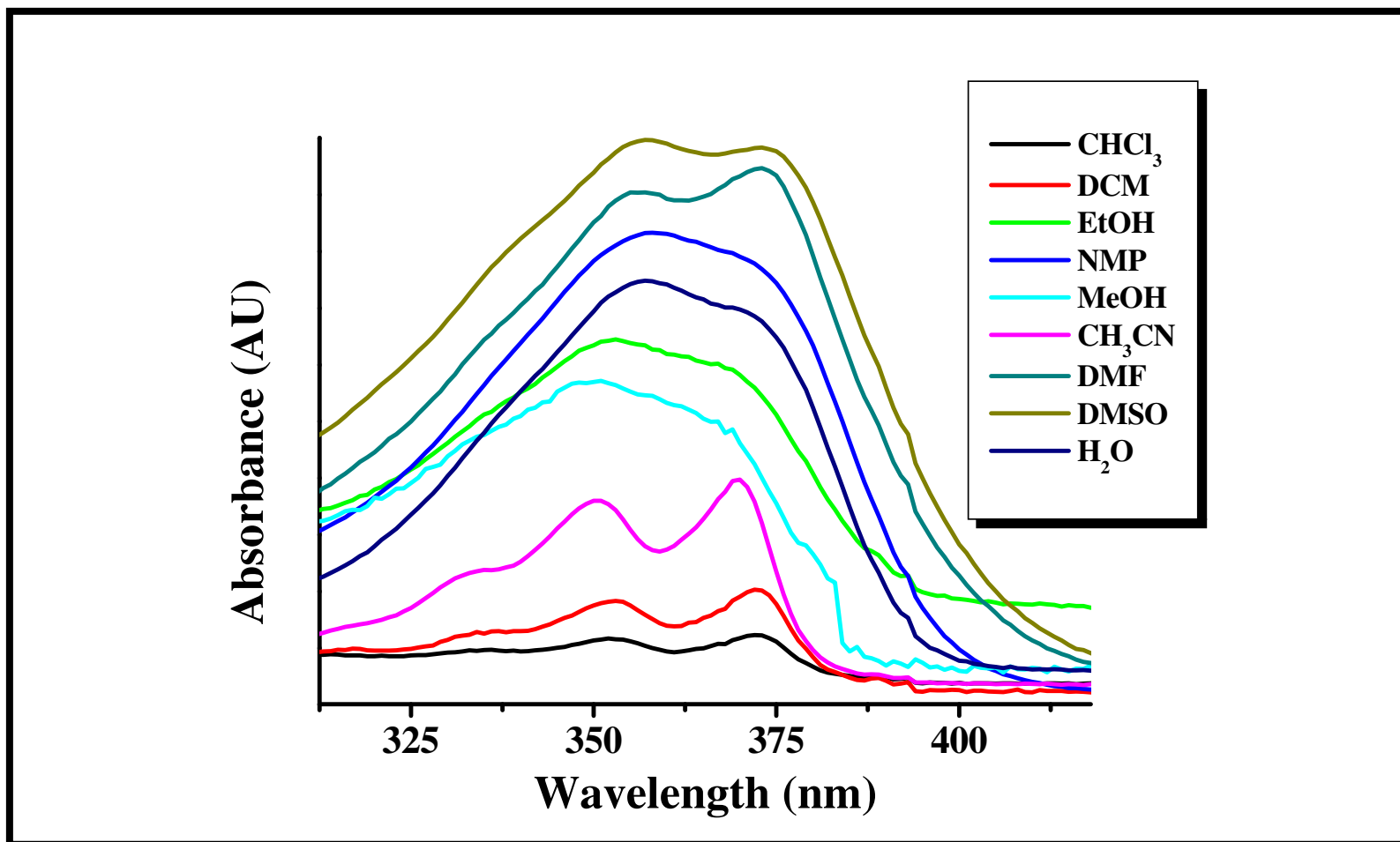


Figure 4.13: Absorption spectra of N-(4-hydroxyphenyl)-1,4,5,8-naphthalenetetracarboxylic-1,8-anhydride-4,5-imide (**1a**) in different solvents.

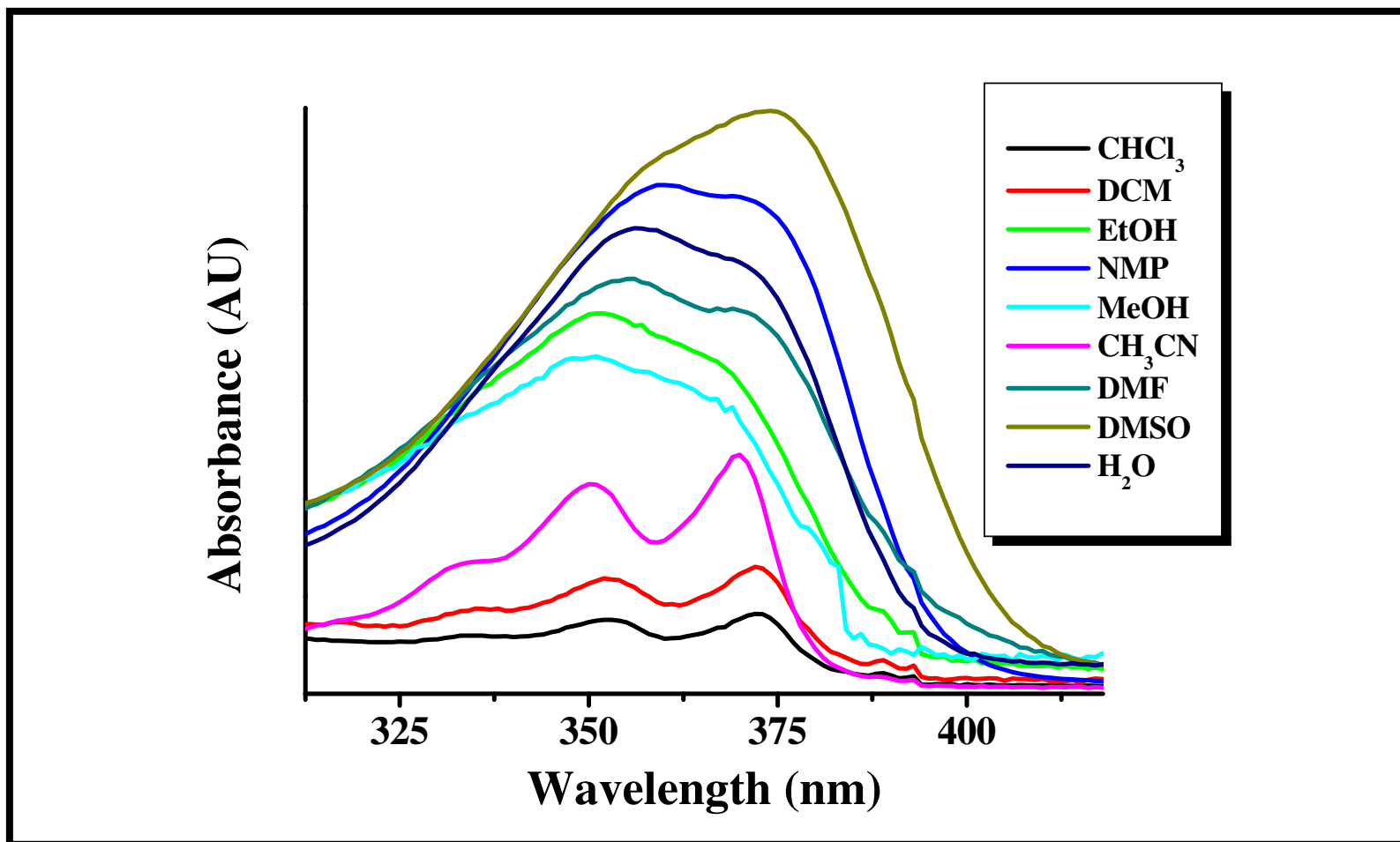


Figure 4.14: Absorption spectra of N-(4-hydroxyphenyl)-1,4,5,8-naphthalenetetracarboxylic-1,8-anhydride-4,5-imide (**1a**) in different solvents after filtration with 0.2 μm microfilter.

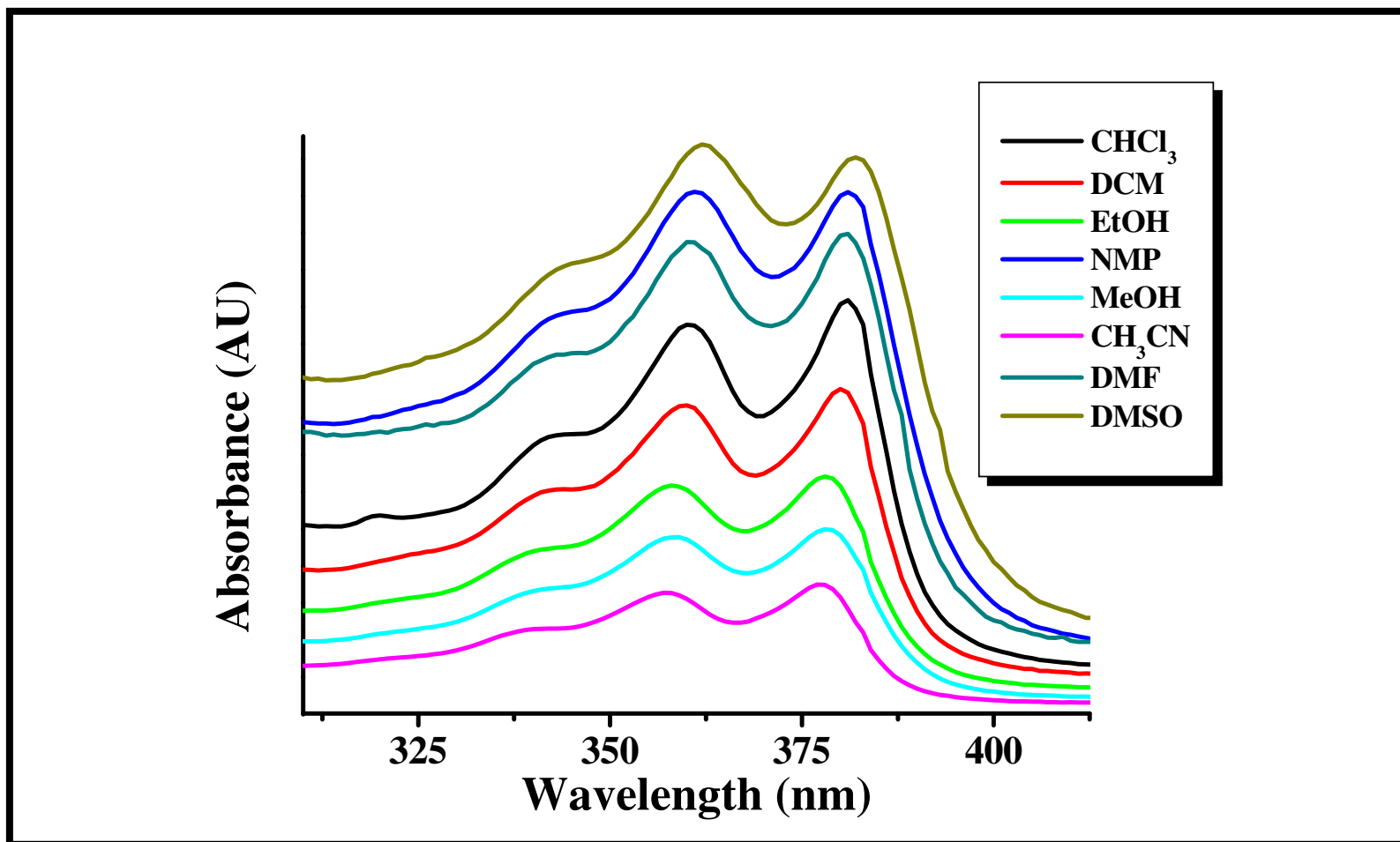


Figure 4.15: Absorption spectra of N-(4-hydroxyphenyl)-N'-[(S)-1-phenylethyl]-1,4,5,8-naphthalenetetracarboxydiimide (**2a**) in different solvents.

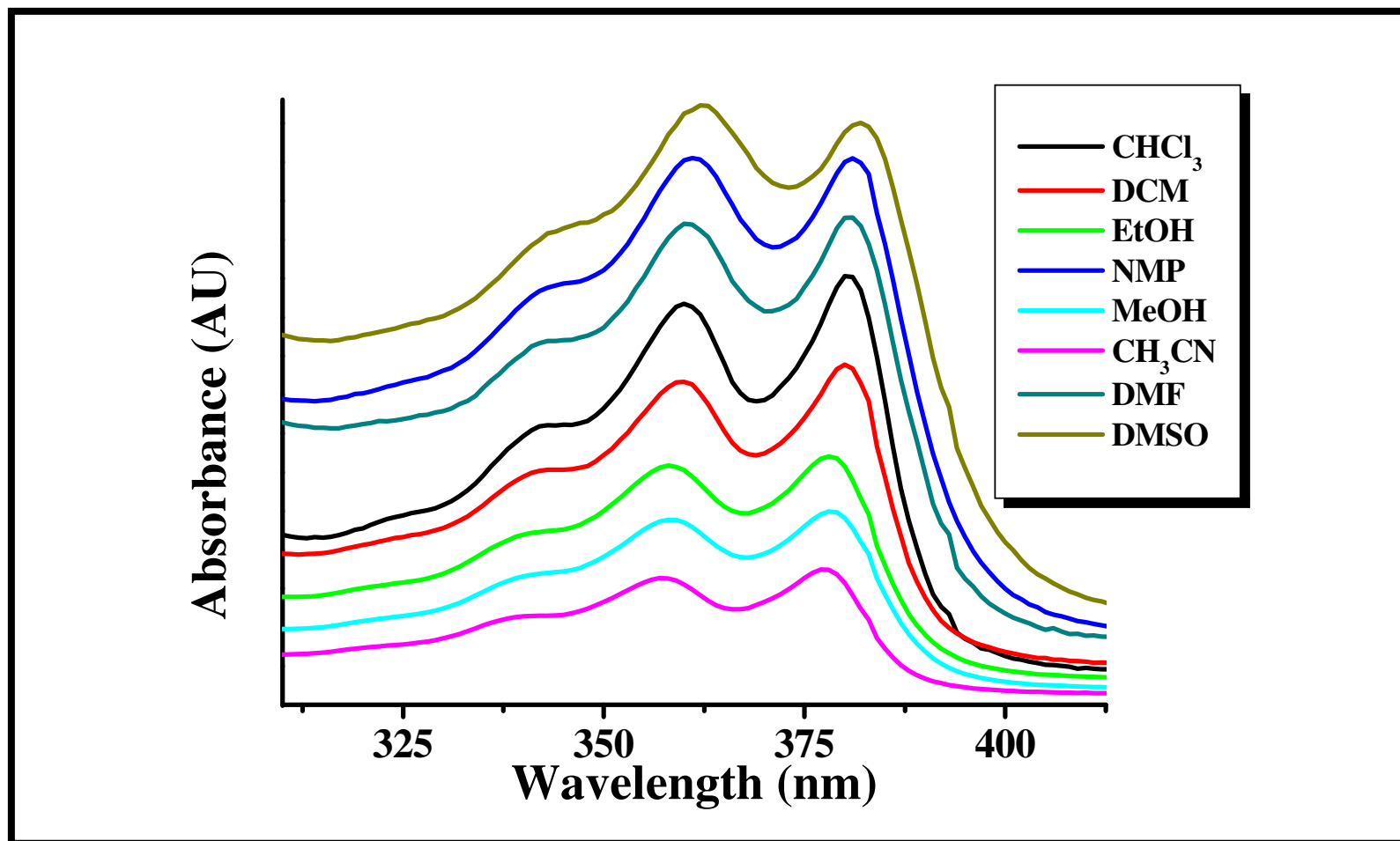


Figure 4.16: Absorption spectra of N-(4-hydroxyphenyl)-N'-[(S)-1-phenylethyl]-1,4,5,8-naphthalenetetracarboxydiimide (**2a**) in different solvents after filtration with 0.2 μm microfilter.

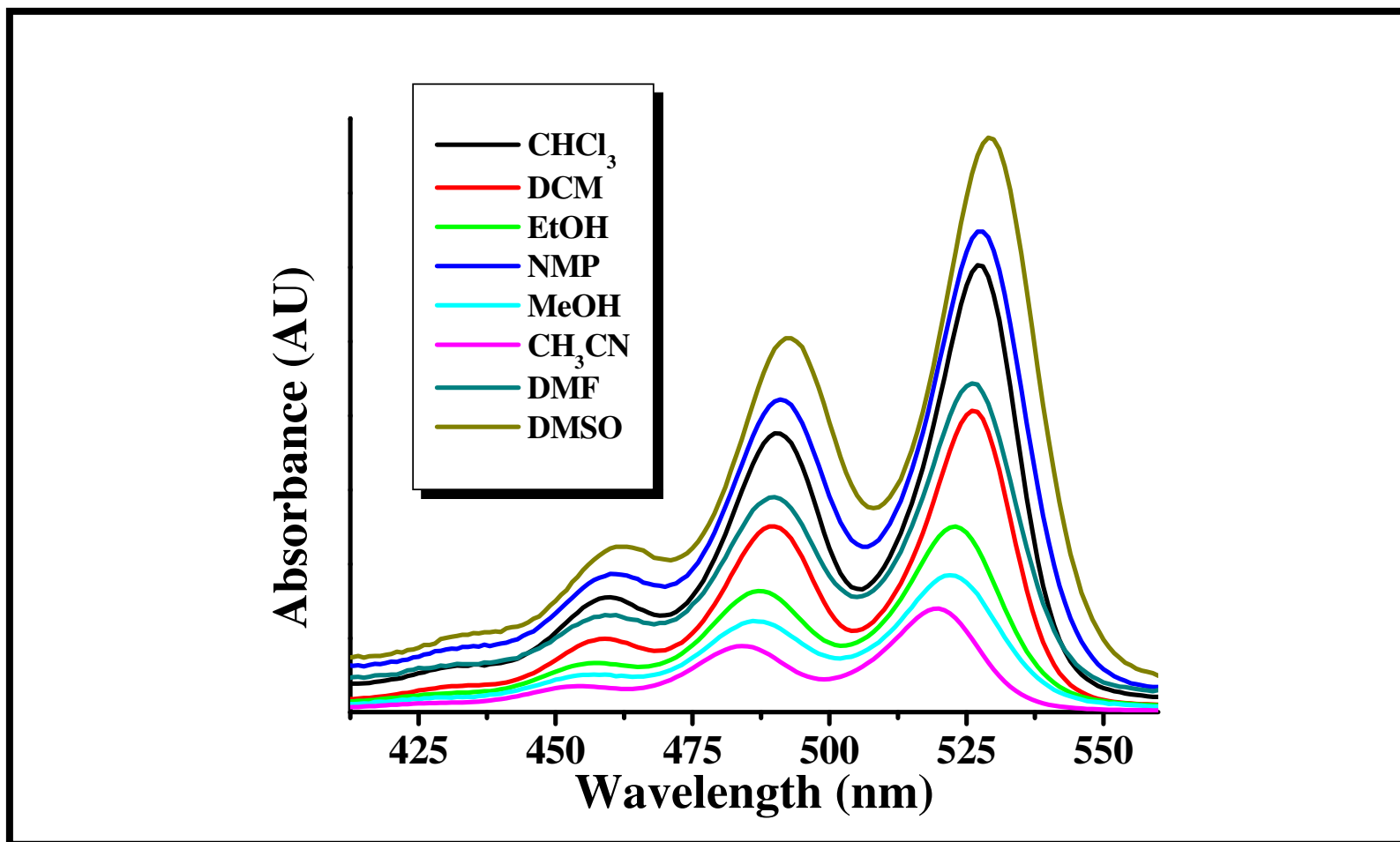


Figure 4.17: Absorption spectra of N-(4-hydroxyphenyl)-N'-[(S)-1-phenylethyl]-3,4,9,10-perylenetetracarboxydiimide (**5a**) in different solvents.

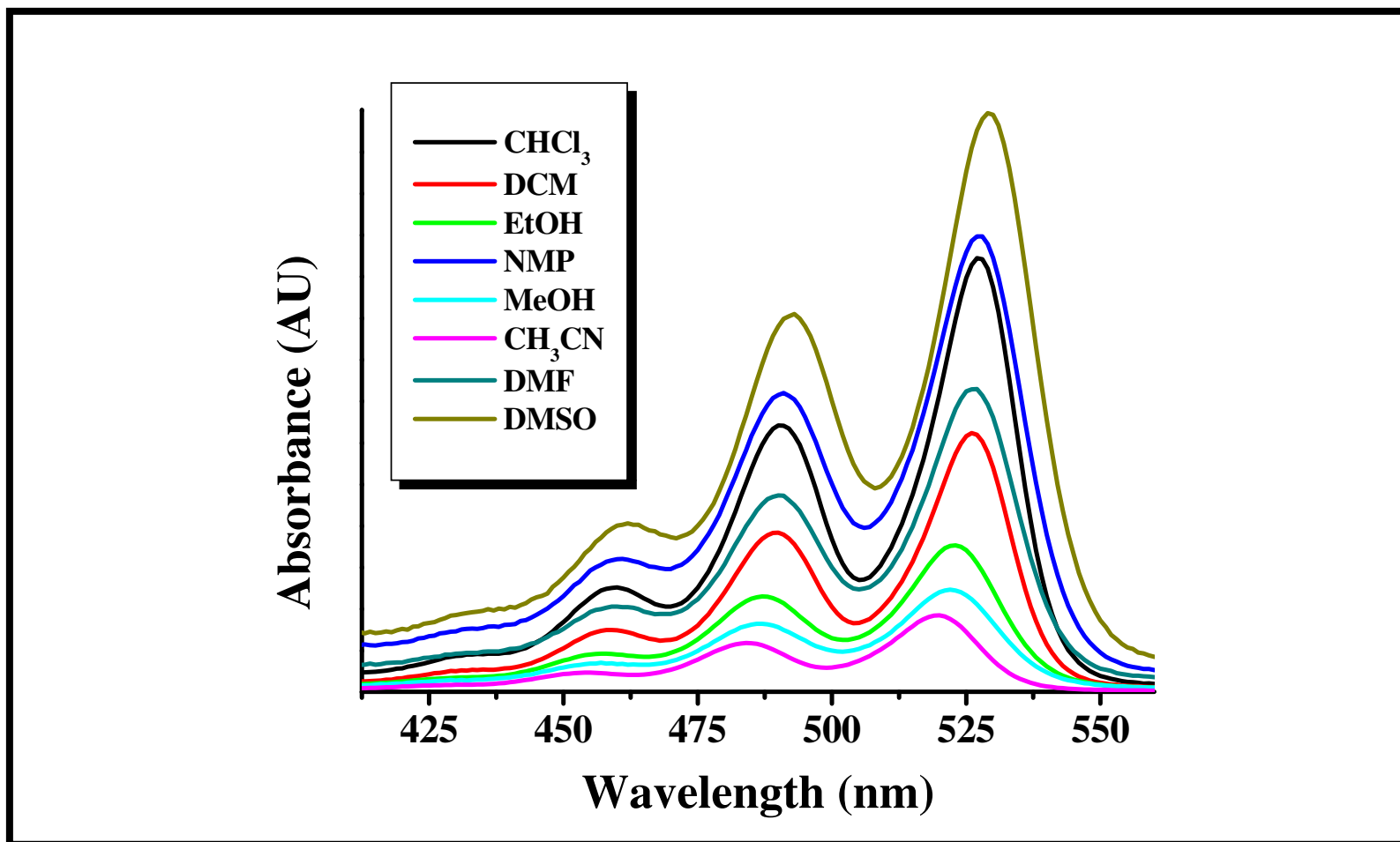


Figure 4.18: Absorption spectra of N-(4-hydroxyphenyl)-N'-[(S)-1-phenylethyl]-3,4,9,10-perylenetetracarboxydiimide (**5a**) in different solvents after filtration with 0.2 μm microfilter.

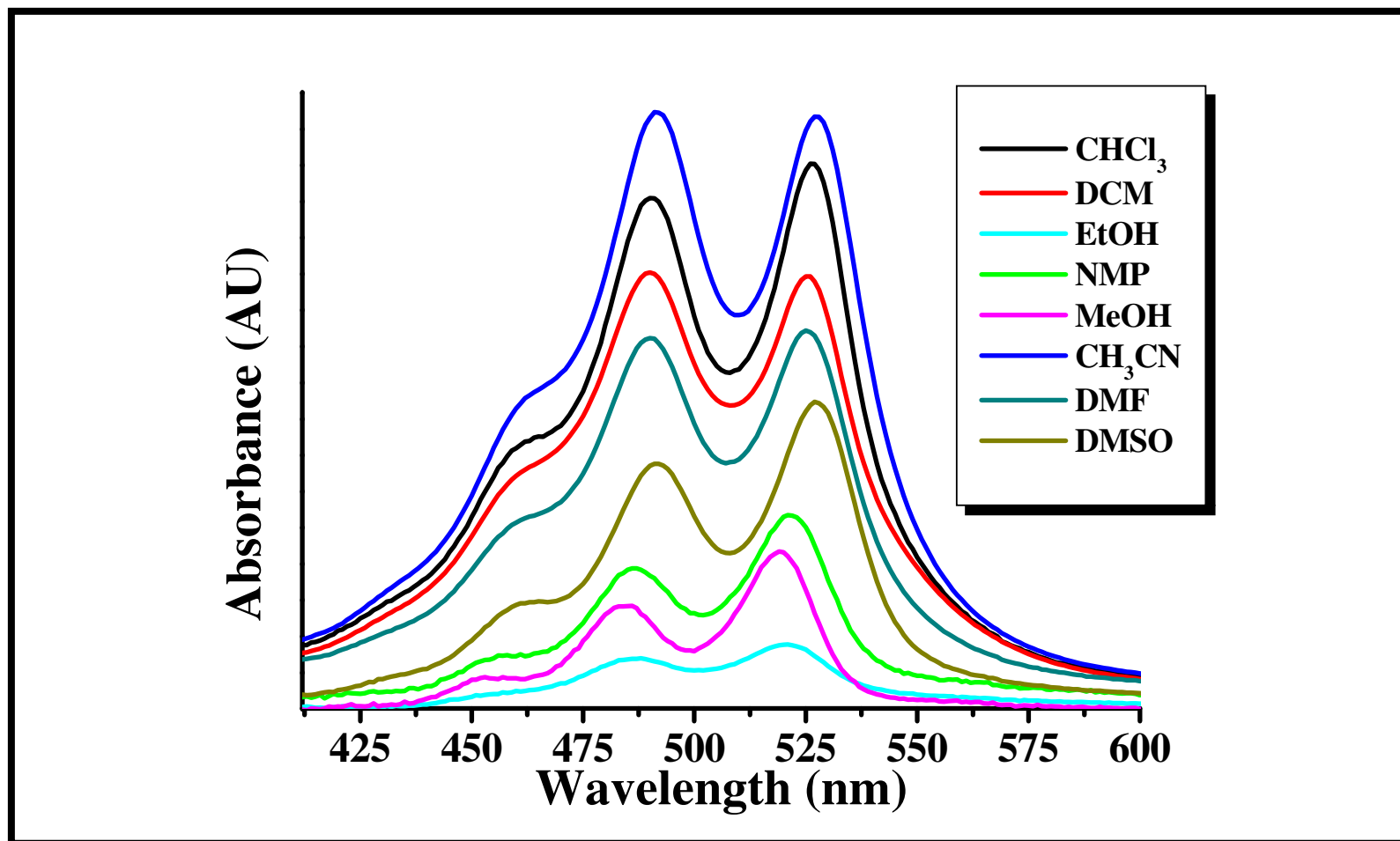


Figure 4.19: Absorption spectra of N-(2-aminohexanoic acid)-N'-(1-dehydroabietyl)-3,4,9,10 perylenetetracarboxydiimide (**5b**) in different solvents.

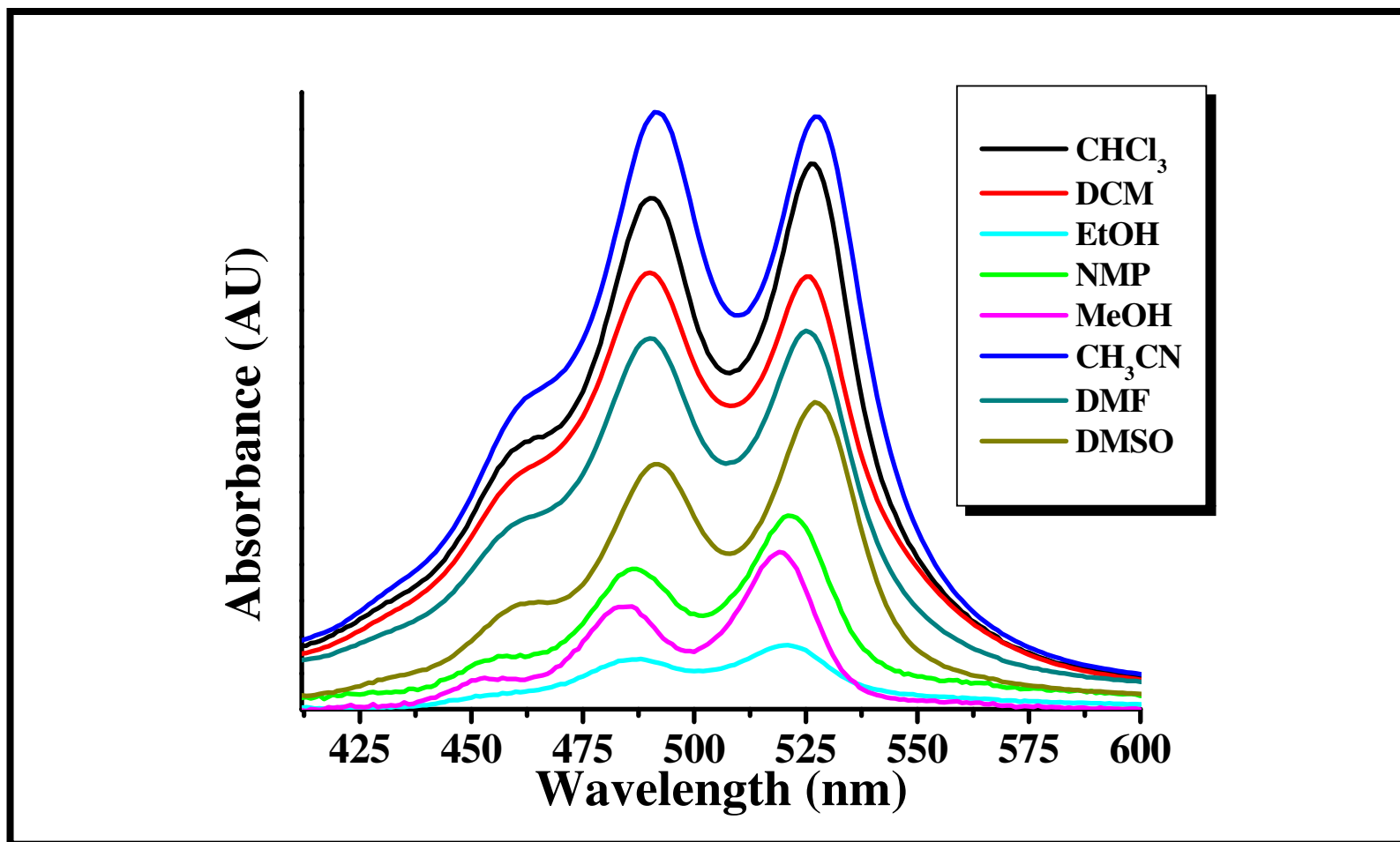


Figure 4.20: Absorption spectra of N-(2-aminohexanoic acid)-N'-(1-dehydroabietyl)-3,4,9,10 perylenetetracarboxydiimide (**5b**) in different solvents after filtration with 0.2 μm microfilter.

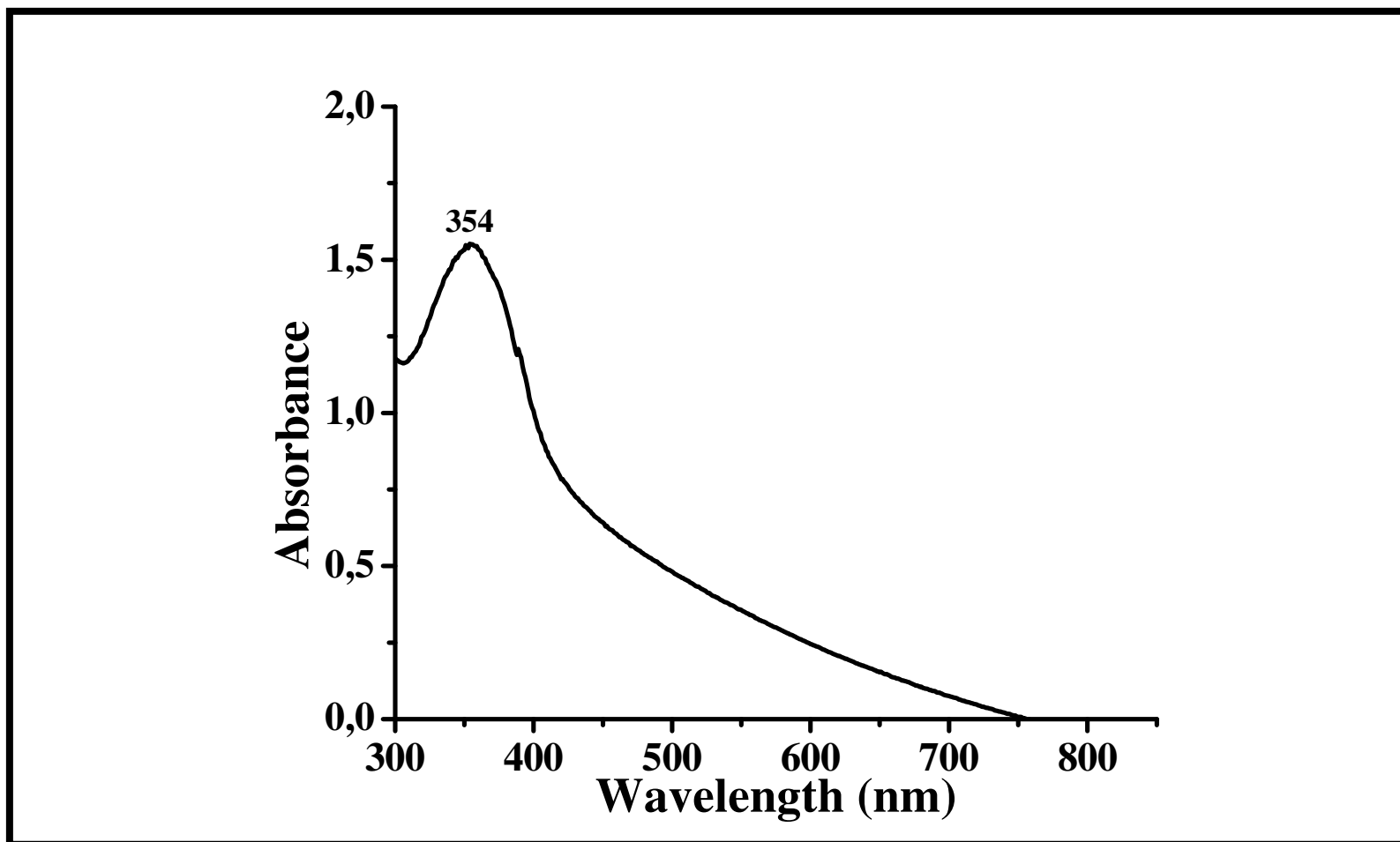


Figure 4.21: Solid-state absorption spectra of N-(4-hydroxyphenyl)-1,4,5,8-naphthalenetetracarboxylic-1,8-anhydride-4,5-imide (**1a**).

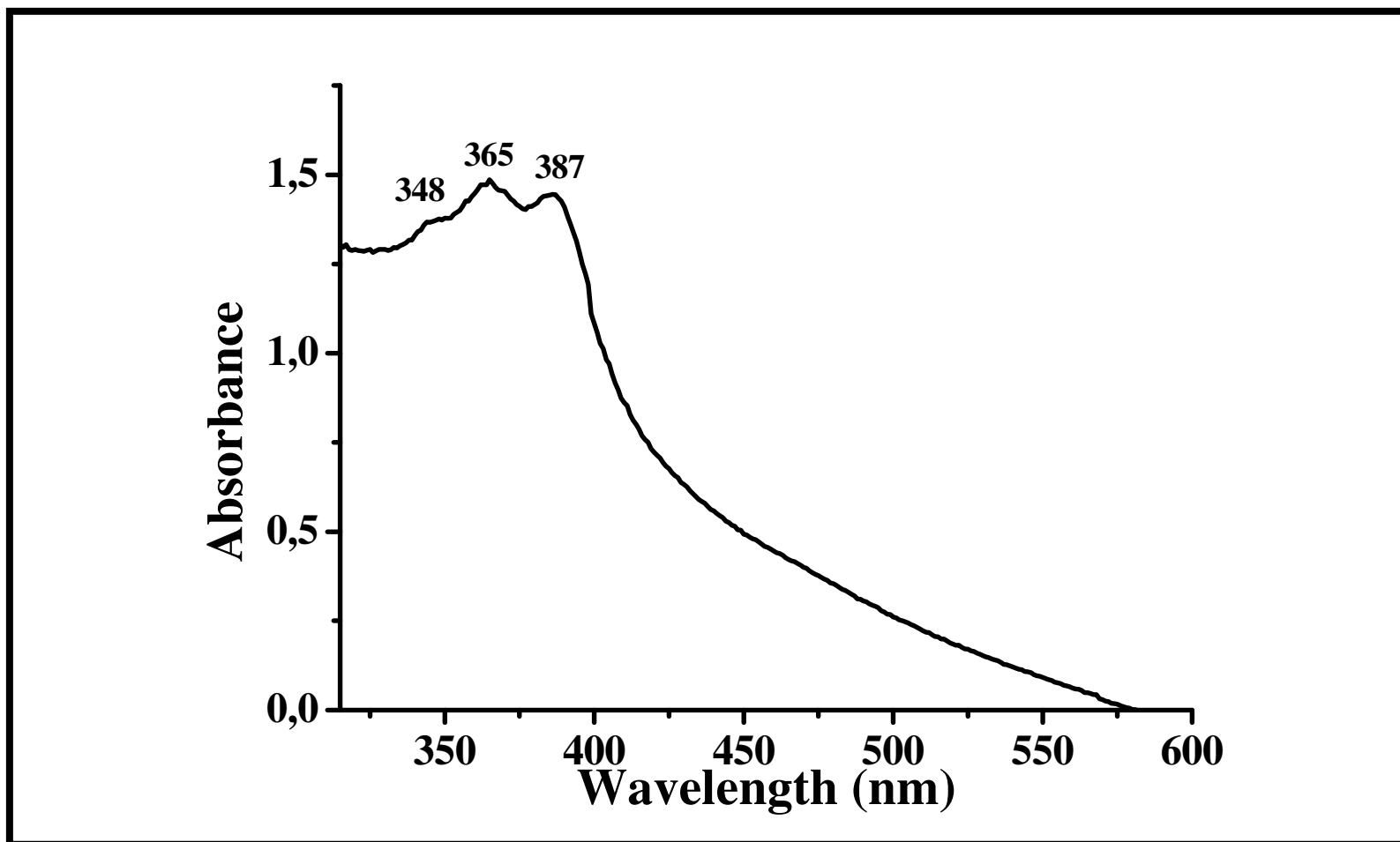


Figure 4.22: Solid-state absorption spectra of N-(4-hydroxyphenyl)-N'-[(S)-1-phenylethyl]-1,4,5,8-naphthalenetetracarboxydiimide (**2a**).

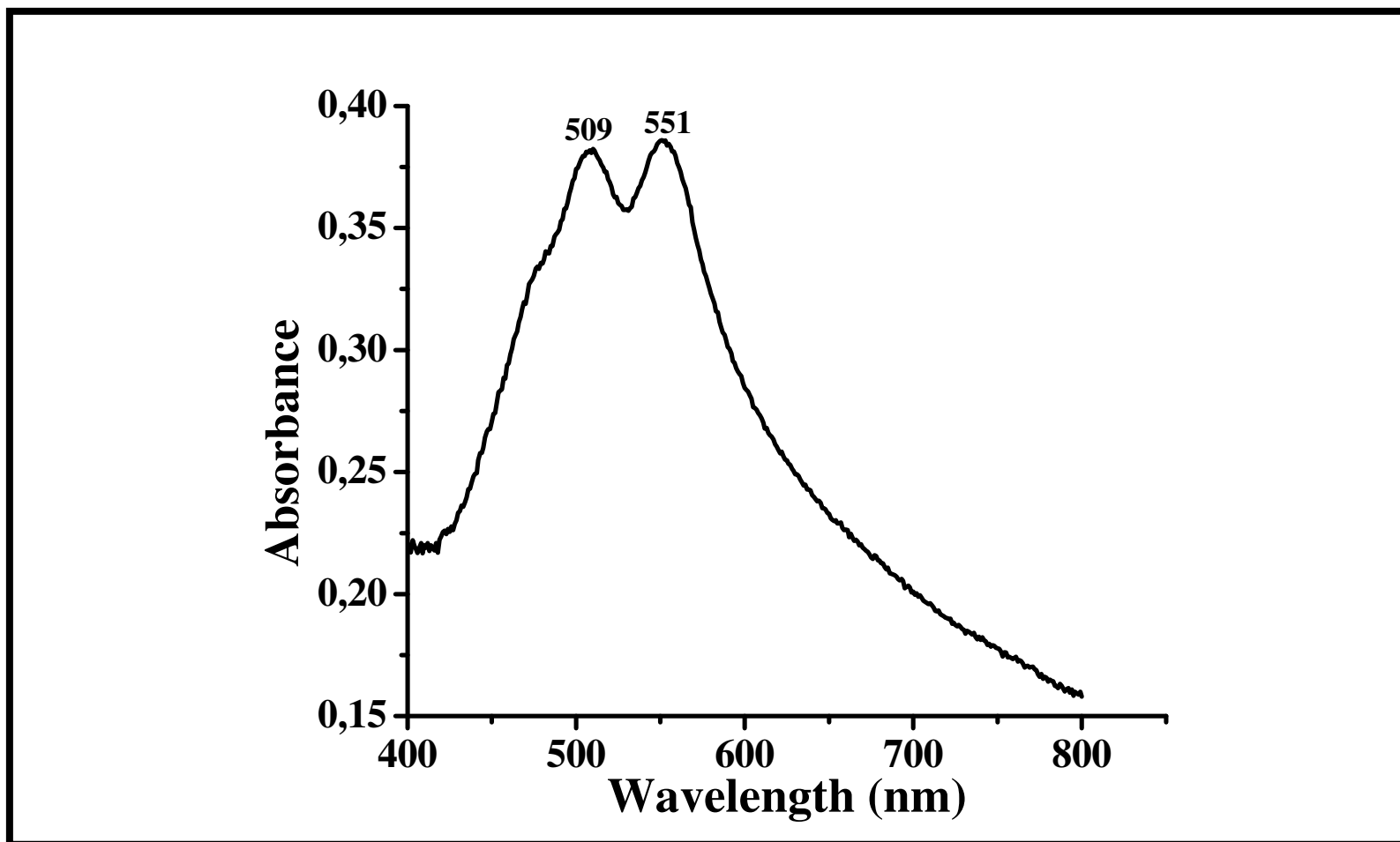


Figure 4.23: Solid-state absorption spectra of N-(4-hydroxyphenyl)-N'-[(S)-1-phenylethyl]-3,4,9,10-perylenetetracarboxydiimide (**5a**).

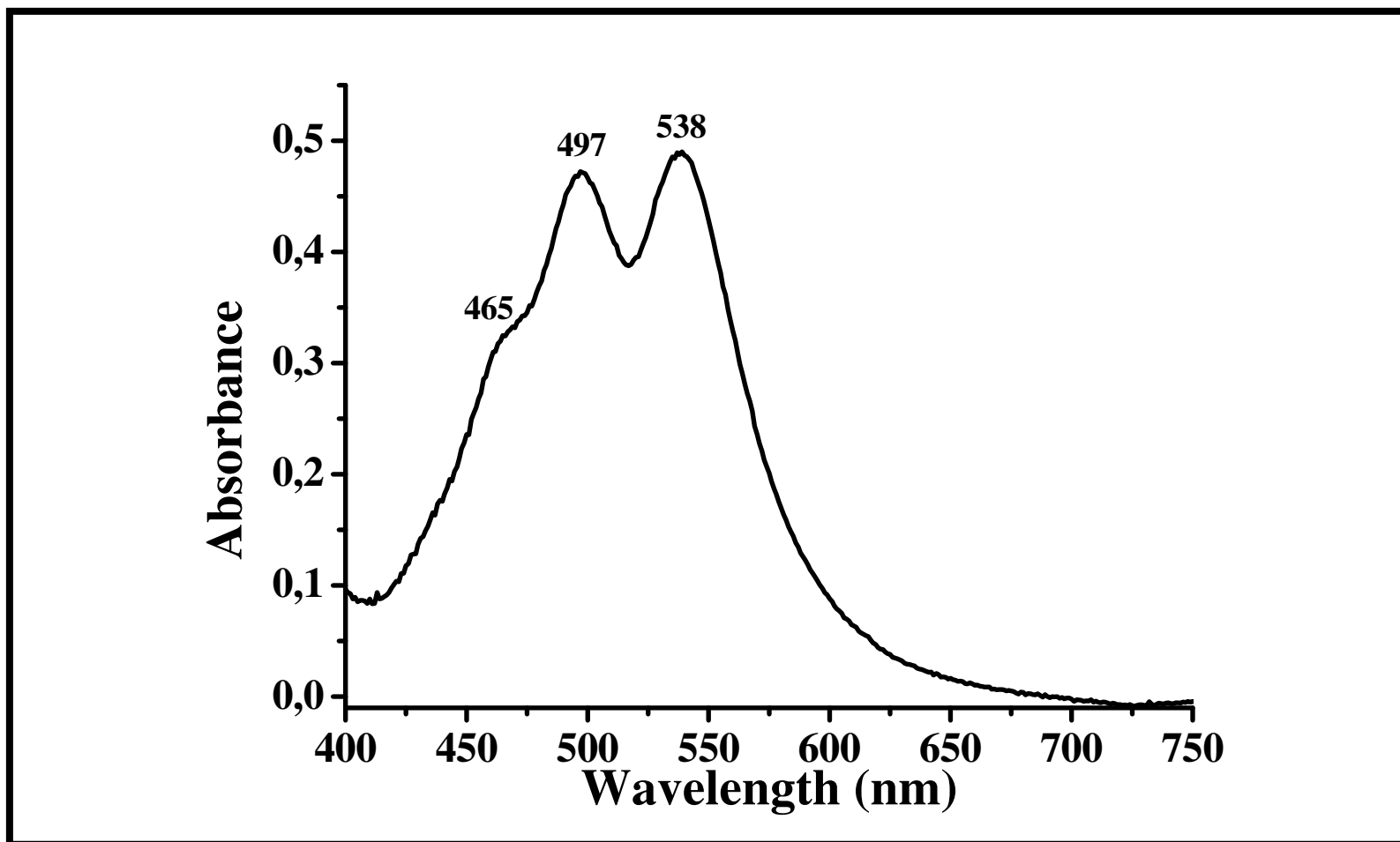


Figure 4.24: Solid-state absorption spectra of N-(2-aminohexanoic acid)-N'-(1-dehydroabietyl)-3,4,9,10 perylenetetracarboxydiimide (**5b**).

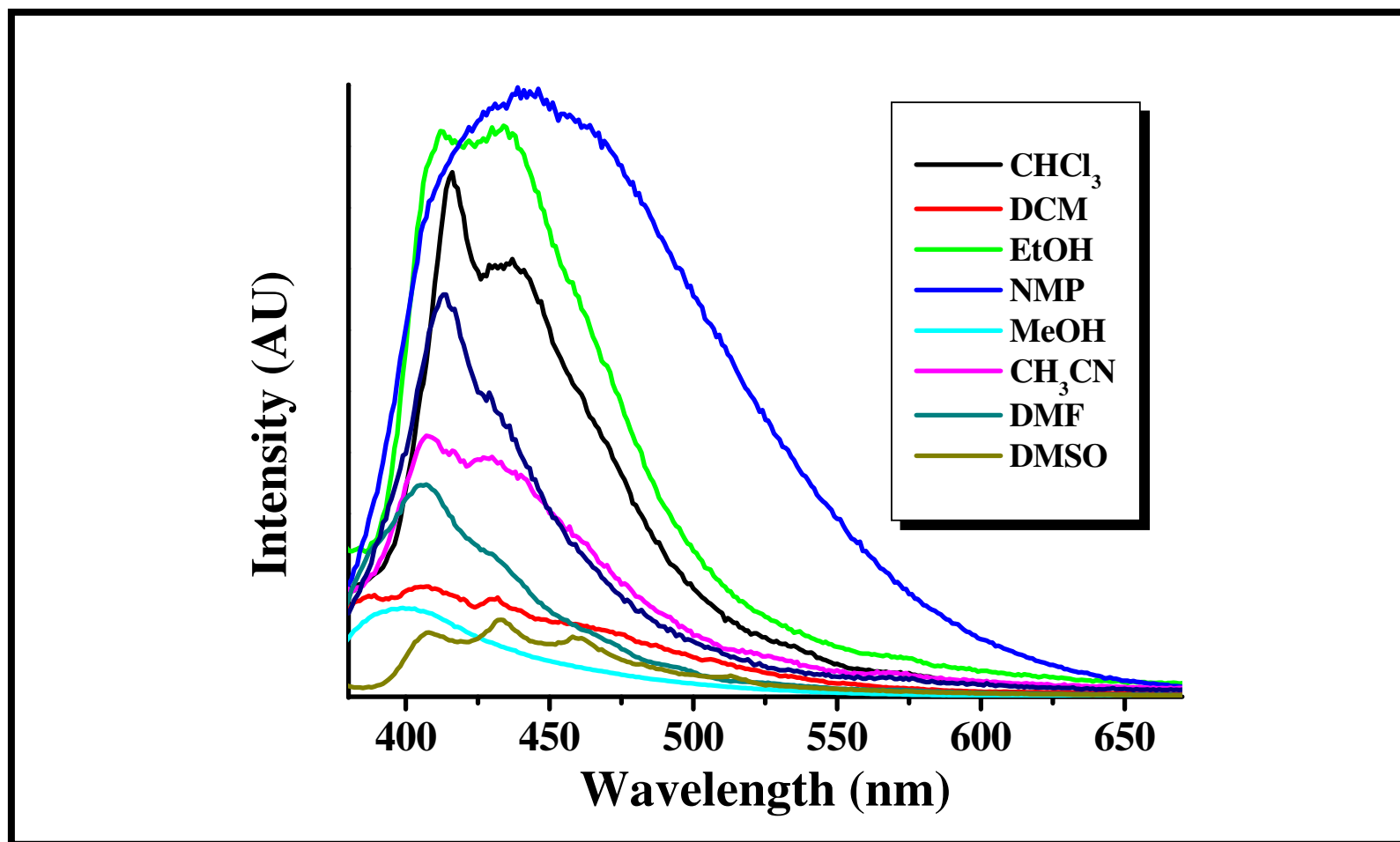


Figure 4.25: Emission spectra of N-(4-hydroxyphenyl)-1,4,5,8-naphthalenetetracarboxylic-1,8-anhydride-4,5-imide (**1a**) in different solvents.

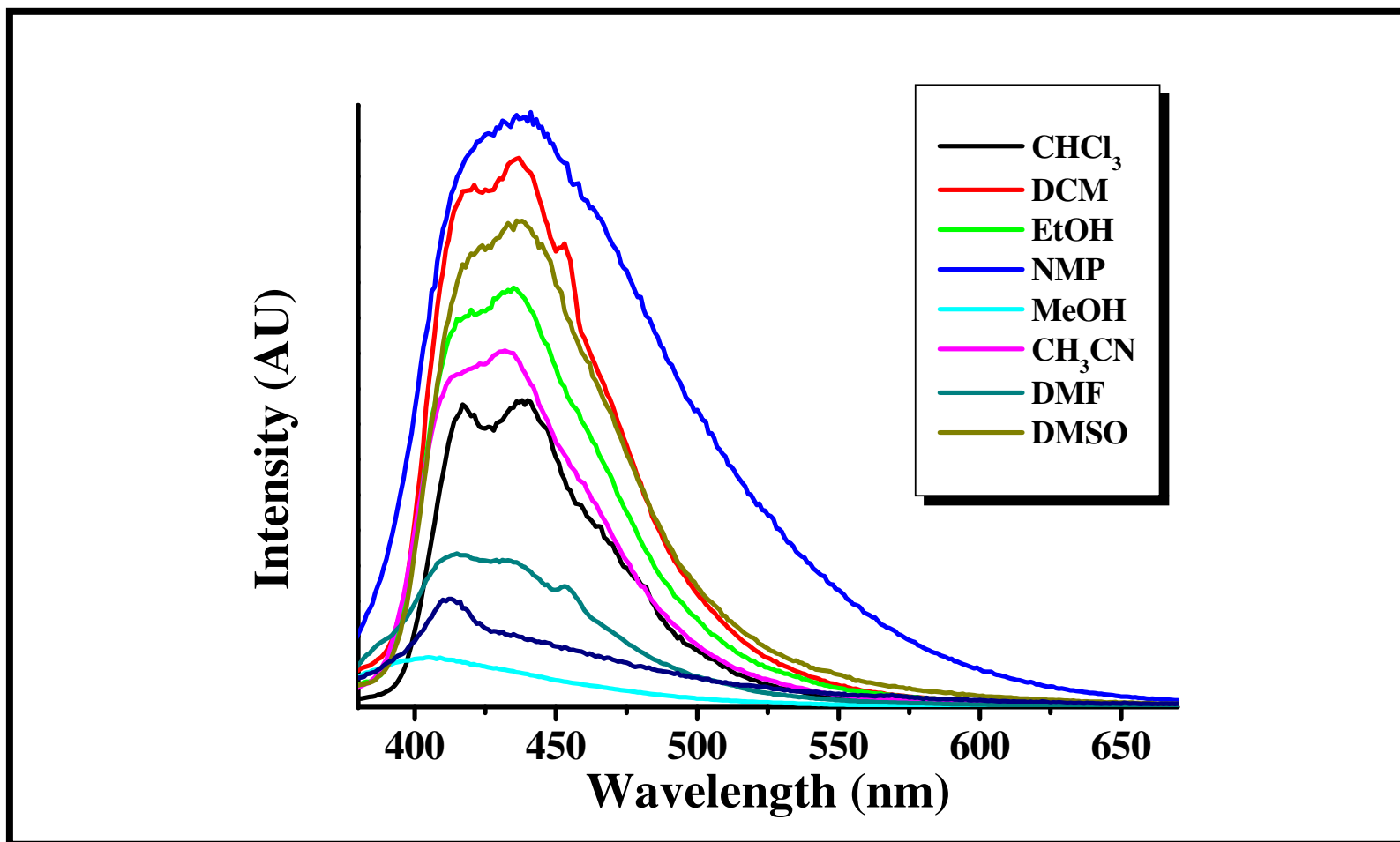


Figure 4.26: Emission spectra of N-(4-hydroxyphenyl)-1,4,5,8-naphthalenetetracarboxylic-1,8-anhydride-4,5-imide (**1a**) in different solvents after filtration with 0.2 μm microfilter.

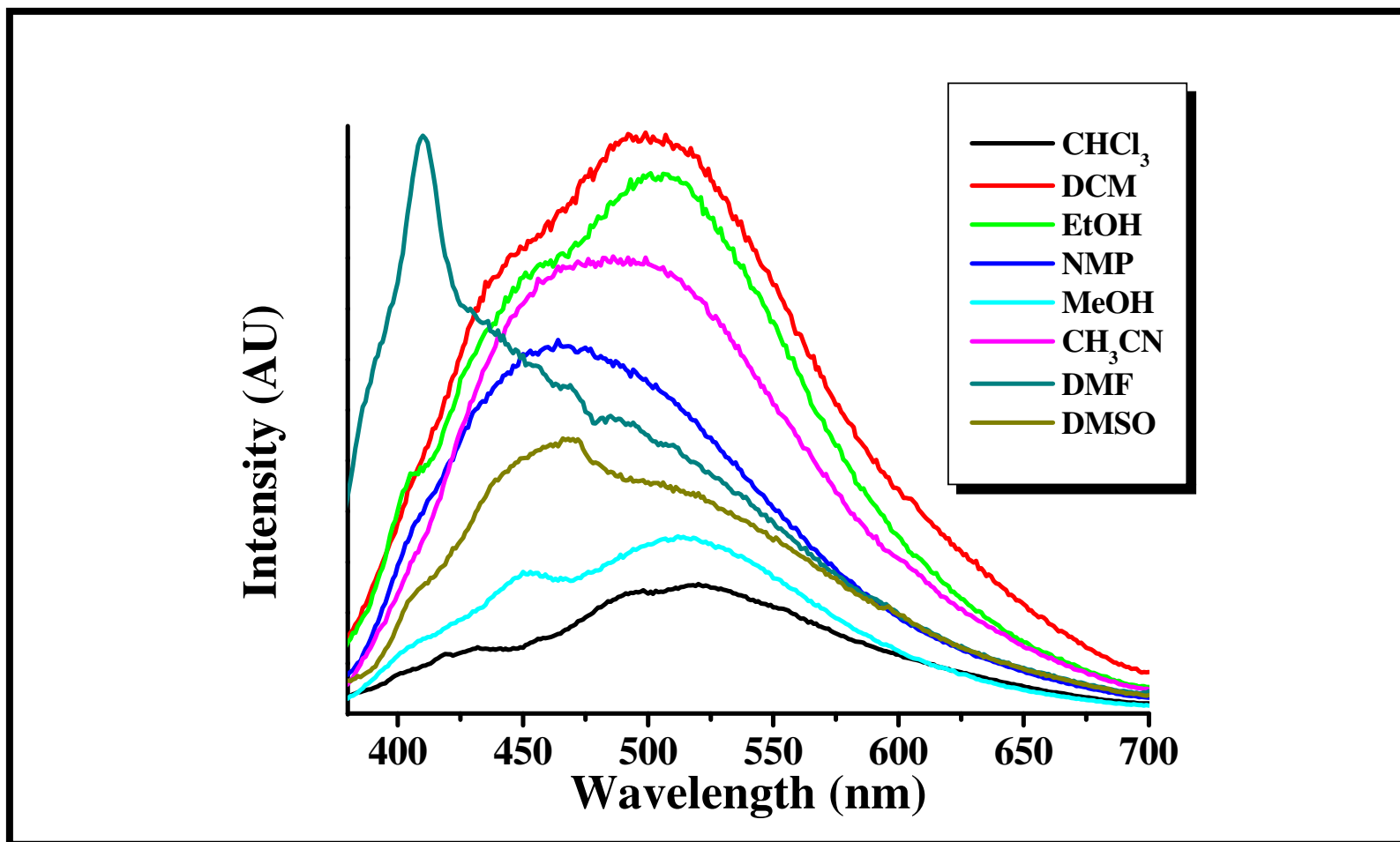


Figure 4.27: Emission spectra of N-(4-hydroxyphenyl)-N'-[(S)-1-phenylethyl]-1,4,5,8-naphthalenetetracarboxydiimide (**2a**) in different solvents.

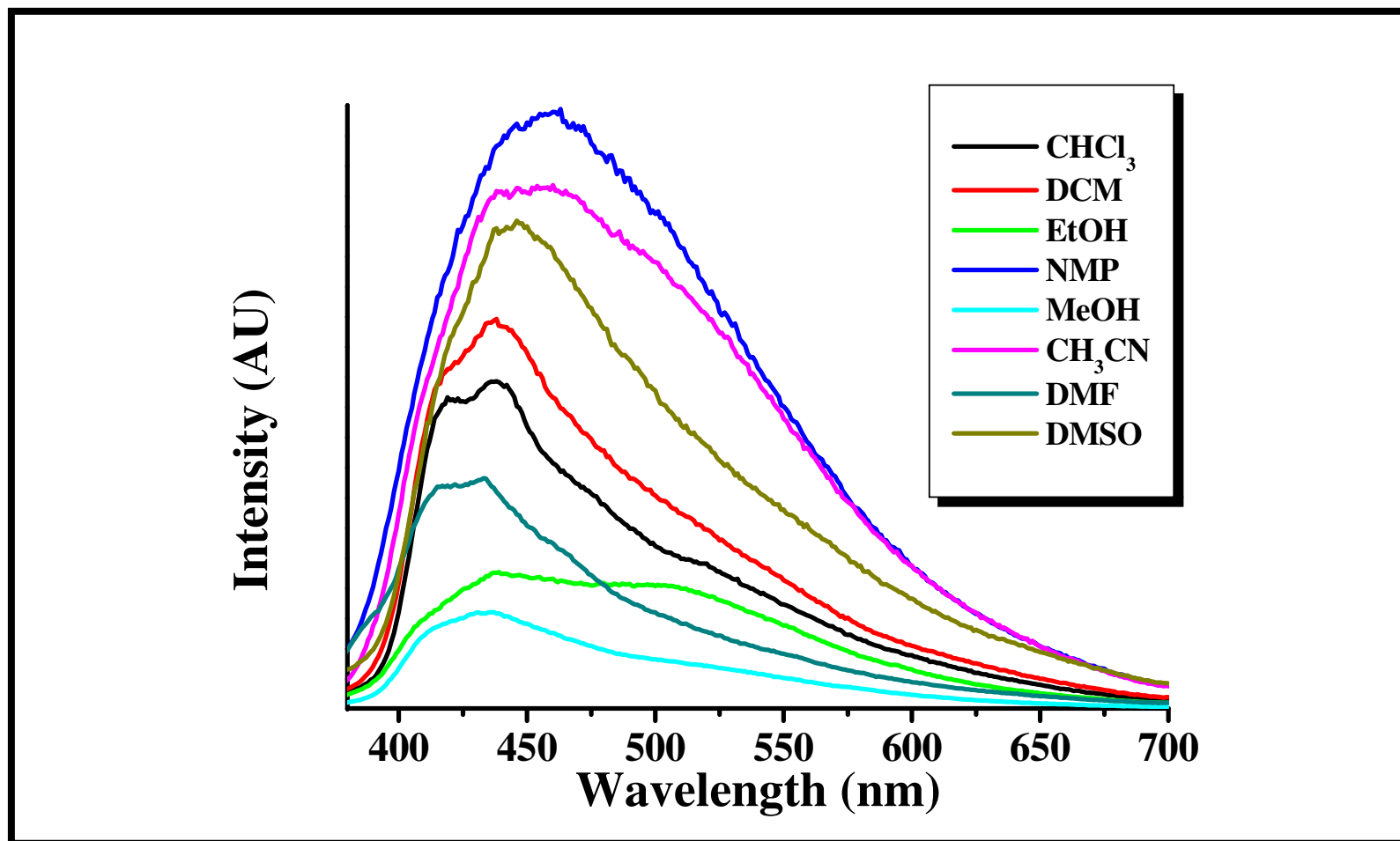


Figure 4.28: Emission spectra of N-(4-hydroxyphenyl)-N'-[(S)-1-phenylethyl]-1,4,5,8-naphthalenetetracarboxydiimide (**2a**) in different solvents after filtration with 0.2 μm microfilter.

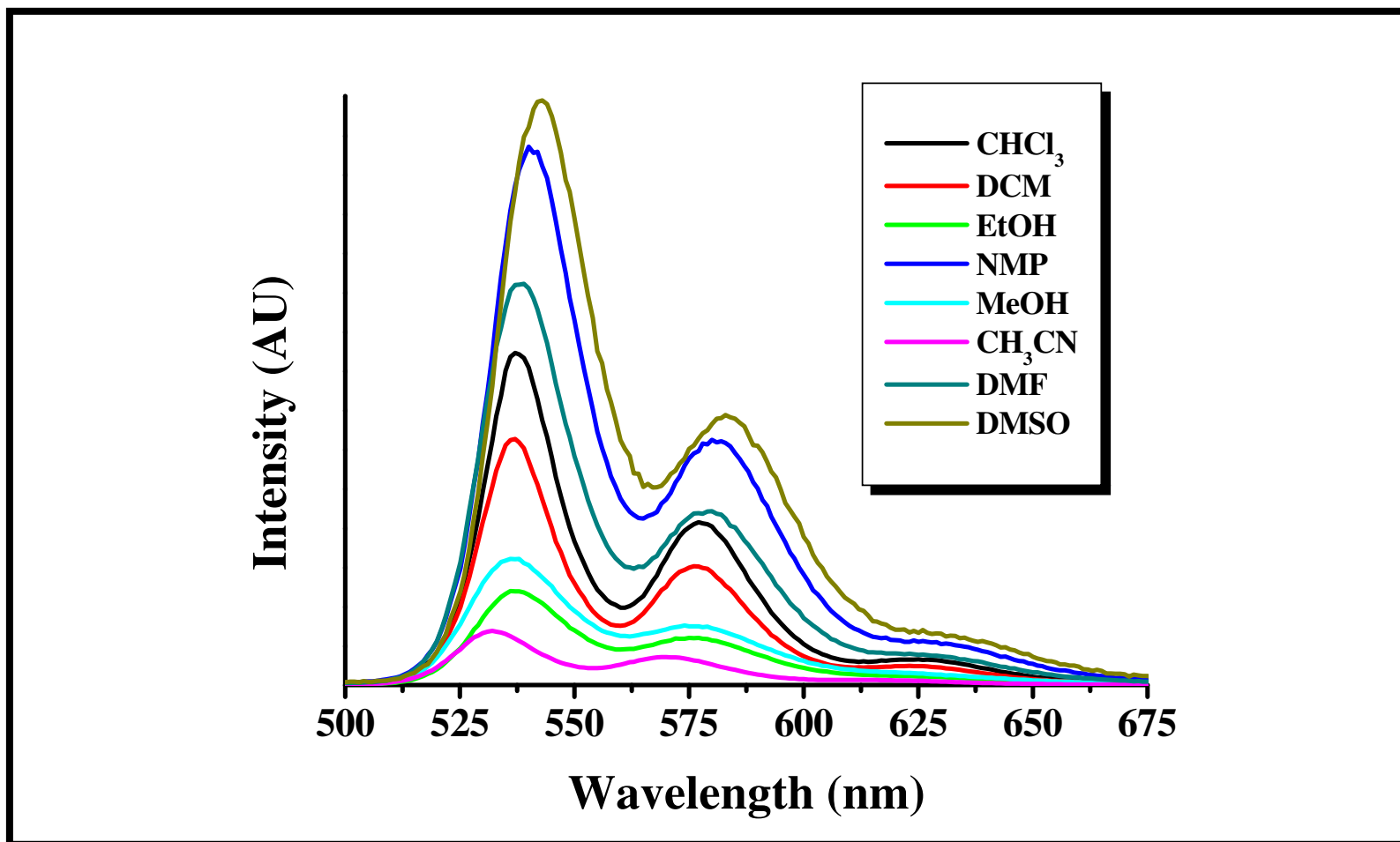


Figure 4.29: Emission spectra of N-(4-hydroxyphenyl)-N'-[(S)-1-phenylethyl]-3,4,9,10-perylenetetracarboxydiimide (**5a**) in different solvents.

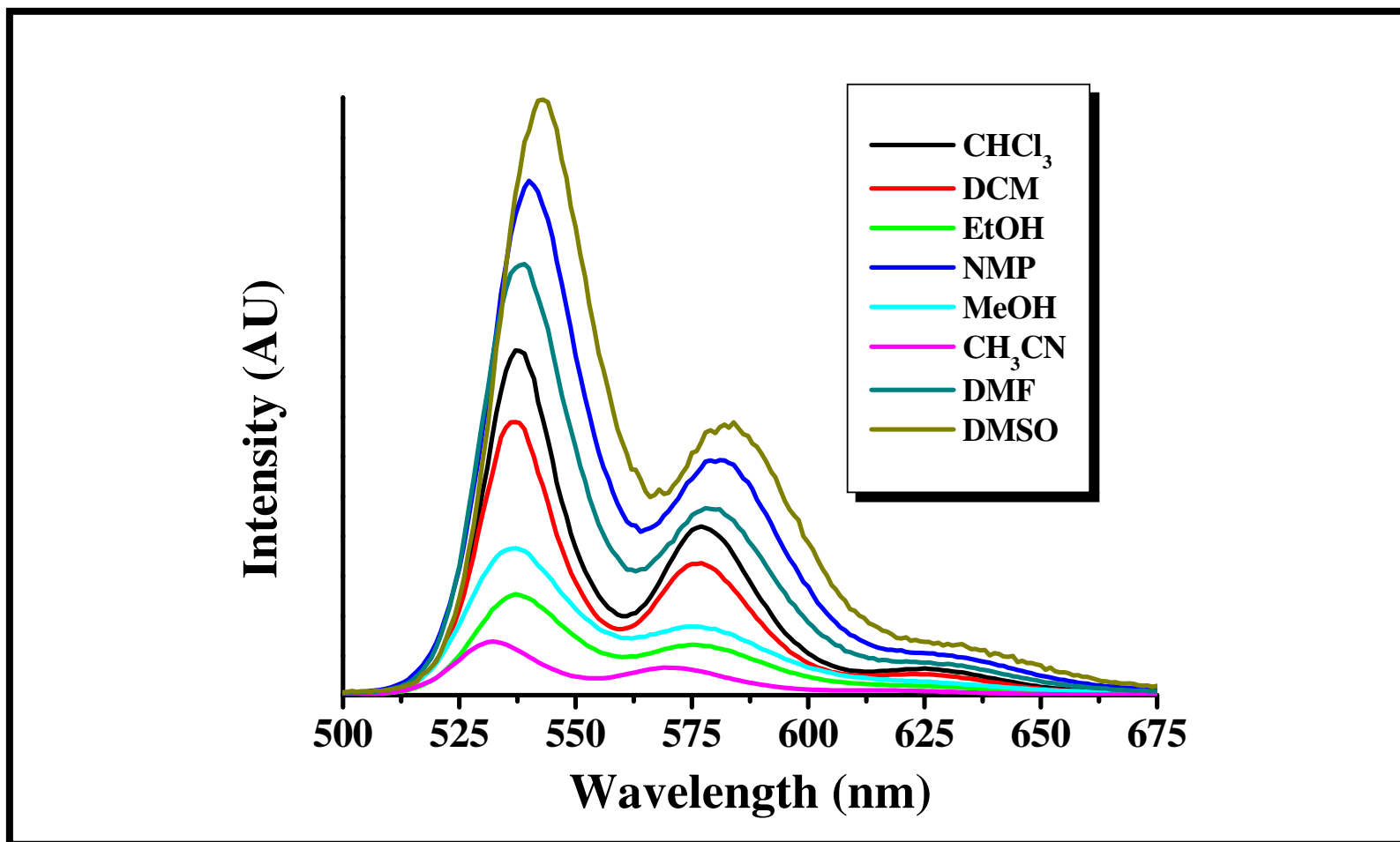


Figure 4.30: Emission spectra of N-(4-hydroxyphenyl)-N'-[(S)-1-phenylethyl]-3,4,9,10-perylenetetracarboxydiimide (**5a**) in different solvents after filtration with 0.2 μm microfilter.

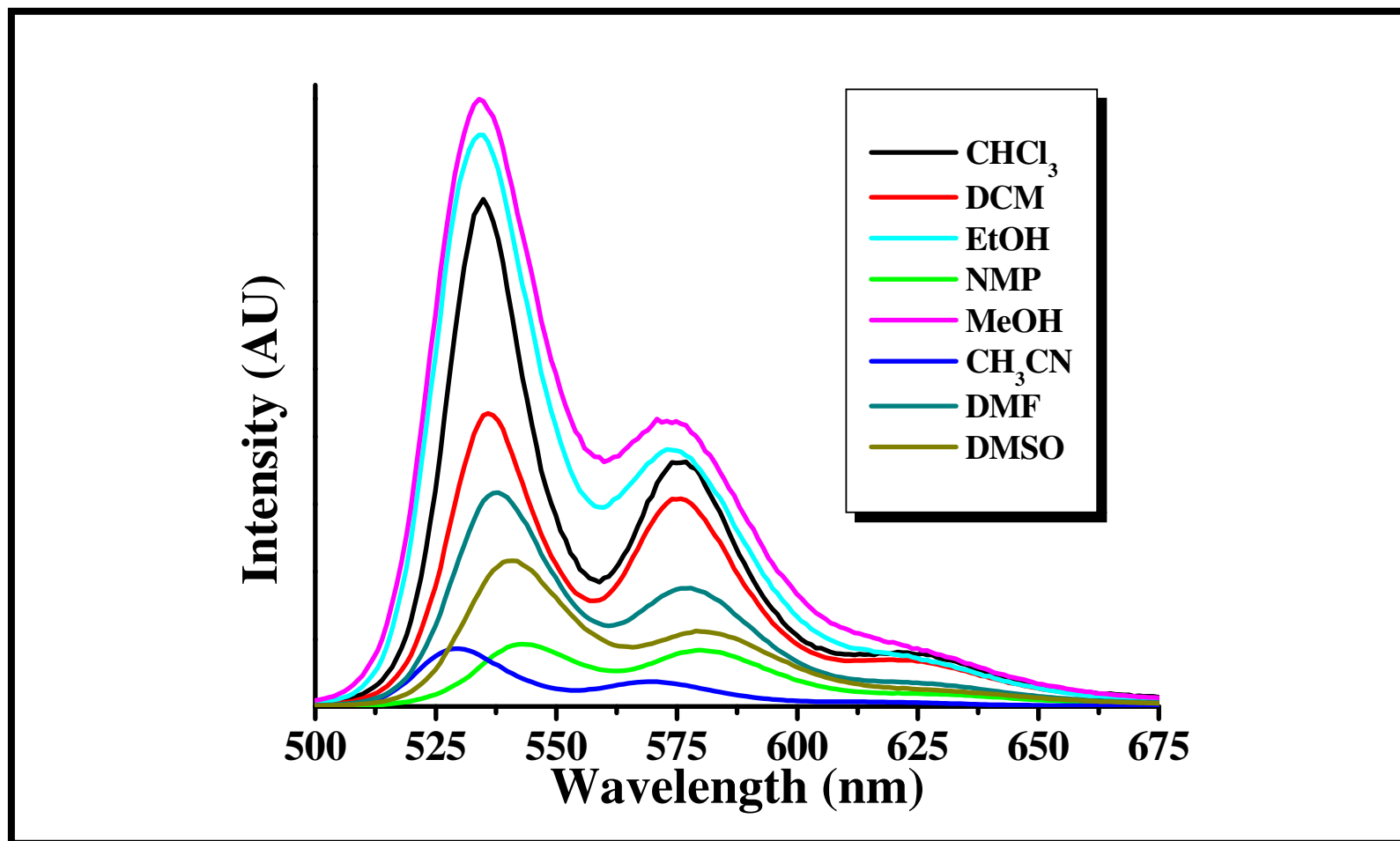


Figure 4.31: Emission spectra of N-(2-aminohexanoic acid)-N'-(1-dehydroabietyl)-3,4,9,10 perylenetetracarboxydiimide (**5b**) in different solvents.

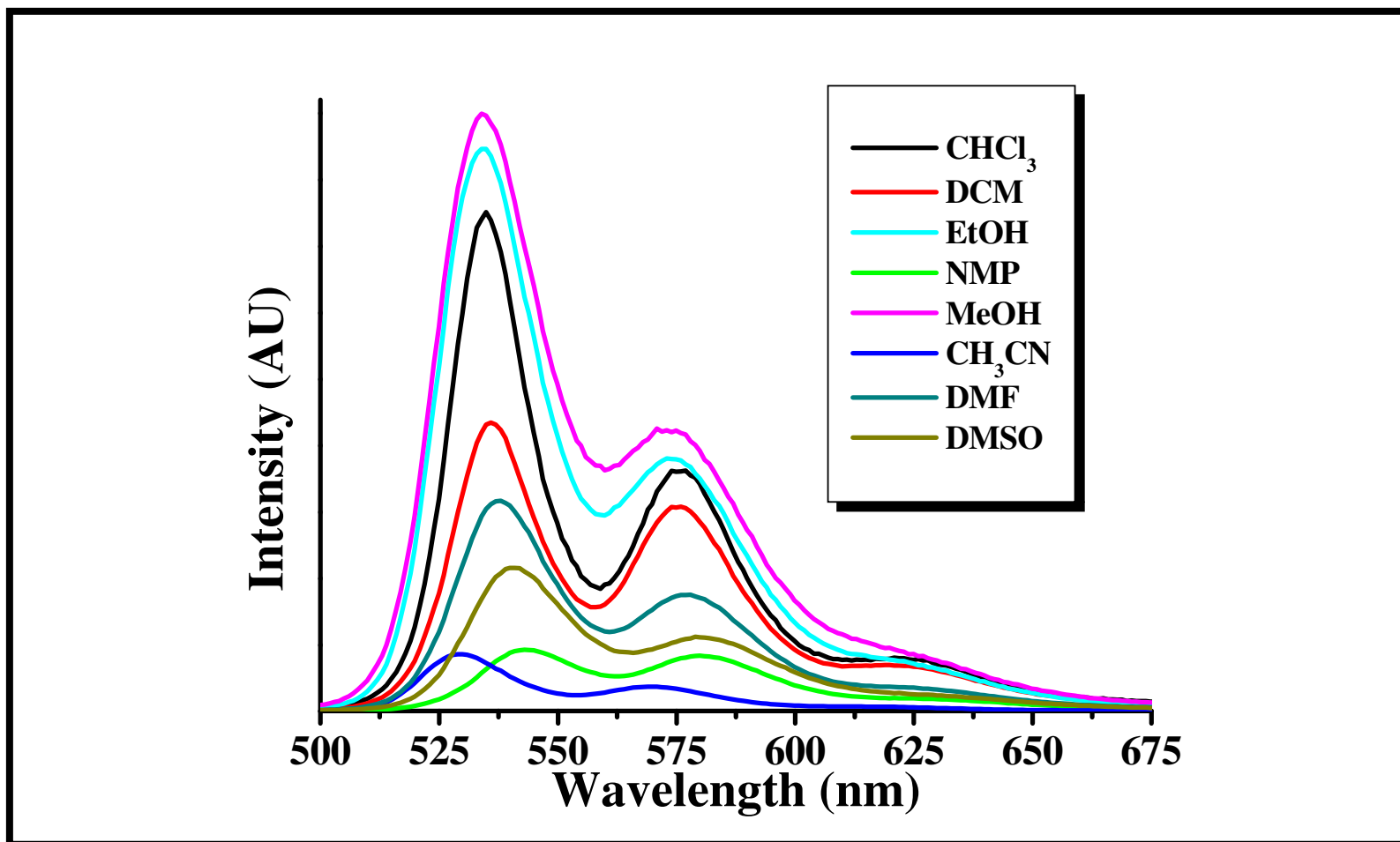


Figure 4.32: Emission spectra of N-(2-aminohexanoic acid)-N'-(1-dehydroabietyl)-3,4,9,10 perylenetetracarboxydiimide (**5b**) in different solvents after filtration with 0.2 μm microfilter.

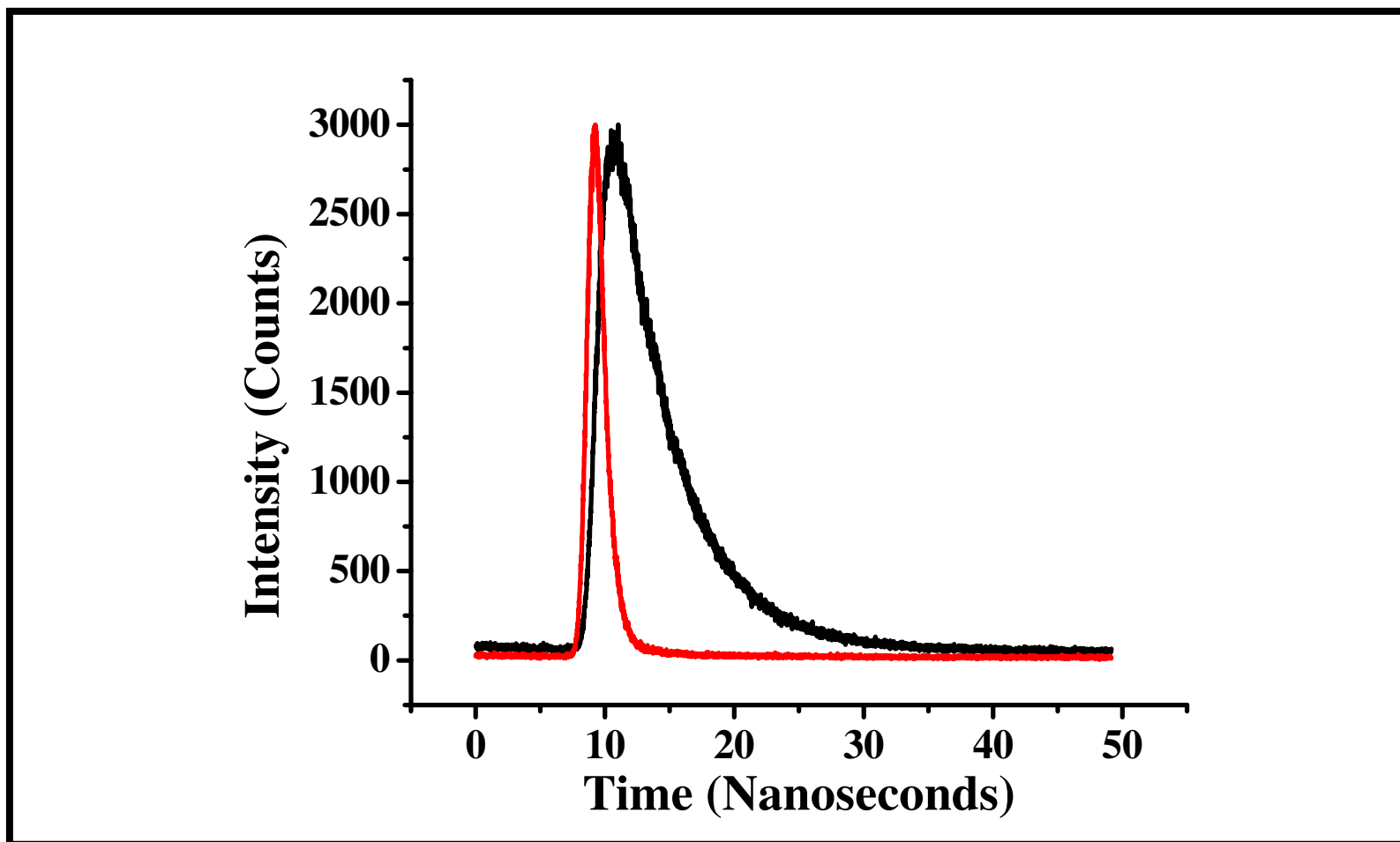


Figure 4.33: Fluorescence decay curve of 10^{-5} M N-(4-hydroxyphenyl)-N'-[(S)-1-phenylethyl]-3,4,9,10-perylenetetracarboxydiimide (**5a**) ($\lambda_{\text{excit.}}=530$ nm and $\lambda_{\text{em}}=580$ nm) in DMF.

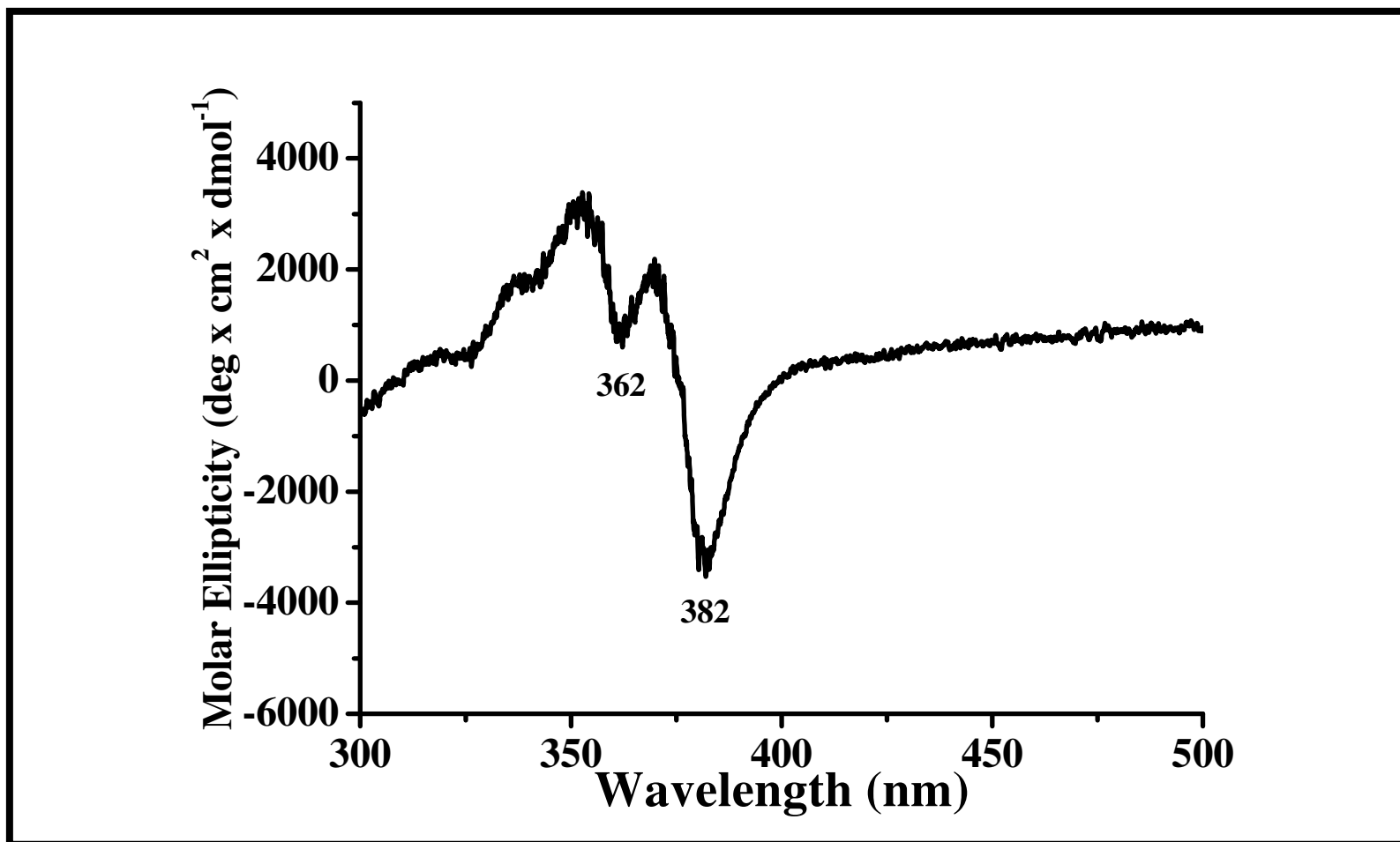


Figure 4.34: CD spectrum of N-(4-hydroxyphenyl)-N'-[(S)-1-phenylethyl]-1,4,5,8-naphthalenetetracarboxydiimide (**2a**) in acetonitrile.

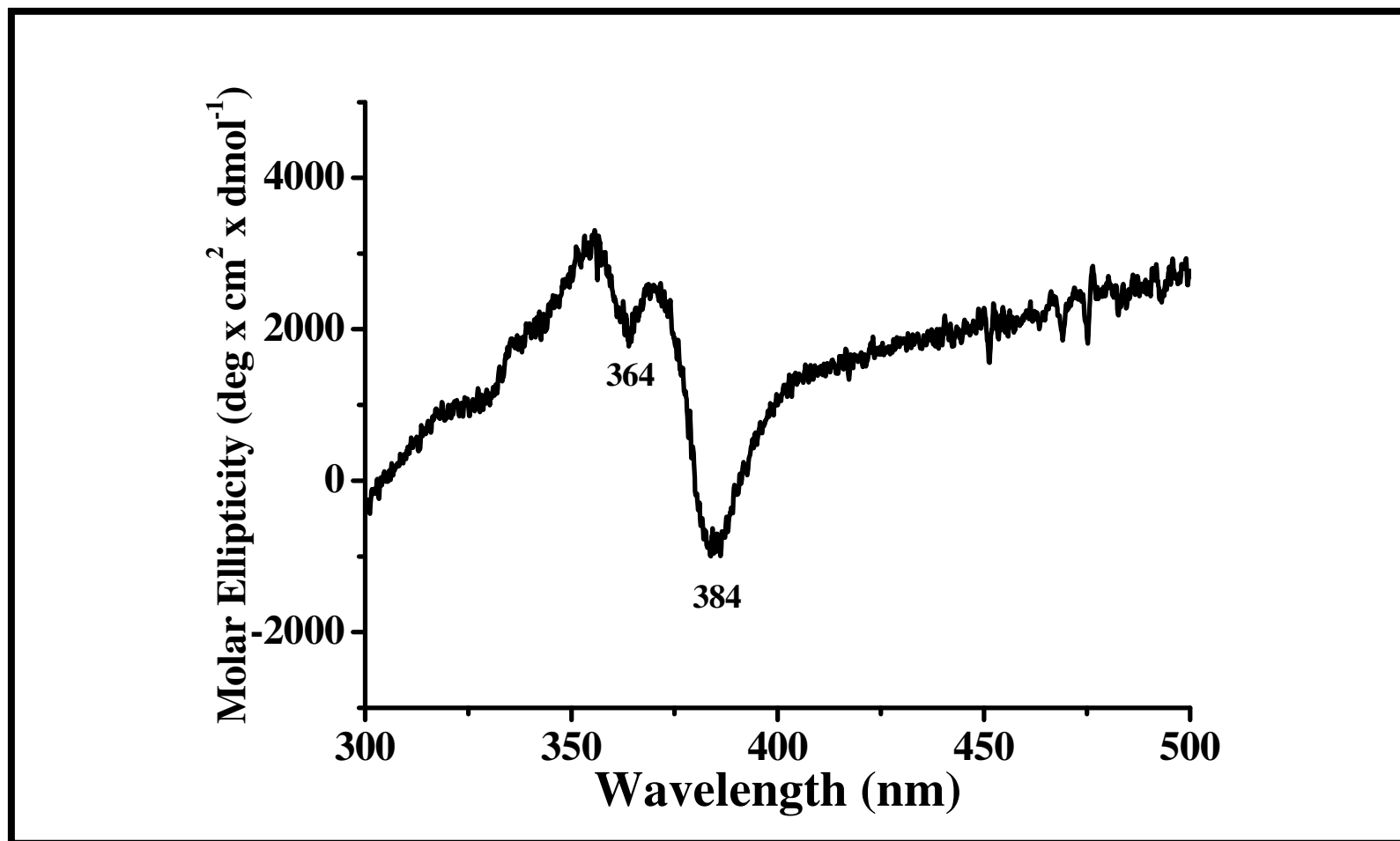


Figure 4.35: CD spectrum of N-(4-hydroxyphenyl)-N'-[(S)-1-phenylethyl]-1,4,5,8-naphthalenetetracarboxydiimide (**2a**) in ethanol.

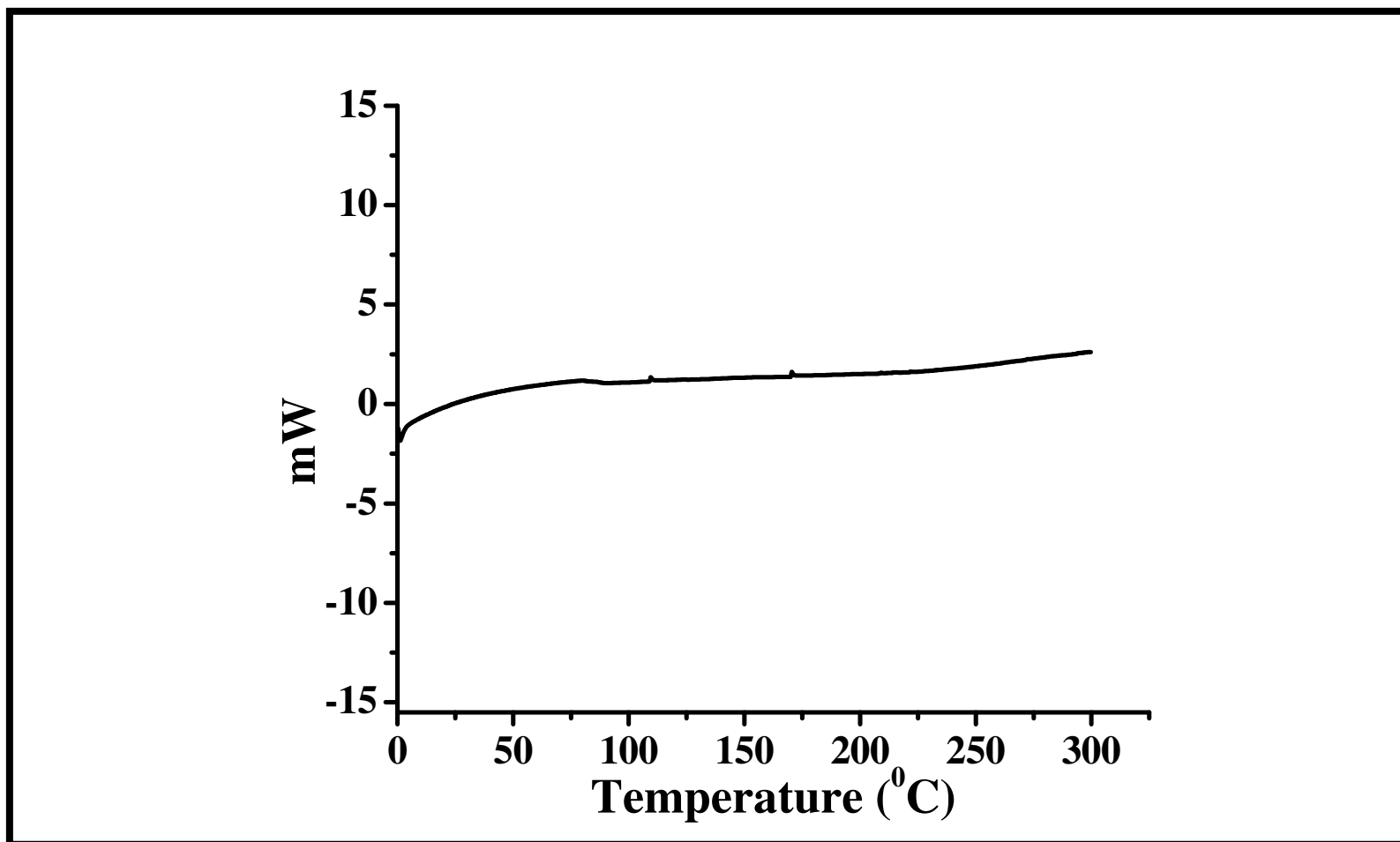


Figure 4.36: DSC thermogram of compound N-(4-hydroxyphenyl)-1,4,5,8-naphthalenetetracarboxylic-1,8-anhydride-4,5-imide (**1a**) (heating rate 10 K min⁻¹).

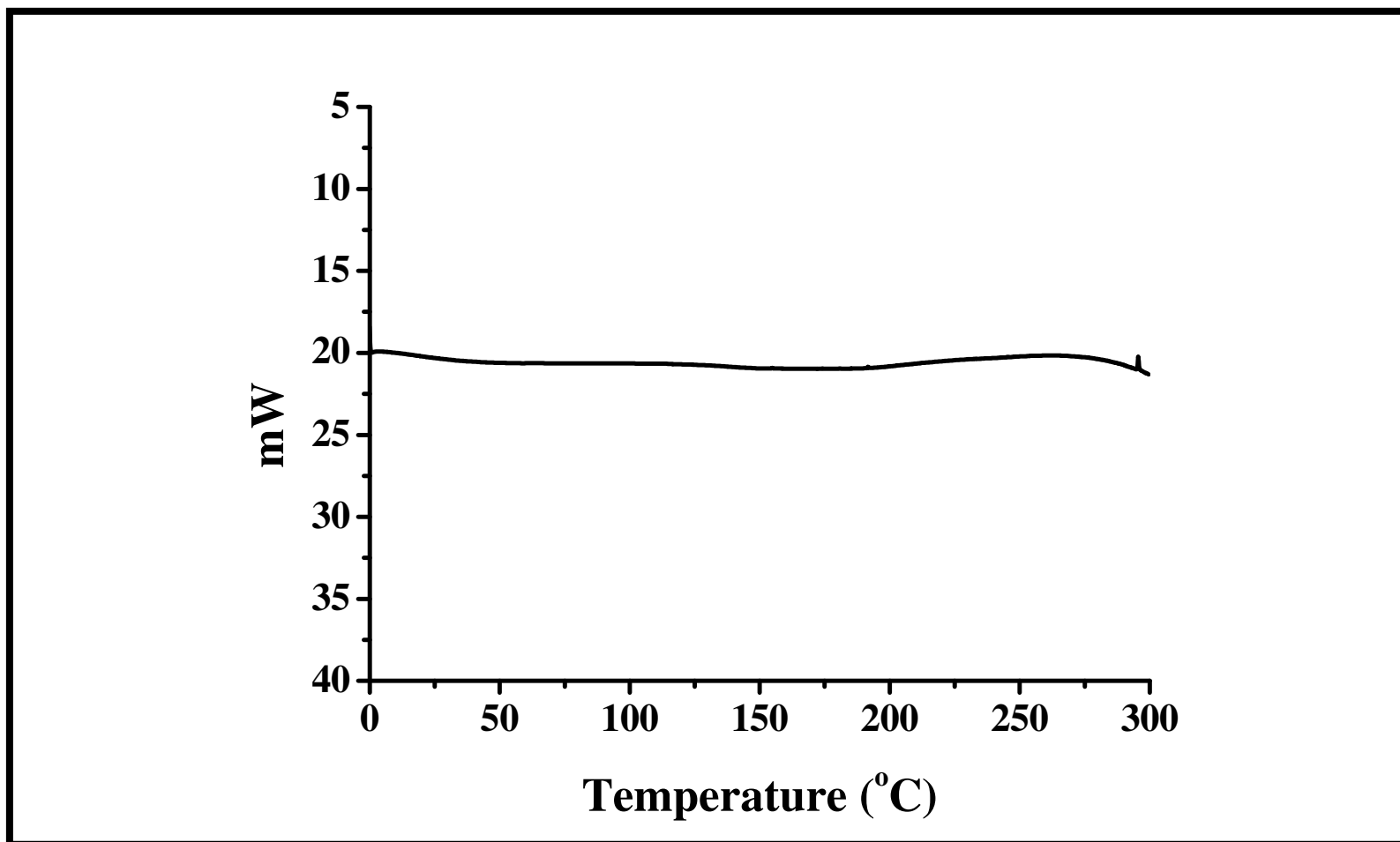


Figure 4.37: DSC thermogram of compound N-(4-hydroxyphenyl)-N'-[(S)-1-phenylethyl]-1,4,5,8-naphthalenetetracarboxydiimide (**2a**) (heating rate 10 K min⁻¹).

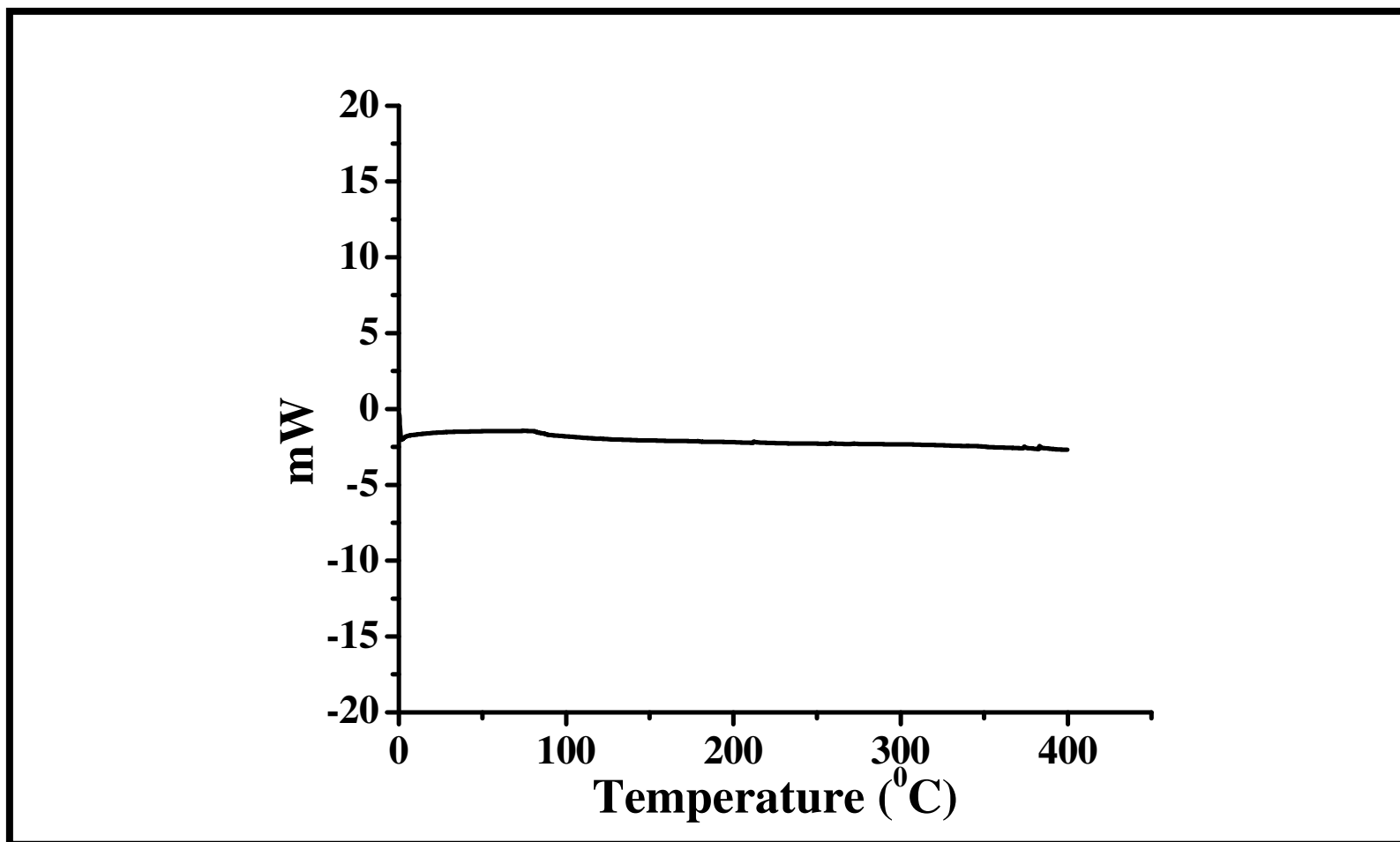


Figure 4.38: DSC thermogram of compound N-(4-hydroxyphenyl)-N'-[(S)-1-phenylethyl]-3,4,9,10-perylenetetracarboxydiimide (**5a**) (heating rate 10 K min⁻¹).

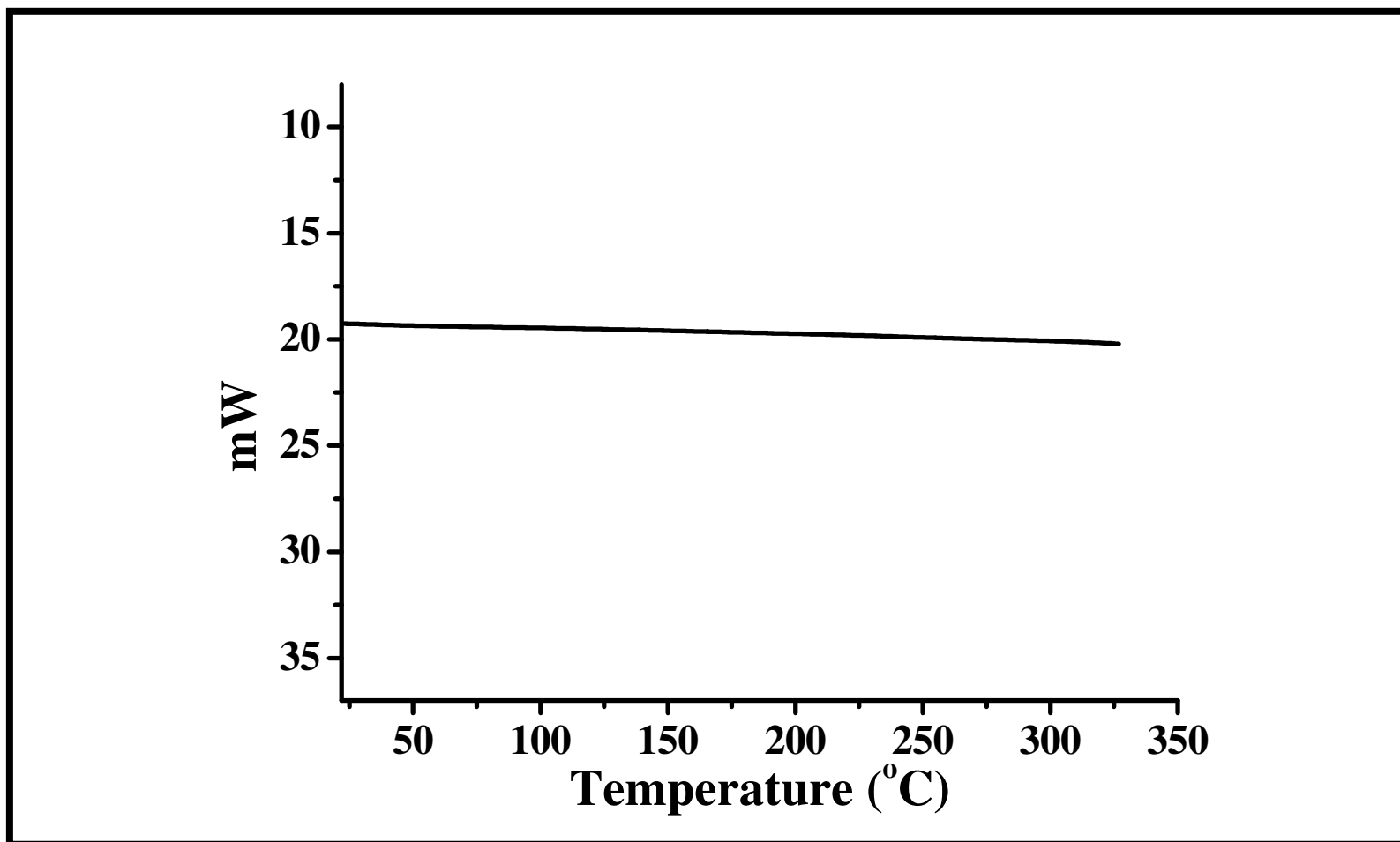


Figure 4.39: DSC thermogram of compound N-(2-aminohexanoic acid)-N'-(1-dehydroabietyl)-3,4,9,10 perylenetetracarboxydiimide (**5b**) (heating rate 10 K min⁻¹).

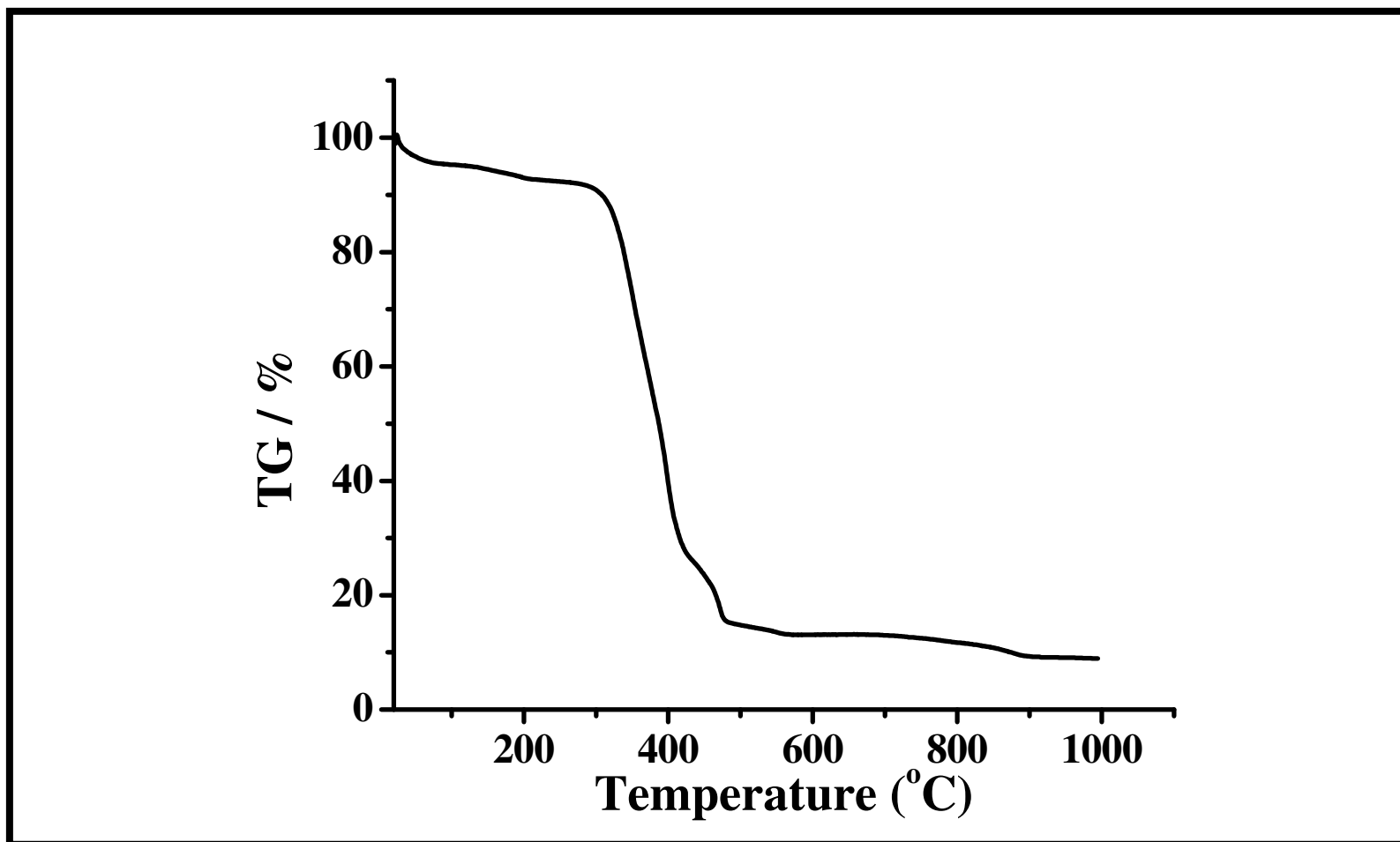


Figure 4.40: Thermal gravimetric analysis (TGA) of compound N-(4-hydroxyphenyl)-1,4,5,8-naphthalenetetracarboxylic-1,8-anhydride-4,5-imide (**1a**) (heating rate 5 K min⁻¹).

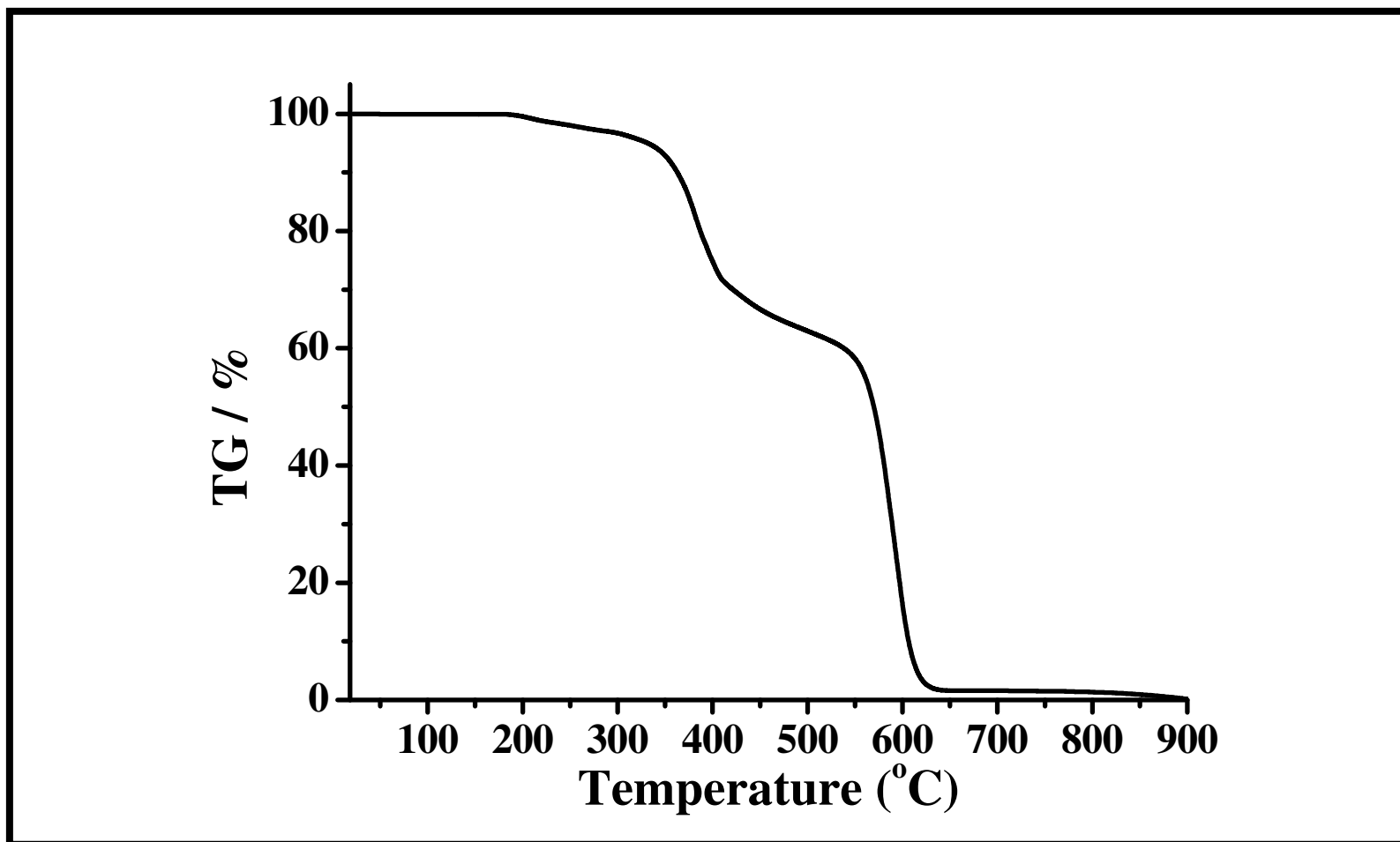


Figure 4.41: Thermal gravimetric analysis (TGA) of compound N-(4-hydroxyphenyl)-N'-[(S)-1-phenylethyl]-1,4,5,8-naphthalenetetracarboxydiimide (**2a**) (heating rate 5 K min⁻¹).

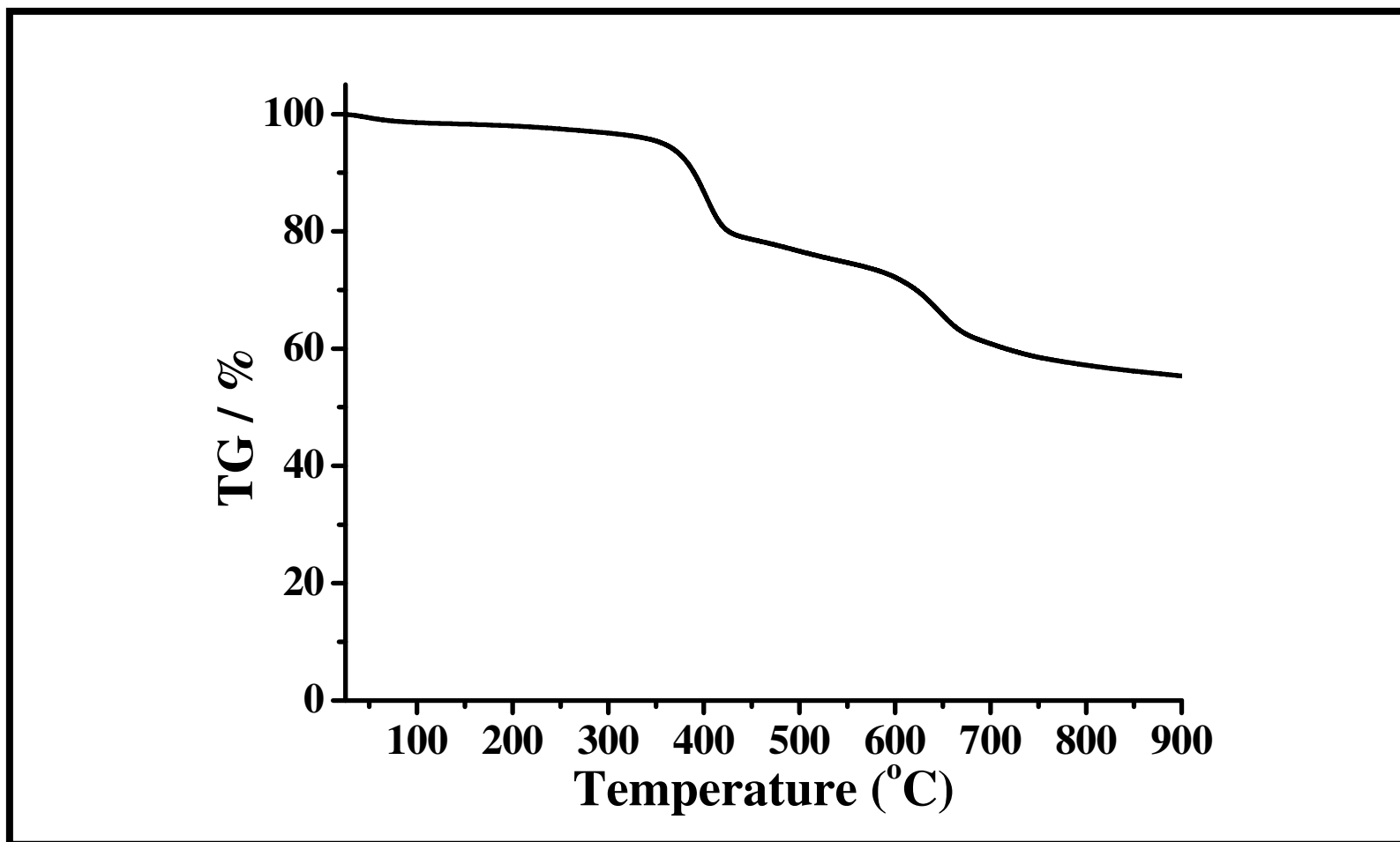


Figure 4.42: Thermal gravimetric analysis (TGA) of compound N-(4-hydroxyphenyl)-N'-[(S)-1-phenylethyl]-3,4,9,10-perylenetetracarboxydiimide (**5a**) (heating rate 5 K min⁻¹).

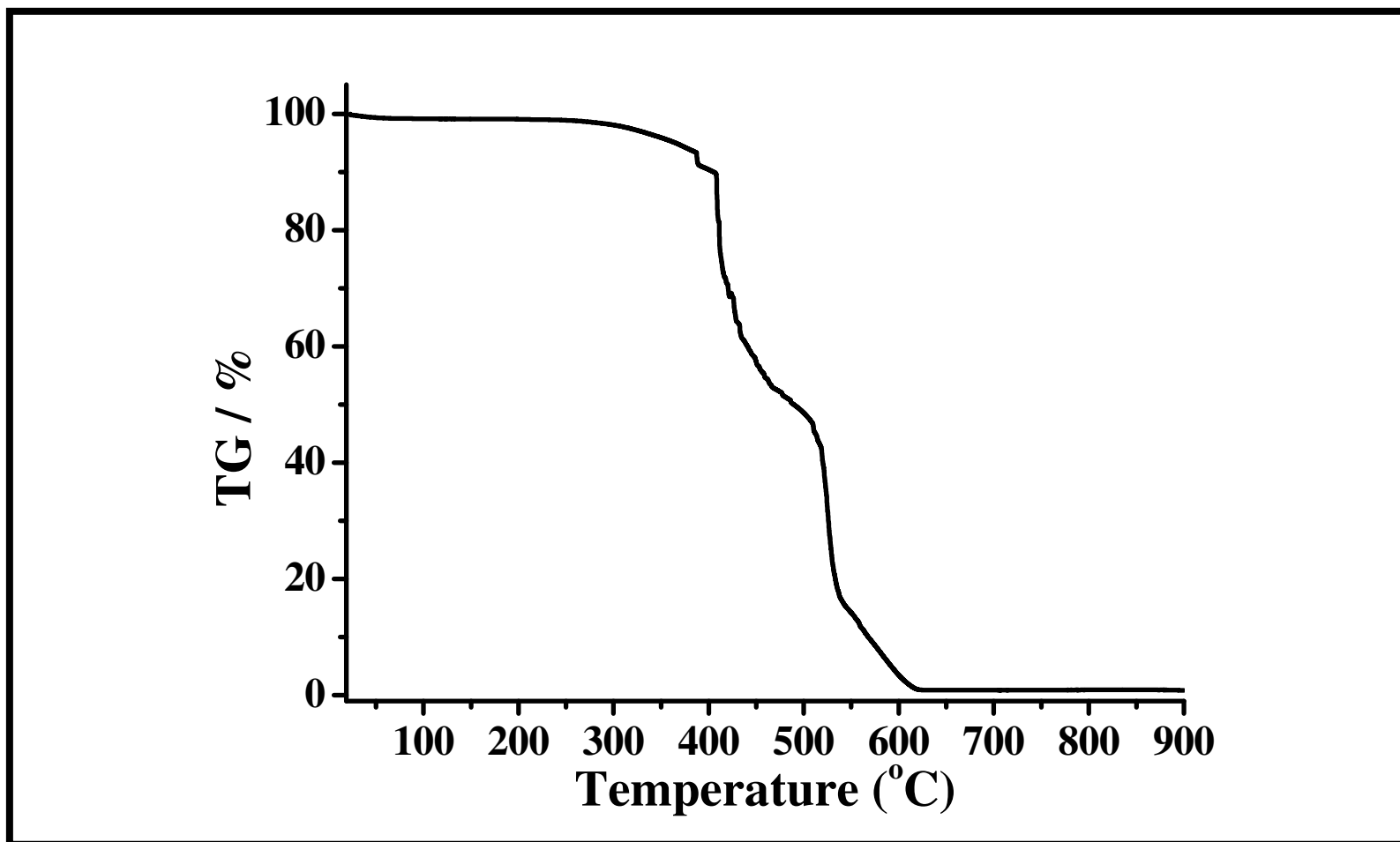


Figure 4.43: Thermal gravimetric analysis (TGA) of compound N-(2-aminohexanoic acid)-N'-(1-dehydroabietyl)-3,4,9,10 perylenetetracarboxydiimide (**5b**) (heating rate 5 K min⁻¹).

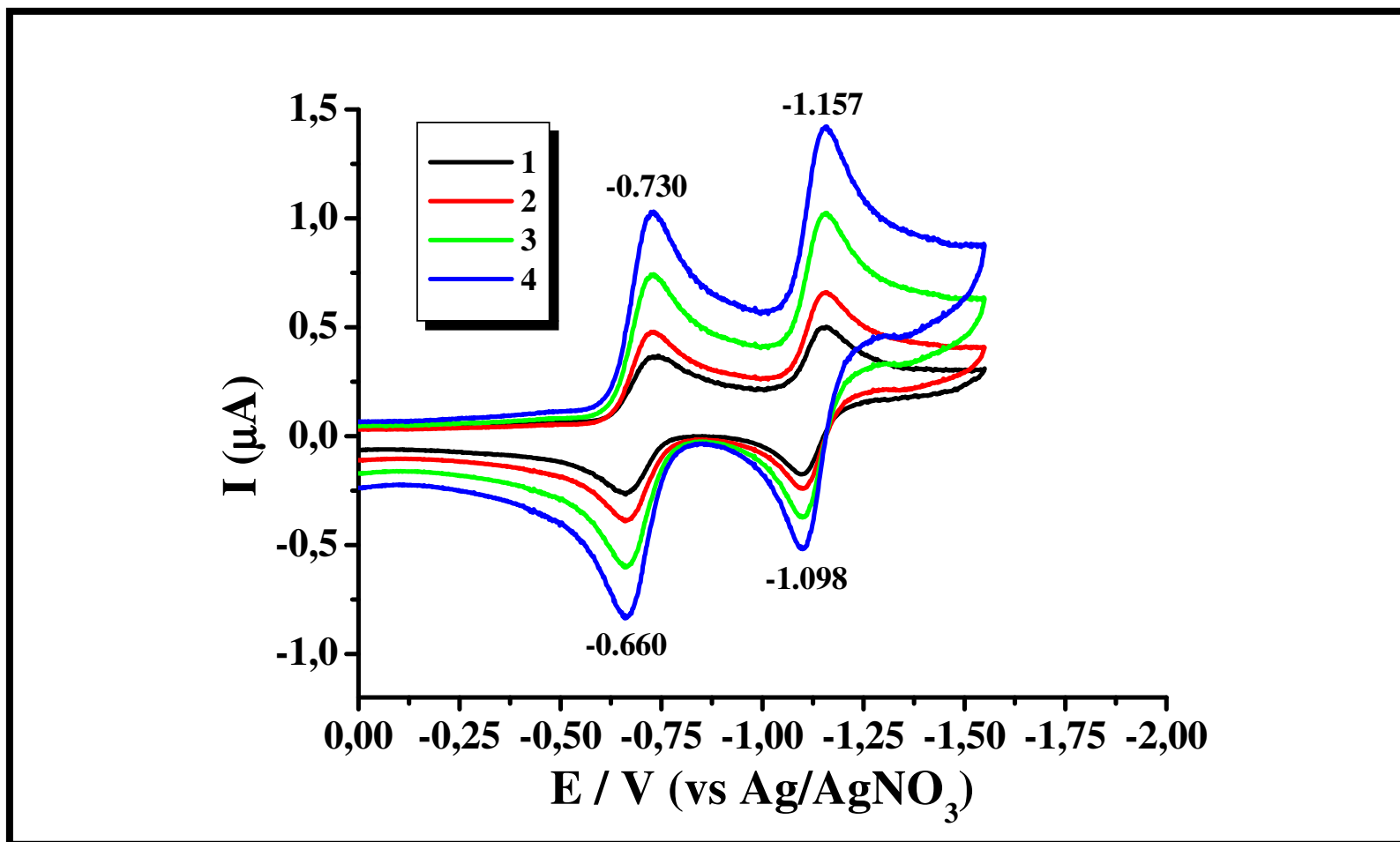


Figure 4.44: Cyclic voltammograms of compound N-(4-hydroxyphenyl)-1,4,5,8-naphthalenetetracarboxylic-1,8-anhydride-4,5-imide (**1a**) in dichloromethane; supporting electrolyte: TBAPF₆, scan rates (mVs⁻¹): 1 (50), 2 (100), 3 (200), 4 (300) at 25 °C.

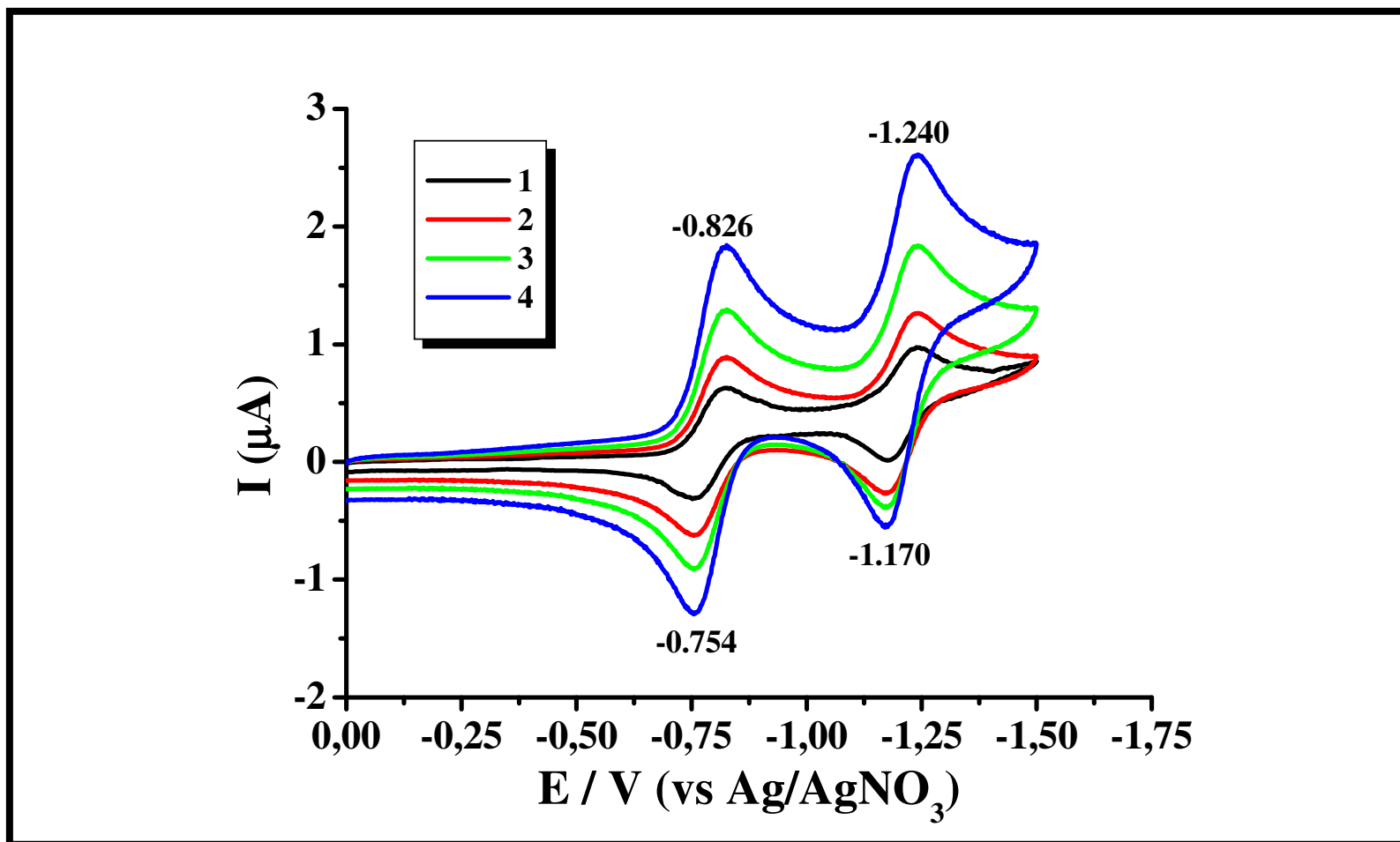


Figure 4.45: Cyclic voltammograms of compound N-(4-hydroxyphenyl)-1,4,5,8-naphthalenetetracarboxylic-1,8-anhydride-4,5-imide (**1a**) in acetonitrile; supporting electrolyte: TBAPF₆, scan rates (mVs⁻¹): 1 (50), 2 (100), 3 (200), 4 (300) at 25 °C.

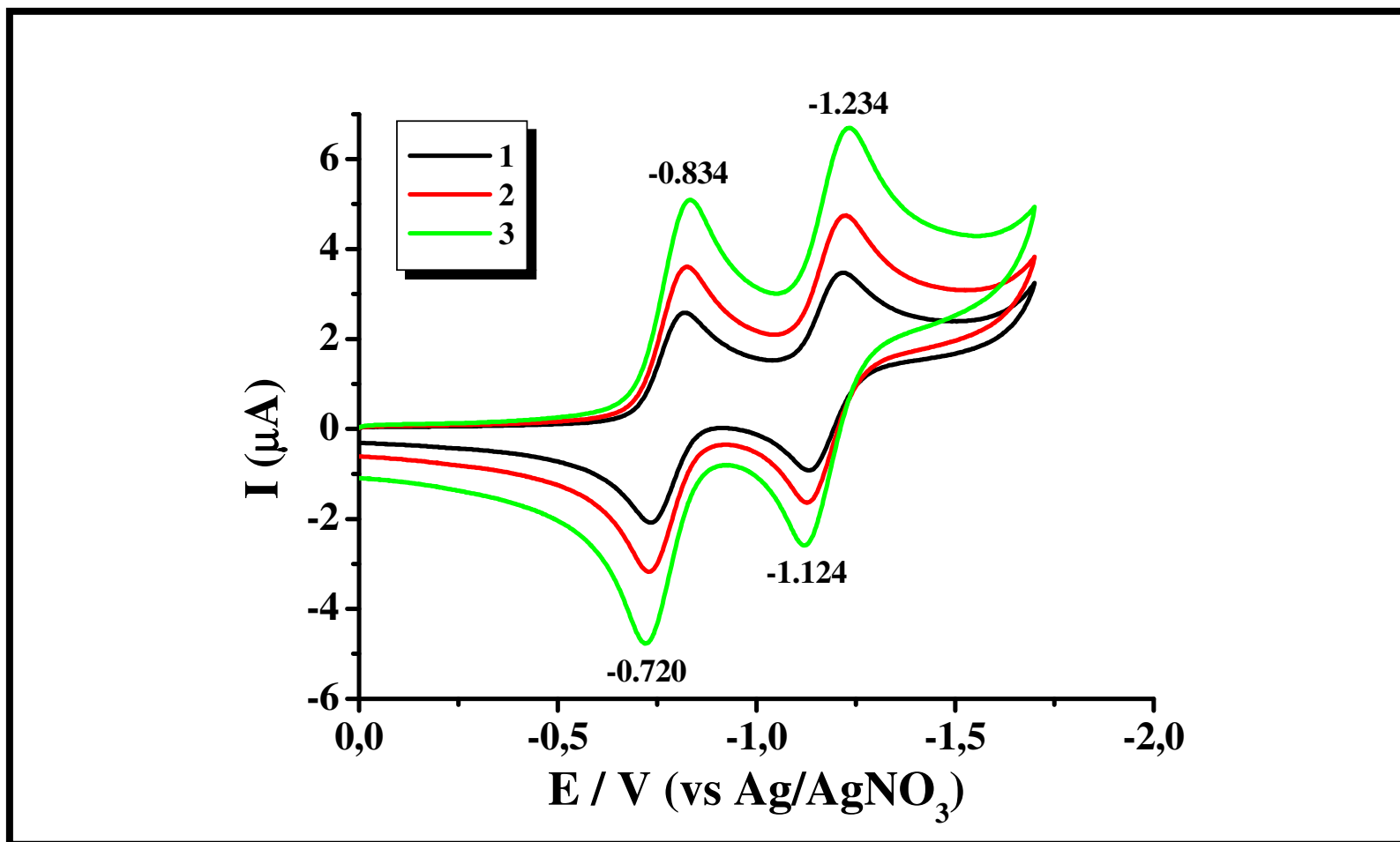


Figure 4.46: Cyclic voltammograms of compound N-(4-hydroxyphenyl)-N'-[(S)-1-phenylethyl]-1,4,5,8-naphthalenetetracarboxydiimide (**2a**) in chloroform; supporting electrolyte: TBAPF₆, scan rates (mVs⁻¹): 1 (50), 2 (100), 3 (200) at 25 °C.

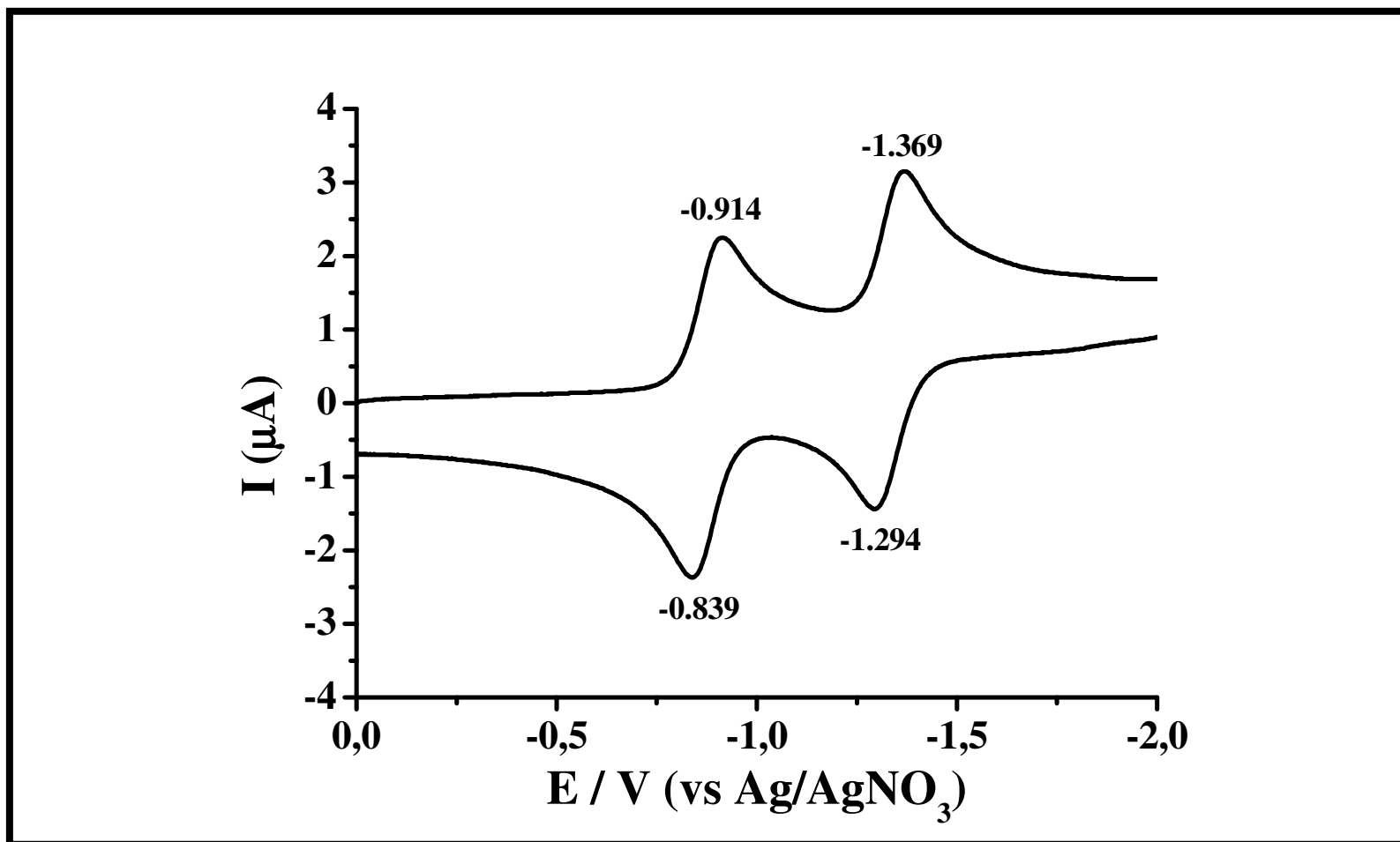


Figure 4.47: Cyclic voltammogram of compound N-(4-hydroxyphenyl)-N'-[(S)-1-phenylethyl]-1,4,5,8-naphthalenetetracarboxydiimide (**2a**) in DMSO; supporting electrolyte: TBAPF₆, scan rate (mVs⁻¹): 50 at 25 °C.

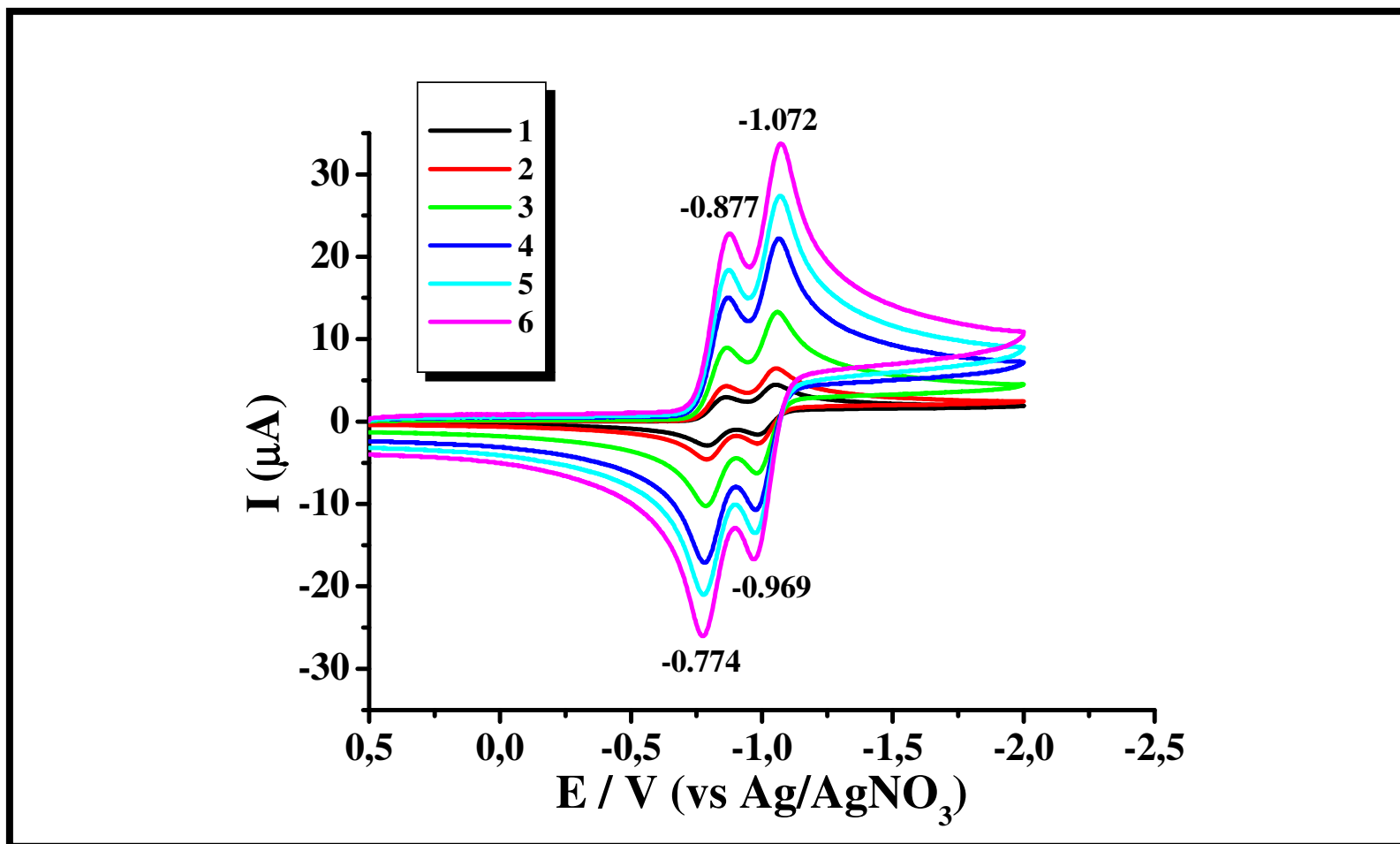


Figure 4.48: Cyclic voltammograms of compound N-(4-hydroxyphenyl)-N'-[(S)-1-phenylethyl]-3,4,9,10-perylenetetracarboxydiimide (**5a**) in chloroform; supporting electrolyte: TBAPF₆, scan rates (mVs⁻¹): 1 (50), 2 (100), 3 (300), 4 (600), 5 (800), 6 (1000) at 25 °C.

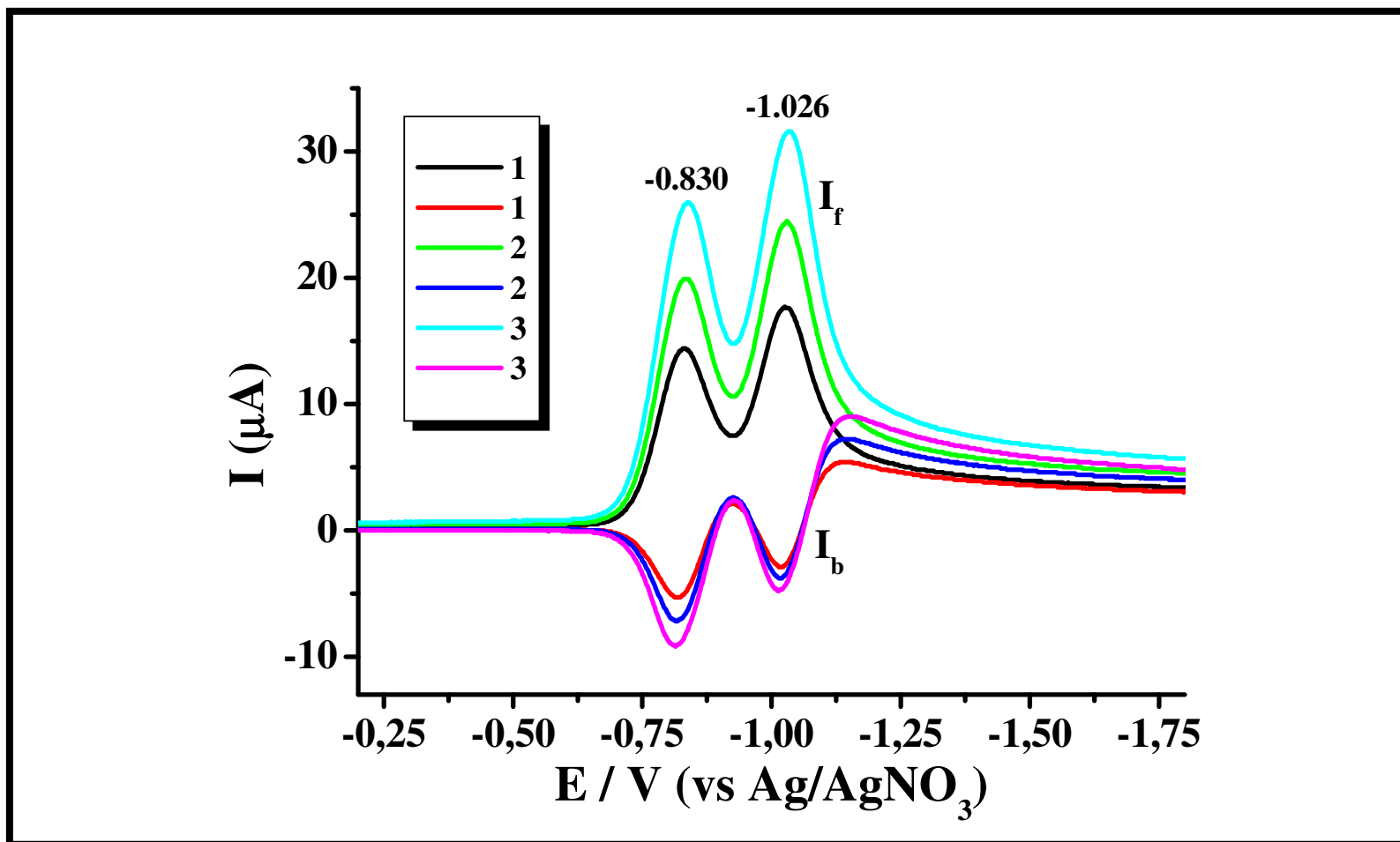


Figure 4.49: Square-wave voltammograms of compound N-(4-hydroxyphenyl)-N'-[(S)-1-phenylethyl]-3,4,9,10-perylenetetracarboxydiimide (**5a**) in chloroform; supporting electrolyte: TBAPF₆, ν (Hz): 1 (60), 2 (100), 3 (150) at 25 °C.

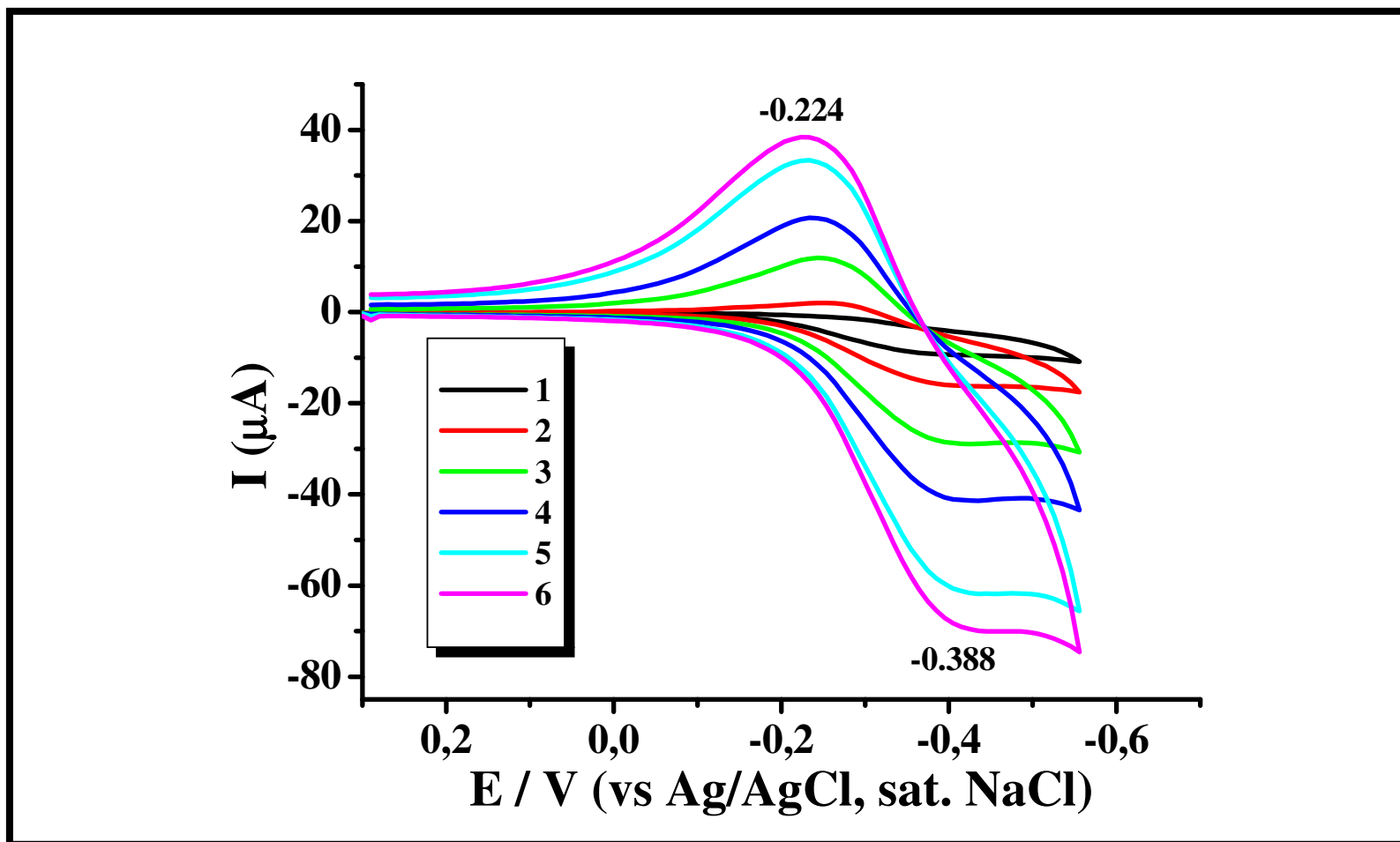


Figure 4.50: Solid state cyclic voltammograms of compound N-(4-hydroxyphenyl)-N'-[(S)-1-phenylethyl]-3,4,9,10-perylenetetracarboxydiimide (**5a**); supporting electrolyte: HCl, scan rates (mVs⁻¹): 1 (25), 2 (50), 3 (100), 4 (200), 5 (400), 6 (600) at 25 °C.

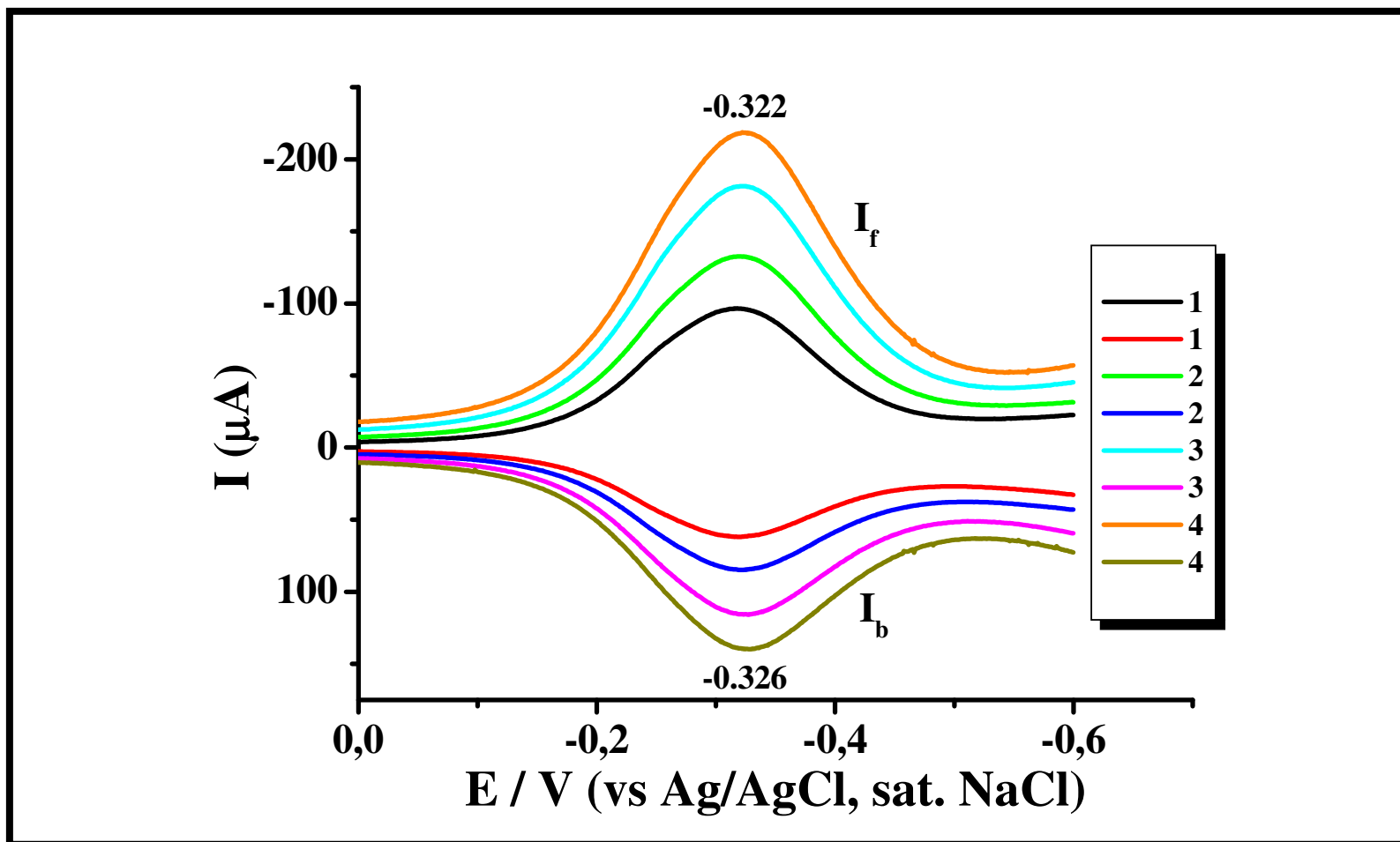


Figure 4.51: Solid state square-wave voltammograms of compound N-(4-hydroxyphenyl)-N'-[(S)-1-phenylethyl]-3,4,9,10-perylenetetracarboxydiimide (**5a**); supporting electrolyte: HCl, ν (Hz): 1 (50), 2 (100), 3 (200), 4 (300) at 25 °C.

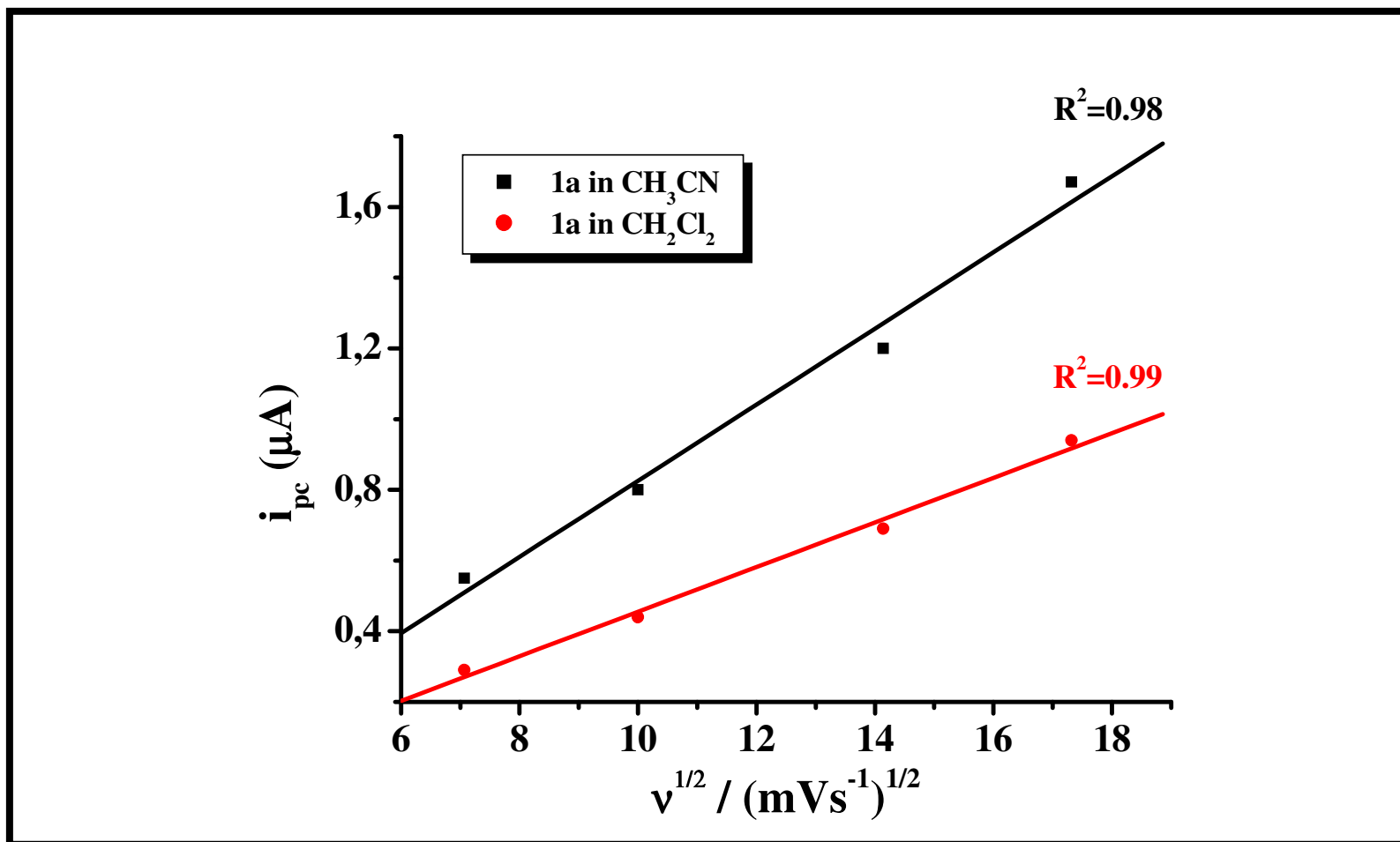


Figure 4.52: Effect of variation of scan rates on the cathodic peak currents of compound N-(4-hydroxyphenyl)-1,4,5,8-naphthalenetetracarboxylic-1,8-anhydride-4,5-imide (**1a**).

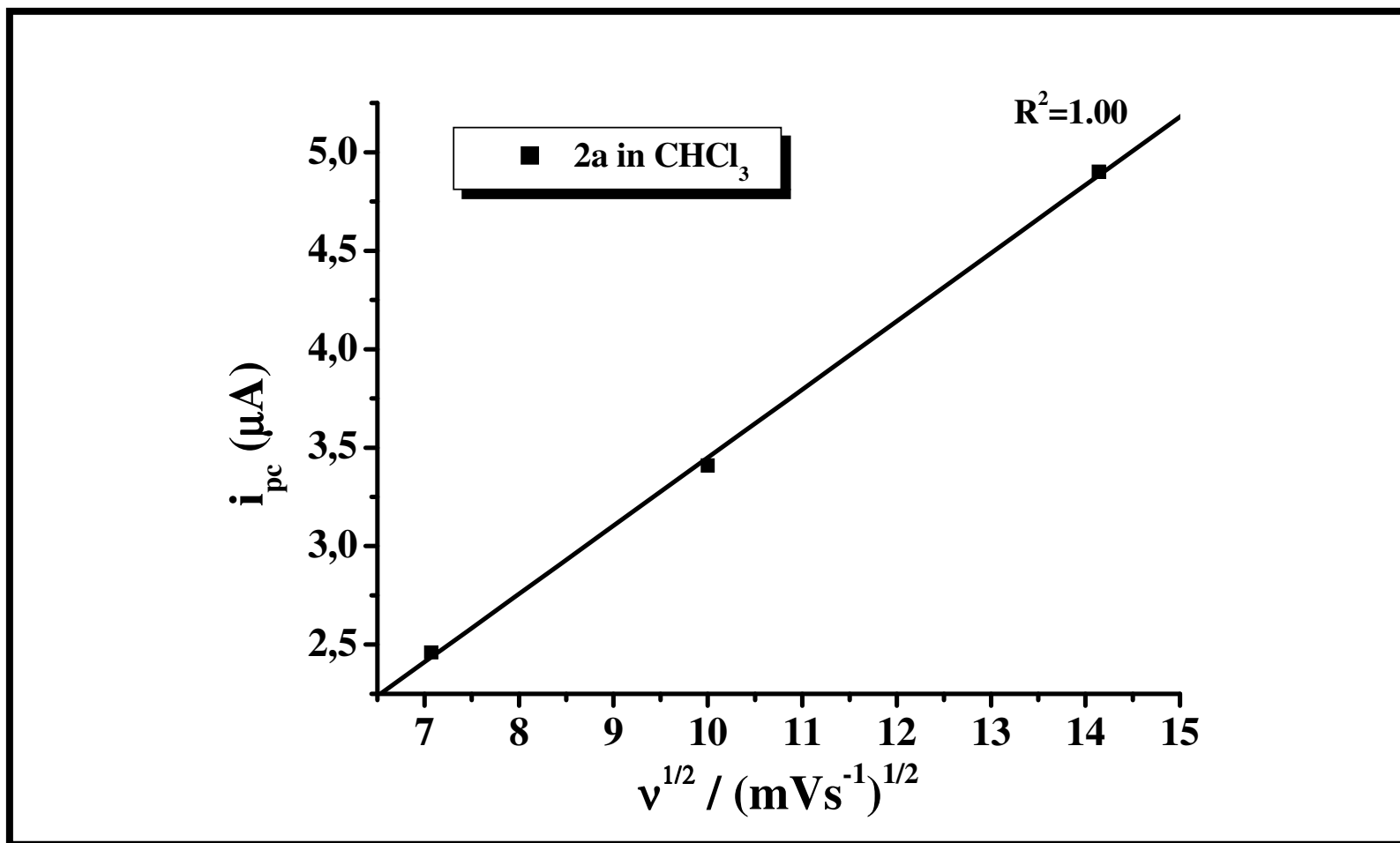


Figure 4.53: Effect of variation of scan rates on the cathodic peak currents of compound N-(4-hydroxyphenyl)-N'-[(S)-1-phenylethyl]-1,4,5,8-naphthalenetetracarboxydiimide (**2a**).

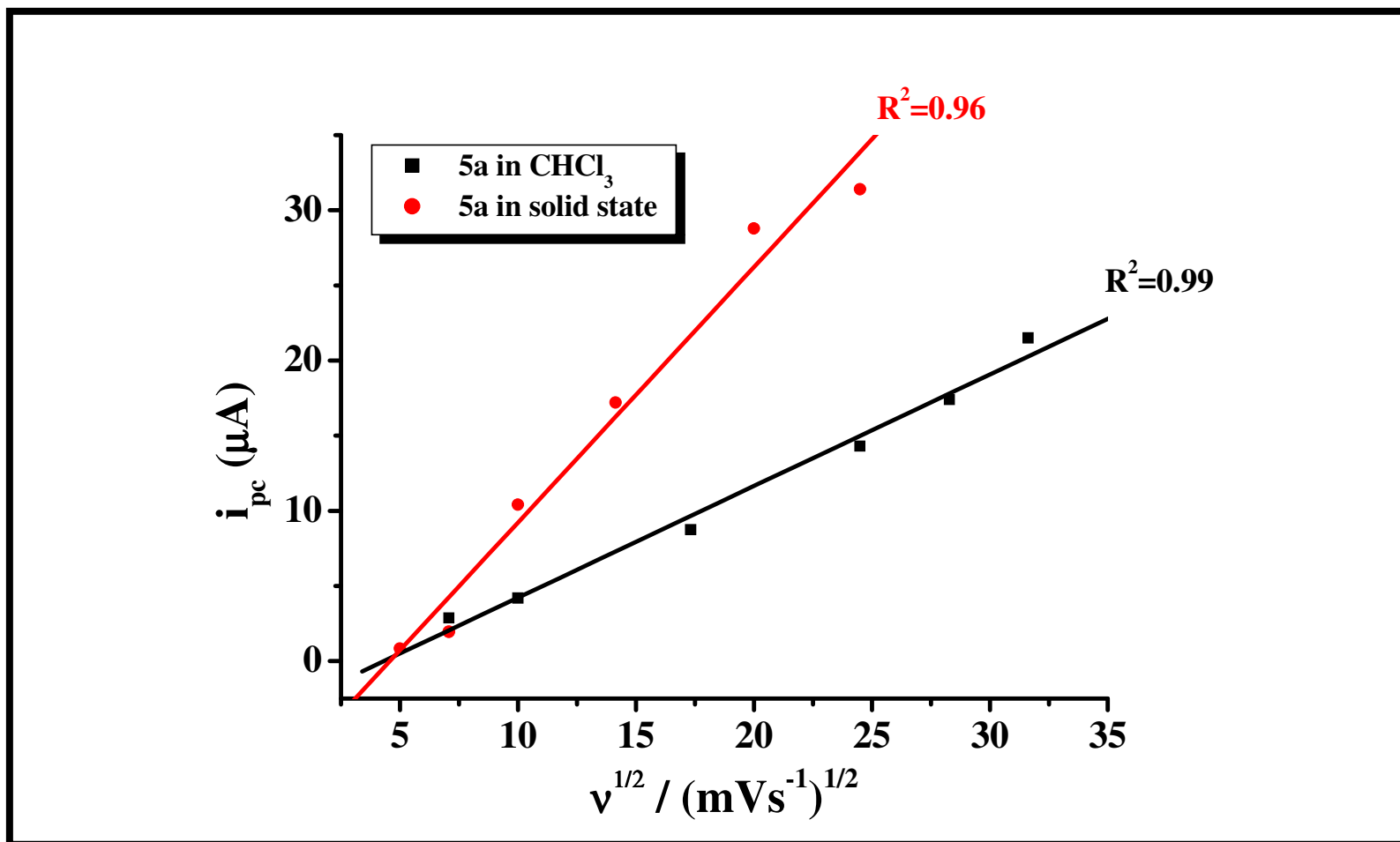


Figure 4.54: Effect of variation of scan rates on the cathodic peak currents of compound N-(4-hydroxyphenyl)-N'-[(S)-1-phenylethyl]-3,4,9,10-perylenetetracarboxydiimide (**5a**).

CHAPTER 5

RESULTS AND DISCUSSION

5.1 Synthesis and Characterization

Unsymmetrically substituted chiral naphthalene and perylene diimides were prepared according to the synthetic routes shown in Scheme 3.1 and Scheme 3.2, respectively. The diacid naphthalenetetracarboxylic acid monoanhydride was directly converted to naphthalene monoimide (**1a**) via condensation with 4-aminophenol at 110 °C for 10 h. The chiral unsymmetrical naphthalene diimide was synthesized via condensation of N-(4-hydroxyphenyl)-1,4,5,8-naphthalenetetracarboxylic-1,8-anhydride-4,5-imide (**2a**) with corresponding amine using m-cresol and isoquinoline as solvent mixture. Compounds **3** and **4** were synthesized according to the methods given in previous works (Pasaogullari, 2006). The unsymmetrical chiral perylene diimides (**5a** and **5b**) was synthesized via condensation of corresponding amine with N-alkyl-3,4,9,10-perylenetetracarboxylic-3,4-anhydride-9,10-imide using m-cresol and isoquinoline as solvent mixture. The structures of the compounds were characterized by ¹HNMR,

^{13}C NMR, MS, IR, and elemental analysis; the results clearly support the predicted chemical structures of all the compounds.

All IR spectra were consistent with the assigned structures as shown in Figures 4.2, 4.3, 4.4 and 4.5. The IR spectrum of **1a** exhibited characteristic absorption bands at 3430 (O-H stretch); 1783 (anhydride C=O stretch); 1709, 1660 (imides C=O stretch); 1609, 1591 (conjugated C=C stretch); 1351 (C-N stretch); 1102 (C-O-C stretch); 861 and 770 (C-H bend) cm^{-1} . In the IR spectrum of **2a**, the characteristic bands of the anhydride carbonyl stretching band (1783 cm^{-1}) had disappeared and were replaced by N-imides carbonyl stretching bands (1708 and 1660 cm^{-1}). Similarly, the characteristic band of the C-O-C stretching (1102 cm^{-1}) had disappeared and was replaced by C-N stretching band (1350 cm^{-1}). Other absorption bands of **2a** were very similar to those of **1a**. The IR spectrum of **5a** exhibited characteristic absorption bands at 3370 (O-H stretch); 3063 (aromatic C-H stretch); 2926 (aliphatic C-H stretch); 1698, 1659 (imides C=O stretch); 1594, 1577 (conjugated C=C stretch); 1354 (C-N stretch) 837 and 746 (C-H bend) cm^{-1} . The IR spectrum of **5b** exhibited characteristic absorption bands at 3480 (O-H stretch); 3083 (aromatic C-H stretch); 2955, 2930, 2867 (aliphatic C-H stretch); 1695, 1658 (imides C=O stretch); 1595, 1578 (conjugated C=C stretch); 1340 (C-N stretch) 856 and 748 (C-H bend) cm^{-1} .

Table 5.1 lists the solubility properties of **1a**, **2a**, **4a**, **4b**, **5a** and **5b**. Solubility of monoimides is lower than that of diimides which is dependent on intermolecular interactions that is affected by the rigidity and symmetry. The presence of secondary carbon atoms next to nitrogen atoms force the other substituents out of the plane of the

molecule and thereby hamper to face-to-face π - π stacking of the **2a**, **5a** and **5b**. The sterically hindered chiral substituents prevented the short π - π contacts of fluorophores and caused to higher solubility. With a less rigid **2a**, these effects are more pronounced comparing to **5a** and **5b** which contribute to the higher solubility. Similarly, chiral **5a** was poorly soluble compared to prior symmetrically substituted chiral perylene diimide (Amiralaei, 2008).

Table 5.1: Solubility of compounds **1a**, **2a**, **4a**, **4b**, **5a** and **5b**.

	Solubility ^a / Colour					
	1a	2a	4a	5a	4b	5b
CHCl₃	+ - Colorless	+ Brown	-	+ - Orange	-	+ Dark Red
CH₂Cl₂	+ - Colorless	+ Brown	-	+ - Orange	-	+ Dark Red
Pyridine	+ - Colorless	+ Brown	-	+ Yellow	-	+ Dark Red
Acetone	+ - Colorless	+ Brown	-	+ - Yellow	-	+ - Light Orange
EtOH	+ - Colorless	+ Brown	-	+ - Yellow	-	+ - Light Orange
NMP	+ - Pale Yellow	+ Brown	+ Red	+ Red	+ Orange	+ - Dark Red
MeOH	+ - Colorless	+ Brown	-	+ - Yellow	-	+ - Light Pink
CH₃CN	+ - Colorless	+ Brown	-	+ - Yellow	-	+ - Light Orange
DMF	+ Pale Yellow	+ Brown	+ Red	+ - Light Pink	-	+ - Light Red
DMSO	+ Pale Yellow	+ Brown	+ Red	+ - Red	-	+ - Light Red
H₂O	+ - Colorless	-	-	-	-	-

^a 0.1 mg in 1.0 mL of solvent. + soluble; + - partially soluble; - insoluble at RT. NMP: N-methylpyrrolidinone; DMF: dimethylformamide; DMSO: dimethyl sulfoxide.

The main fragmentation routes of the compounds **1a**, **2a** and **5a** are shown in Figures 4.6, 4.7 and 4.8. The mass spectrum of compound **1a** showed the corresponding molecular ion peak at 359 m/z , which was also the base peak. The fragment of 250 m/z was produced by the breakage of C_6H_4NO (Figure 4.6). The base peak again coincided with the molecular ion peak for compound **2a** at 463.5 m/z (M+1) (Figure 4.7). The fragment of 372.4 m/z was produced by the breakage of C_7H_7 . The mass spectrum of **5a** (Figure 4.8) showed the corresponding molecular ion peak at 587.7 m/z (M+1). The base peak occurred at 302.3 m/z was produced by the breakage of $C_{16}H_{17}N_2O_3$.

5.2 Absorption and Fluorescence Properties

The absorption and emission spectra of **1a** in nonpolar, polar protic and aprotic solvents are shown in Figures 4.13, 4.14, 4.25 and 4.26 (4.13: absorption spectra at 10^{-5} M concentration, 4.14: absorption spectra of filtered solution through a 0.2 μm SPR microfilter, 4.25: emission spectra at 10^{-5} M concentration, 4.26: emission spectra of filtered solution through a 0.2 μm SPR microfilter). The absorbance is significantly dependent on the polarity of solvent. Characteristically three absorption bands are observed in solvents (nonpolar and polar) where compound **1a** dissolves poorly such as $CHCl_3$, CH_2Cl_2 and CH_3CN (in $CHCl_3$: 334, 350, 370 nm). The broad long wavelength absorption band of **1a** in polar solvents EtOH, NMP, MeOH, DMF, DMSO and H_2O presents a solvent dependent charge transfer character corresponding to a shift of the electron density from the electron rich moiety (hydroxyl substituent) towards the imide carbonyls and it is significantly red-shifted compared to the bands in nonpolar solvents. The extension of the π conjugation system accounts for the narrowing of the HOMO-LUMO gap in the compound **1a**. Additionally, the lower degree of symmetry of **1a** may

induce a higher number of vibronic modes which results in a broader absorption bands. The small changes on absorption bands regarding to their initial shape upon filtration of the solutions through 0.2 μm SPR microfilter (Figure 4.14) indicate weak aggregated distributions in polar solvents except CHCl_3 , CH_2Cl_2 and CH_3CN . The absorption and emission spectra of **2a**, **5a** and **5b** in the same nonpolar, polar protic and aprotic solvents used in the electronic spectra of **1a** are shown in Figures 4.15, 4.16, 4.17, 4.18, 4.19, 4.20, 4.27, 4.28, 4.29, 4.30, 4.31 and 4.32. In contrast to **1a** the compounds **2a**, **5a** and **5b** exhibit the characteristic three absorption bands of the compounds in their absorption spectra (solvent DMSO; **2a**: 345, 360, 381 nm; **5a**: 461, 492, 529 nm; **5b**: 465, 490, 526 nm) indicating the absence of a strong charge transfer interaction in the ground state. The values of the absorption wavelength maxima for all solvents are nearly same without charge transfer complexation. Consequently, there is more intensive interaction between **1a** and solvent molecules so as to influence its shape of absorption spectra which is not observed for **2a**, **5a** and **5b**.

Interestingly, all the emission spectra of **1a** and **2a** show characteristically red shifted and broad excimer-like emissions (Figures 4.25, 4.26, 4.27, 4.28). The high Stokes shift (Table 5.2; **1a**: 123457 cm^{-1} , filtered solution through a 0.2 μm SPR microfilter (**1a**^{*}): 138889 cm^{-1} , **2a**: 120482 cm^{-1} and filtered solution through a 0.2 μm SPR microfilter (**2a**^{*}): 121951 cm^{-1}) value and broadest band for the spectrum taken in NMP showed the presence of a large number of internal conversions at the excited states. The high difference in Stokes shift between the solution taken at 10^{-5} M concentration and filtered solution through a 0.2 μm SPR microfilter was attributed to aggregation.

Table 5.2: Stokes shifts of **1a**, **2a**, **5a** and **5b**.

	Stokes Shift (cm ⁻¹)							
	1a	1a*	2a	2a*	5a	5a*	5b	5b*
CHCl₃	227273	222222	200000	256410	1000000	1000000	1111111	1111111
CH₂Cl₂	285714	204082	84034	172414	909091	909091	909091	909091
EtOH	169492	144928	81301	166667	714286	714286	769231	769231
NMP	123457	138889	120482	121951	769231	769231	625000	625000
MeOH	208333	277778	133333	192308	666667	666667	769231	769231
CH₃CN	270270	161290	91743	120482	769231	769231	909091	909091
DMF	294118	217391	344828	250000	769231	769231	769231	769231
DMSO	285714	200000	120482	156250	714286	714286	714286	714286
H₂O	178571	232558	-	-	-	-	-	-

* after filtration with 0.2 μm microfilter.

The emission spectra of **1a** and **2a** were very similar to the excimer-like emissions usually observed for π -stacked interacting molecules in solution. Besides the well resolved absorption bands for **2a**, the excimer-like emission of the compound has been thought as an important indication of weaker interacting π -stacks in solution. Additionally, the shape of the emission spectra and obtained peak maxima upon filtration of the solution through a 0.2 μm SPR microfilter indicates aggregated emission besides the excimer emission in the excited state. The fluorescence spectra of **5a** and **5b** taken at $\lambda_{\text{exc}} = 485$ nm showed mirror images of their absorption spectra with close and small Stokes shift and absence of excimer emission which proved the similarity between ground S_0 and excited S_1 states. As expected, dominance of rigidity and planarity gave small Stokes shift and greater reabsorptivity.

The emission spectra of compounds **1a** and **2a** were taken at $\lambda_{\text{exc}} = 360$ nm and the relative fluorescence quantum yields were determined in DMF by using anthracene as a standard in EtOH. The low fluorescence quantum yields of **1a** and **2a** are in good correlation with literature data (**1a**: 0.2% and **2a**: 0.8%) (Uzun, 2003). The emission spectra of **5a** and **5b** were taken at $\lambda_{\text{exc}} = 485$ nm and the relative fluorescence quantum yields were determined by using N, N'-didodecyl-3,4,9,10-perylenebis(dicarboxiimide) in CHCl_3 as standard. The lower fluorescence quantum yield of **5b** could be attributed to conformational changes, torsional movement, or other non-radiative decays (**5a**: 80% and **5b**:40%).

The absorption spectra of the compounds **1a**, **2a**, **5a** and **5b** in the solid state are shown in Figures 4.21, 4.22, 4.23 and 4.24. Table 5.3 provides a summary of the experimental spectroscopic data for all of the compounds together with calculated values. Intermolecular electron-donor-acceptor complex are formed for **1a** in the solid state which give rise to an intermolecular charge transfer absorption at 354 nm as an unresolved band. The main difference between the uv spectra in solid and solution states of **1a** is the shoulder around 373 nm in the solution spectra. Interestingly, the solid state uv spectra of **1a**, and **2a** are very similar to their spectra taken in solution which indicate weakly interacting π -stacks in solid state and similar intermolecular interactions in both states. It is worth noting that the solid state spectra of **5a** and **5b** are different in the absorptions maxima and band shapes which indicate different π interaction in solid state.

Table 5.3: Maximum absorption wavelengths λ_{max} (nm), extinction coefficients ϵ_{max} ($\text{l mol}^{-1} \text{cm}^{-1}$), oscillator strengths f , fluorescence quantum yields Φ_f ($\lambda_{\text{excit.}} = 360 \text{ nm}$ for **1a** and **2a**, $\lambda_{\text{excit.}} = 485 \text{ nm}$ for **5a** and **5b**), radiative lifetimes τ_0 (ns), fluorescence lifetimes τ_f (ns), fluorescence rate constants k_f (10^8 s^{-1}), rate constants of radiationless deactivation k_d (10^8 s^{-1}), optical activities $[\alpha]_D^{20}$, and singlet energies E_s (kcal mol^{-1}) data of **1a**, **2a**, **5a** in DMF and **5b** in CHCl_3 .

	λ_{max}	λ_{max} (solid- state)	ϵ_{max}	f	Φ_f	τ_0	τ_f	k_f	k_d	$[\alpha]_D^{20}$	E_s
1a	373	354	11732	0.4	0.002	5.34	0.01	1.9	948	---	76.7
2a	381	387	18318	0.6	0.008	3.63	0.03	2.8	341	-221.6	75.1
5a^a	526	551	70000	0.4	0.80	10.6	8.48 (4.2)	0.9	0.2	-24	54.4
5b	526	538	65695	0.4	0.40	10.9	4.35	0.9	1.3	+200	54.4

^a Experimental values are given in parantheses.

Solid state fluorescence of all compounds could not be obtained which is attributed to presence of aggregates and excimers, which normally reduce quantum efficiencies of emission in the solid state. Maximum absorption wavelengths (λ_{max} in nm), extinction coefficients (ϵ_{max}), oscillator strengths (f), fluorescence quantum yields Φ_f ($\lambda_{\text{excit.}} = 360 \text{ nm}$ for **1a** and **2a**, $\lambda_{\text{excit.}} = 485 \text{ nm}$ for **5a** and **5b**), radiative lifetimes τ_0 (ns), fluorescence lifetimes τ_f (ns), fluorescence rate constants k_f (10^8 s^{-1}), rate constants of radiationless deactivation k_d (10^8 s^{-1}), optical activities $[\alpha]_D^{20}$, and singlet energies E_s (kcal mol^{-1}) data of **1a**, **2a**, **5a** in DMF and **5b** in CHCl_3 , are given in Table 5.3. Notably, the high solvent sensitivity of the emissions of compounds **1a** and **2a** indicates a polar character for the emitting species. The excimer-like emission and the low fluorescence quantum rate constant in DMF supports the charge transfer complexes in solutions as well. The fluorescence lifetime of **1a** and **2a** are calculated as 10 and 30 ps respectively, which

support the ultra fast intersystem crossing from the singlet excited state. The fluorescence lifetime of **5a** is observed experimentally as 4.2 ns ($\lambda_{\text{exc}} = 530$ nm, Figure 4.33). The technique of time correlated single photon counting was used to record fluorescence lifetimes of the compound **5a**. The decay curve was multi-exponential and analysed by using the standard method of iterative reconvolution and nonlinear least square fitting method (Figure 4.33). The quality of calculated fits was judged using statistical parameters, the reduced χ^2 value and the residual data. Experimental radiative lifetimes, fluorescence lifetimes, fluorescence rate constants, rate constants of radiationless deactivation and singlet energies data of all the compounds were consistent with literature data (Pasaogullari, 2006).

The specific optical rotation ($[\alpha]_D^{20}$, alpha) of **2a**, **5a** and **5b** measured at 20 °C (**2a**: $c = 0.0194$ mg mL⁻¹ in DMF; **5a**: $c = 0.052$ mg mL⁻¹ in DMF; **5b**: $c = 0.012$ mg mL⁻¹ in CHCl₃) as -221.6, -24 and +200, respectively. Figures 4.34 and 4.35 show the CD spectra of **2a** in acetonitrile and ethanol, respectively. The compound **2a** showed prominent negative cotton effect which corresponds to the maximum absorption bands in the uv spectra recorded (acetonitrile: 362 and 382 nm, ethanol: 364 and 384 nm). No significant spectroscopic changes were observed in these two solvents. The CD signal provides support for the helical conformation of the synthesized compound. However no detectable cotton effect was obtained for compound **5a** in different attempts probably due to the aggregates in solution at room temperature.

5.3 Thermal Stability

The thermal behavior of all compounds was investigated by DSC (heating rate 10 K min⁻¹, Figures 4.36, 4.37, 4.38 and 4.39) and TGA (heating rate 5 K min⁻¹, Figures 4.40, 4.41, 4.42 and 4.43). All compounds exhibit no glass transition temperature in the DSC run. The curves showed the high decomposition temperatures (T_d) for the compounds. Compounds **1a**, **2a**, **5a** and **5b** were stable up to 323, 353, 373 and 408 °C, respectively. For compound **1a**, a rapid weight loss of 70% of the initial weight was occurred between 323 and 415 °C. When **1a** was heated to 900 °C, 91% of the initial weight was lost, and about 9% char yield observed. For compound **2a**, a rapid weight lost of 27% of the initial weight occurred between 353 and 405 °C. When **2a** was heated to 650 °C, 98% of the initial weight was lost rapidly and 2% char yield observed. Compound **2a** showed higher thermal stability than compound **1a** that could be attributed to the intermolecular forces, rigidity and symmetry of the structure. For compound **5a**, a rapid weight lost of 20% of the initial weight occurred between 373 and 423 °C. When **5a** was heated to 900 °C, 44% of the initial weight was lost rapidly and 56% char yield observed. For compound **5b**, a rapid weight lost of 54% of the initial weight occurred between 408 and 520 °C. When **5b** was heated to 620 °C, 99% of the initial weight was lost rapidly and 1% char yield observed. Remarkably, the compound **5a** showed better thermal stability at elevated temperature (symmetrical PDI: 2% char yield at 900 °C) with higher char yield compared with the symmetrical PDI bearing the same chiral substituent, and chiral unsymmetrical PDI **5b**.

5.4 Electrochemistry

The electrochemical characterization of all compounds were studied in detail using cyclic (CV: **1a**, **2a** and **5a**) and square-wave (SWV: **5a**) voltammetries in different solvents containing 0.1 M TBAPF₆ as a supporting electrolyte and in solid state (Figures 4.44, 4.45, 4.46, 4.47, 4.48, 4.49, 4.50 and 4.51) which summarized in Tables 4.13, 4.14, 4.15, 4.16 and 4.17. All the measured redox potentials, HOMO (highest occupied molecular orbital)/LUMO (lowest unoccupied molecular orbital) and band gap energy E_g values obtained from those are tabulated in Table 5.4.

All compounds undergo two reversible one electron reductions, the first of which is the reduction of the neutral compound to radical anion (**1a**⁻, **2a**⁻ and **5a**⁻) and the second reduction corresponds to the formation of the dianion (**1a**²⁻, **2a**²⁻ and **5a**²⁻) as shown in Scheme 5.1. Similarly, for compounds **1a**, **2a** and **5a** the values of the half-wave potential ($E_{1/2}$) were found to be independent of the scan rate, as was expected for a reversible system.

As shown in Figure 4.44 and Scheme 5.1, cyclic voltammogram of compound **1a** has shown two fast reversible one-electron reductions at -0.695 and -1.127 V (vs. Ag/AgNO₃, scan rate: 100 mV s⁻¹) with peak potential separations $\Delta E_{p1} = 67$ mV and $\Delta E_{p2} = 60$ mV, respectively in CH₂Cl₂. The calculated ΔE_p in the range 60-70 mV for **1a** shows that reversibility of electron transfer was fairly well maintained in this system.

Table 5.4: Cyclic^a voltammetry data and optical band gap energy E_g , HOMO, LUMO values of compounds **1a**, **2a** and **5a**.

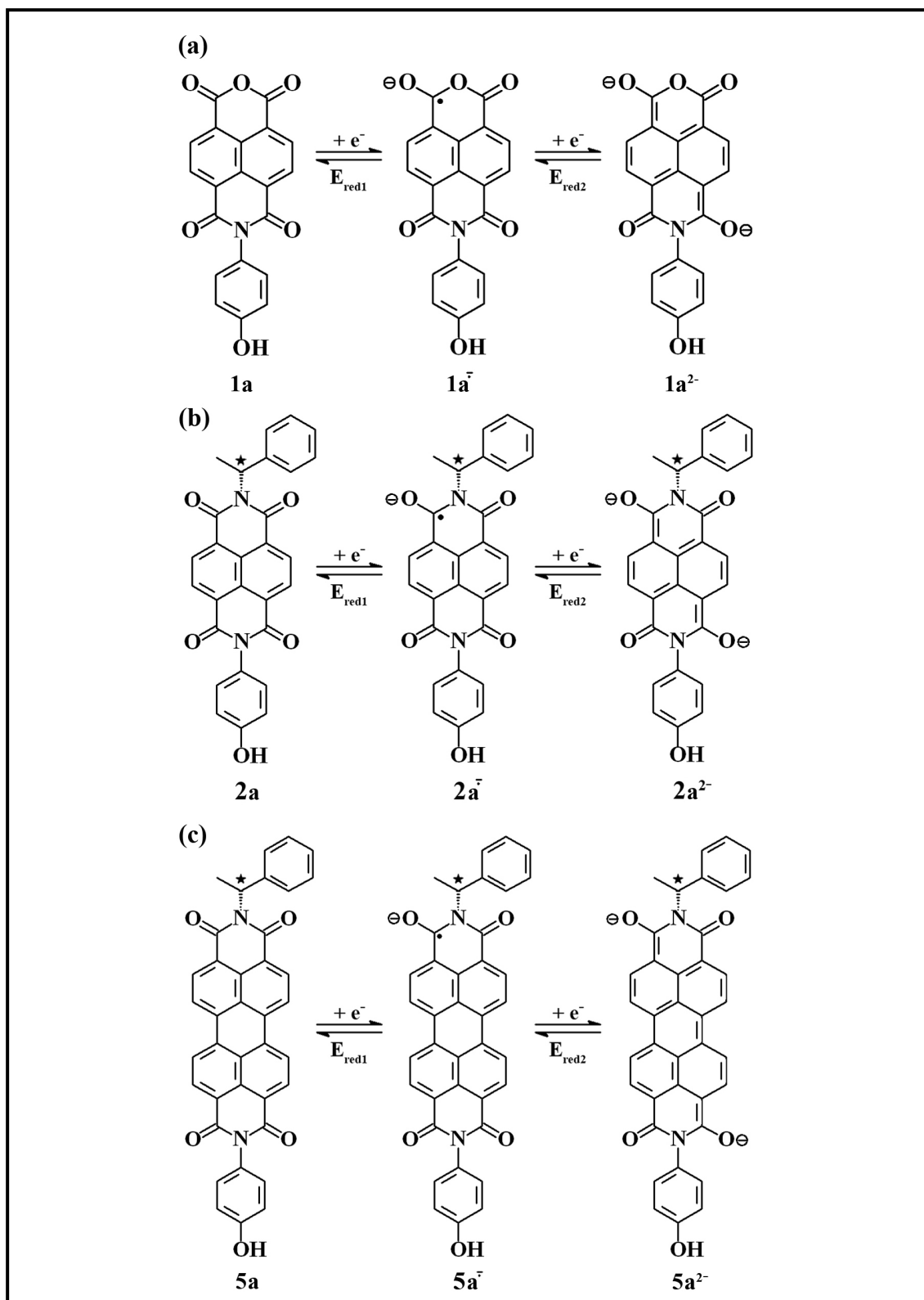
	1a^b (DCM)	2a^b (CHCl ₃)	5a^b (CHCl ₃)	5a^c (solid state)
E_{pc} / V	-0.729 -1.157	-0.825 -1.226	-0.865 -1.054	-0.244
E_{pa} / V	-0.662 -1.097	-0.728 -1.127	-0.789 -0.982	-0.378
ΔE_p / mV	67 60	97 99	76 72	134
E_{1/2} / V vs. Ag/AgNO ₃	-0.695 -1.127	-0.776 -1.176	-0.827 -1.018	-0.311 ^d
E_{Fc} / V vs. Ag/AgNO ₃	0.172 0.172	0.234 0.234	0.196 0.196	0.360 ^d
E_{1/2} / V vs. Fc	-0.867 -1.299	-1.010 -1.411	-1.023 -1.214	-0.671
E_g / eV	3.21	3.15	2.28	1.92
HOMO / eV	-7.14	-6.94	-6.06	-6.05
LUMO / eV	-3.93	-3.79	-3.78	-4.13

^a Scan rate of 100 mV s⁻¹.

^b Supporting electrolyte: 0.1 M tetrabutylammonium hexafluorophosphate (TBAPF₆).

^c Supporting electrolyte: 1 M HCl.

^d vs. Ag/AgCl



Scheme 5.1: Proposed two-step reduction mechanism for (a) **1a**; (b) **2a**; and (c) **5a**.

The reduction couples for **1a** were observed at $E_{1/2} = -0.790$ and -1.205 V (vs. Ag/AgNO₃, scan rate: 100 mV s⁻¹) in more polar solvent CH₃CN (Figure 4.45 and Scheme 5.1, $\Delta E_{p1} = 68$ mV and $\Delta E_{p2} = 68$ mV). **2a** has shown two fast reversible one-electron reductions at -0.776 and -1.176 V (vs. Ag/AgNO₃, scan rate: 100 mV s⁻¹) with peak potential separations $\Delta E_{p1} = 97$ mV and $\Delta E_{p2} = 99$ mV, respectively in CHCl₃ (Figure 4.46 and Scheme 5.1). These values were observed at -0.777 and -1.175 V at scan rate of 50 mV s⁻¹ with peak potential separations $\Delta E_{p1} = 86$ mV and $\Delta E_{p2} = 87$ mV. The reduction couples for **2a** were observed at $E_{1/2} = -0.876$ and -1.331 V (vs. Ag/AgNO₃, scan rate: 50 mV s⁻¹) in more polar solvent DMSO (Figure 4.47 and Scheme 5.1, $\Delta E_{p1} = 75$ mV and $\Delta E_{p2} = 75$ mV). Notably, $E_{1/2}$ shifts toward high negative potentials in more polar solvents indicating a more difficult reduction probably due to the stable complex formation (**1a**: CH₂Cl₂ and CH₃CN, **2a**: CHCl₃ and DMSO, Tables 4.13, 4.14 and 4.15).

In order to calculate the absolute energies of LUMO level of **1a** and **2a** with respect to the vacuum level, the redox data are standardized to the ferrocene/ferricenium couple which has a calculated absolute energy of -4.8 eV (Bredas, 1983; Peng, 1998). The LUMO energies of the **1a** and **2a** were calculated from cyclic voltammograms (Table 5.4) as -3.93 and -3.79 eV, respectively. The optical band gap, E_g values, were calculated approximately 3.21 and 3.15 eV for the compound **1a** and **2a**, respectively where E_g was obtained from the edge of the electronic absorption band with E_g (eV) = hc/λ ($h = 6.626 \times 10^{-34}$ J s, $c = 3 \times 10^{10}$ cm s⁻¹, 1 eV = 1.602×10^{-19} J). From this value, the HOMO energies of **1a** and **2a** were estimated from the relationship $E_{\text{HOMO}} = E_{\text{LUMO}} - E_g$, as -7.14 and -6.94 eV, respectively.

The electrochemical stability and reversibility of the redox processes of **1a** and **2a** were examined using cyclic voltammetry in different solvents (**1a**: CH₂Cl₂ and CH₃CN, **2a**: CHCl₃). Electrochemical stability of the compounds was examined by measuring repeated cycles of redox processes. Compound **1a** showed completely reversible reduction steps for the entire scanning rate in a region of 50 to 300 mV s⁻¹. As shown in Table 4.14, the ΔE_p was about 59-78 mV for each cycle of **1a** in CH₂Cl₂. Similar results were attained with the solvent CH₃CN. Compound **2a** showed completely reversible reduction steps for the entire scanning rate in a region of 50 to 200 mV s⁻¹. At the large ΔE_p values (114 mV at 200 mV s⁻¹) which indicate the limitation due to charge transfer kinetics the reversibility of the compound **2a** showed poor reversibility. According to standard reversibility criteria, each reduction process indicates reversible, diffusion-controlled one-electron transfer. A plot of peak current against square root of scan rate was found to be linear as shown in Figures 4.52 and 4.53 for compounds **1a** and **2a** (**1a**: in CH₂Cl₂ R² = 0.99 and CH₃CN R² = 0.99, **2a**: in CHCl₃ R² = 1.00), which fulfils the conditions for diffusion controlled processes.

The diffusion coefficients D were measured by cyclic voltammetry according to Randles-Sevick equation (Bard, 1980). The diffusion coefficients (D) of **1a** and **2a** in solution were estimated from the slope of the plot i_{pc} vs. v^{1/2} (Figures 4.52 and 4.53). Accordingly, the diffusion coefficients were determined as 8.73 x 10⁻⁸ and 2.55 x 10⁻⁷ cm² s⁻¹ for **1a** in CH₂Cl₂ and CH₃CN, respectively, and 2.63 x 10⁻⁶ cm² s⁻¹ for **2a** in CHCl₃.

The electrochemical behaviour of **5a** was investigated using cyclic (CV) and square-wave (SWV) voltammetries in chloroform containing 0.1 M TBAPF₆ as a supporting electrolyte and in solid state containing HCl as supporting electrolyte (Figures 5.48, 5.49, 5.50 and 5.51). All the measured redox potentials, HOMO (highest occupied molecular orbital)/LUMO (lowest unoccupied molecular orbital) and band gap energy E_g values obtained from those are tabulated in Table 5.4. As shown in Figures 4.48, 4.49 and Scheme 5.1, compound **5a** displays reduction processes in cyclic and square-wave voltammetries. Cyclic voltammogram of compound **5a** has shown two fast reversible one-electron reductions at -0.827 and -1.018 V (vs. Ag/AgNO₃, scan rate: 100 mV s⁻¹) with peak potential separations $\Delta E_{p1} = 76$ mV and $\Delta E_{p2} = 72$ mV, respectively in CHCl₃ (Figure 4.48 and Scheme 5.1). For compound **5a**, the calculated ΔE_p in the range of 60-70 mV shows that reversibility of electron transfer was fairly well maintained in this system. The square-wave voltammograms of **5a** (Figure 4.49) showed reversible reduction potentials at -0.830 and -1.026 V (vs. Ag/AgNO₃, frequency: 60 Hz). Similar results were found via cyclic and square-wave voltammetric studies. These properties are in agreement with the literature data (Pasaogullari, 2006).

In order to investigate the solid state electrochemical properties of compound **5a** the voltammetry of immobilized microparticles was applied. This technique is a simple and powerful tool for characterizing the thermodynamics and elucidating the redox mechanisms of electroactive compounds which are poorly soluble in water (Kahlert, 1998; Lovric, 1999; Lovric, 2000; Schröder, 2000; Hermes, 2001; Widmann, 2002; Grygar, 2002). The basic principle of the voltammetry of immobilized microparticles comprises mechanical attachment of the substance on the surface of the working

electrode (paraffin impregnated graphite electrode, i.e., PIGE), and immersing the modified electrode in an aqueous electrolyte solution. If the substance is electroactive, and if its product is insoluble in water, for reasons of charge neutrality, ions must be exchanged with the solution. In case of a reduction, either anions, if available, must leave the solid, or cations must be transferred from the solution into the solid phase. The processes of coupled electron and ion transfer occur simultaneously and give rise to a single voltammetric response. All the voltammetric measurements were repeated several times and the values of the reduction potentials were found to be reproducible within ± 3 mV.

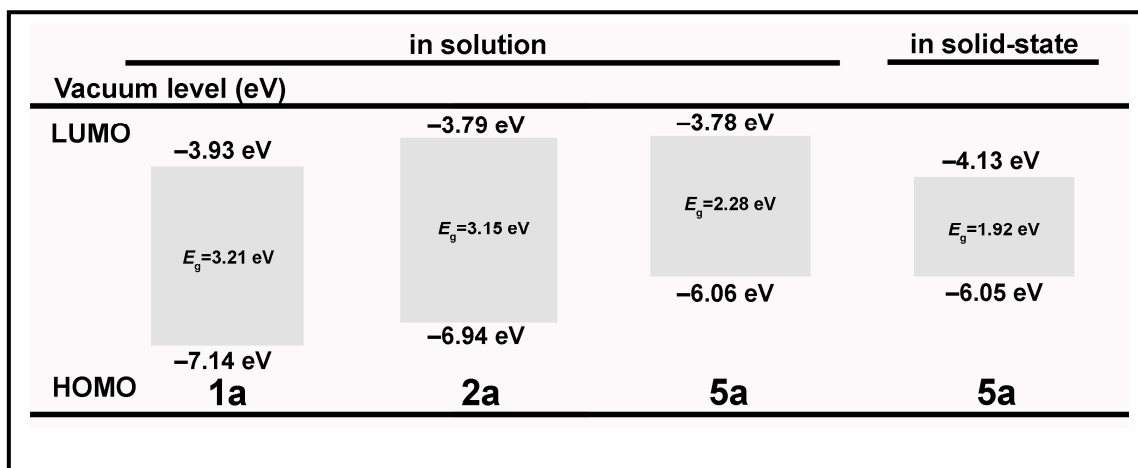
The solid-state electrochemical property of **5a** was determined with cyclic (CV) and square-wave (SWV) voltammetries (CV: Figure 4.50, SWV: Figure 4.51). All the measured redox potentials, HOMO (highest occupied molecular orbital)/LUMO (lowest unoccupied molecular orbital) and band gap energy E_g values obtained from those are tabulated in Table 5.4. The cyclic voltammograms of compound **5a** showed one reversible reduction wave (Figure 4.50), implying the formation of anions (**5a**⁻) at -0.311 V (vs. Ag/AgNO₃, scan rate: 100 mV s⁻¹) with peak potential separation $\Delta E_{p1} = 134$ mV (Table 5.4). Similarly, the square-wave voltammograms of **5a** (Figure 4.51) showed reversible reduction potential at -0.325 V (vs. Ag/AgNO₃, frequency: 50 Hz). Cyclic and square-wave voltammetric results were in good agreement. The reduction potential value is more positive than that observed for free **5a** in solution indicating the easier reduction with higher reduction rate (Table 5.4). Interestingly, the compound **5a** has shown lower solid state reduction potentials comparing to the reductions of CN-substituted derivatives (CN-NDI and CN-PDI) and same with the symmetrical substituted chiral

perylene diimide bearing the same chiral substituent which were measured with similar way at earlier published work (Uzun, 2003; Amiralaei, 2008). The differing results could be attributed to the intermolecular forces, rigidity and symmetry of the structure.

The electrochemical stability and reversibility of the redox processes of **5a** was examined using cyclic voltammetry and square-wave voltammetries in CHCl_3 (Figures 4.48, 4.49 and Table 4.16) and solid state (Figures 4.50, 4.51 and Table 4.17). Electrochemical stability in CHCl_3 was examined by measuring repeated cycles of redox processes. **5a** showed completely reversible reduction steps for the entire scanning rate in a region of 50 to 1000 mV s^{-1} . As shown in Table 4.16, the calculated peak current ratio, i_{pa} (anodic current) / i_{pc} (cathodic current) was equal to unity and the ΔE_p was about 70-103 mV for each cycle in CHCl_3 . Notably, higher ΔE_p value (103 mV) at 1000 mV s^{-1} scanning rate shows more difficult reduction. According to standard reversibility criteria, each reduction process indicates reversible, diffusion-controlled one-electron transfer. Similarly, the solid state electrochemical stability and reversibility of the redox processes of **5a** was examined using cyclic and square-wave voltammetries (Figures 4.50, 4.51 and Table 4.17). Electrochemical stability of **5a** was examined by measuring repeated cycles of redox processes. Compound **5a** showed completely reversible reduction steps for the entire scanning rate in a region of 25 to 600 mV s^{-1} and 50 to 300 Hz. All voltammograms have shown only a slight shift of peak (SWV) or formal potentials (CV) of all compounds by 10 mV which indicate the electrochemical reversibility of the investigated system. As shown in Table 4.17, the calculated peak current ratio, $i_{\text{pa}} / i_{\text{pc}}$ was equal to unity and the ΔE_p was about 134-164 mV for each cycle.

A plot of peak current against square root of scan rate was found to be linear as shown in Figure 4.54 for compound **5a** (in CHCl₃ R² = 0.99, in solid state R² = 0.96), which fulfils the conditions for diffusion controlled processes. Additionally, at the large ΔE_p values which indicate the limitation due to charge transfer kinetics the reversibility of the compound showed poor reversibility.

The LUMO energies of **5a** in CHCl₃ and solid-state were calculated from cyclic voltammograms (Figures 4.50, 4.51 and Table 5.4) as -3.78 and -4.13 eV, respectively. The optical band gap, E_g values, were calculated approximately 2.28 and 1.92 eV for the compound **5a** in CHCl₃ and solid-state, respectively. From these values, the HOMO energies of **5a** were estimated as -6.06 and -6.05 eV, respectively. The remarkably smaller LUMO and E_g value were obtained at the solid state characterization of **5a** as compared to those obtained from its solution state (Scheme 5.2).



Scheme 5.2: Schematic energy diagram of **1a**, **2a** and **5a**.

The diffusion coefficients D of **5a** in CHCl₃ and solid state were measured by cyclic voltammetry according to Randles-Sevcik equation (Bard, 1980). Accordingly, the

diffusion coefficients were determined as 1.21×10^{-5} and $1.62 \times 10^{-6} \text{ cm}^2 \text{ s}^{-1}$ for **5a** in CHCl_3 and solid state, respectively.

CHAPTER 6

CONCLUSION

In conclusion, one new naphthalene monoimide (**1a**) and three new unsymmetrically substituted chiral diimides (**2a**, **5a** and **5b**) having large π -conjugated systems have been successfully synthesized. Their structures have been well determined and the photophysical, thermal, electrochemical, chiroptical and intramolecular charge transfer properties have been investigated. **1a**, **2a**, **5a** and **5b** showed high thermal stability. Compound **1a** exhibits an intramolecular charge transfer complexation in its absorption spectrum in polar solvents corresponding to a shift of the electron density from the electron rich moiety (hydroxyl substituent) towards the imide carbonyls. Additionally, the lower degree of symmetry of **1a** may induce a higher number of vibronic modes which results in broader absorption bands. The difference in complex formation between polar and non-polar solvents was attributed to the higher concentration of free reactive compound **1a**. Excimer-like emissions were obtained in nonpolar, polar protic and aprotic solvents for **1a** and **2a**. Interestingly, all the emission spectra of **1a** and **2a** show characteristically red shifted and broad excimer-like emissions. The high Stokes shift ($123457 - 120482 \text{ cm}^{-1}$) value and broadest band for the spectrum taken in NMP

showed the presence of a large number of internal conversions at the excited states. The fluorescence spectra of **5a** and **5b** showed mirror images of their absorption spectra with close and small Stokes shifts and absence of excimer emission in the same solvents used in the electronic spectra of **1a** and **2a** which proved the similarity between ground S_0 and excited S_1 states and high fluorescence quantum yield values. Solid-state fluorescence of chiral compounds **5a** and **5b** could not be obtained which is attributed to presence of aggregates and excimers, which normally reduce quantum efficiencies of emission in the solid state. The electrochemical characteristics of compounds **1a**, **2a** and **5a** were investigated from dilute solution to solid state. In solution, compounds **1a**, **2a** and **5a** showed two one-electron reduction. However in solid state, chiral compound **5a** has shown only one one-electron reduction which is consistent with the high molecular symmetry. Chiral **2a** showed prominent Cotton effect centered at 362 and 382 nm.

In summary, the results could lead to further development of sterically and stereochemically controlled conductive unsymmetrical diimides which could guide to design important photo-, electro-, and optoelectronic devices.

REFERENCES

- Abdalla M. A., Bayer J., Rädler J. O., Müllen K. (2004) *Angew. Chem. Int. Ed.* 43, 3967-3970.
- Amiralaei S., Uzun D., Icil H. (2008) *Photochem. Photobiol. Sci.* 7, 936-947.
- Andric G., Boas J. F., Bond A. M., Fallon G. D., Ghiggino K. P., Hogan C. F., Hutchison J. A., Lee M. A. P., Langford S. J., Pilbrow J. R., Troup G. J., Woodward C. P. (2004) *Aust. J. Chem.* 57, 1011-1019.
- Ashkenasy N., Horne W. S., Ghadiri M. R. (2006) *Small* 2, 99-102.
- Asseline U., Cheng E. (2001) *Tetrahedron Lett.* 42, 9005-9010.
- Balzani V., Credi A., Venturi M. (2003) *Molecular Devices and Machines – A Journey into the Nano World*, Wiley-VCH Verlag GmbH & Co. KGaA, Weinheim.
- Balzani V., Scandola F. (1991) *Supramolecular Photochemistry*, Ellis Horwood, New York.
- Bard A. J., Faulkner L. R. (1980) *Electrochemical Methods, Fundamentals and Applications*, Wiley & Sons Inc, New York.

Bevers S., O_Dea T.P., McLaughlin L. W. (1998) *J. Am. Chem. Soc.* 120, 11004–11005.

Bevers S., Schutte S., McLaughlin L. W. (2000) *J. Am. Chem. Soc.* 122, 5905–5915.

Bevers S., Schutte S., McLaughlin L. W. (2002) *J. Am. Chem. Soc.* 122, 5905–5915.

Bredas J. L., Silbey R., Boudreaux D. S., Chance R. R. (1983) *J. Am. Chem. Soc.* 105, 6555–6559.

Brown G. H. (1971) *Photochromism in Techniques of Chemistry*, Vol 3, Wiley-Interscience, New York.

Cahn R. S., Ingold C. K., Prelog V. (1966) *Angew Chem Int Ed* 5, 335–415.

Chu Y. J., Sorey S., Hoffman D. W., Iverson B. L. (2007) *J. Am. Chem. Soc.* 129, 1304–1311.

Crick F. (1981) *Life Itself*, McDonald & Co., London.

Debreczeny M.P., Svec W.A., Marsh E.M., Wasielewski M.R. (1996) *J. Am. Chem. Soc.* 118, 8174.

Dehm V., Chen Z., Baumeister U., Prins P., Siebbeles L. D. A., Würthner F. (2007) *Org. Lett.* 9, 1085-1088.

Dixon D. W., Thornton N. B., Steullet V., Netzel T. L. (1999) *Inorg. Chem.* 38, 5526-5534.

Dou Z., Li X., Zhong S., Zhao C., Na H. (2006) *Polymer Bulletin* 57, 351-358.

Drayer D. (1993) The early history of stereochemistry. In: *Drug Stereochemistry, Analytical Methods and Pharmacology*, 2nd edn., Marcel Dekker, New York.

Drexler K. E. (1991) *Unbounding the Future: the Nanotechnology Revolution*, Marrow, New York.

Duan R. G., Miller L. L., Tomalia D. A. (1995) *J. Am. Chem. Soc.* 117, 10783-10784.

Dürr H. (1989) *Angew. Chem. Int. Ed. Engl.* 28, 413.

Dürr H., Bouas H., Laurent H. (1990) *Photochromism, Molecules and Systems in Studies in Organic Chemistry*, Elsevier, Amsterdam.

Ebeid E., El-Daly S. A. (1988) *J. Phys. Chem* 93, 4565-4568.

El'tsov A. V. (1990) *Organic Photochromes*, Plenum Press, New York.

Fedoroff O. Y., Salazar M., Han H. Y., Chemeris V. V., Kerwin S. M., Hurley L. H. (1998) *Biochemistry* 37, 12367-12374.

Feringa B. L. (2001) *Molecular Switches*, Wiley-VCH GmbH, Weinheim, Germany.

Feringa B. L., Huck N. P. M., Schoevaars A. M. (1996) *Adv. Mater.*, 8, 681.

Feringa B. L., Jager W. F., de Lange B. (1993) *Tetrahedron* 49, 8267.

Feringa B. L., van Delden R. A., Koumura N., Geertsema E. M. (2000) *Chem. Rev.* 100, 1789.

Feynman R. P. (1960) *Eng. Sci.* 23, 22.

Figueiredo K. M., Marcon R. O., Campos I. B., Nantes I. L., Brochsztain S. (2005) *J. Photochem. Photobiol. B* 79, 1-9.

Franceschin M., Alvino A., Ortaggi G., Bianco A. (2004) *Tetrahedron Lett.* 45, 9015-9020.

Francotte E. (1997) Preparation of drug enantiomers by chromatographic resolution on chiral stationary phases. In: *The Impact of Stereochemistry on Drug Development and Use*, John Wiley & Sons, New York.

Franke D., Vos M., Antonietti M., Sommerdijk N. A. J. M., Faul C. F. J. (2006) *Chem. Mater.* 18, 1839-1847.

Gabriel G. J., Sorey S., Iverson B. L. (2005) *J. Am. Chem. Soc.* 127, 2637-2640.

Gardner M. (1974) *The Ambidextrous Universe*, Penguin.

Gawroński J., Brzostowska M., Kacprzak K., Kołbon H., Skowronek P. (2000) *Chirality* 12, 263-268.

Gianolio D. A., McLaughlin L.W. (2001) *Bioorg. Med. Chem.* 9, 2329-2334.

Gianolio D. A., Segismundo J. M., McLaughlin L. W. (2000) *Nucleic Acids Res.* 28, 2128-2134.

Gómez-López M., Stoddart J. F. (1997) *Bull. Chim. Soc. Belg* 106, 491.

Gregg B. A., Ferrere S. (2002) *New J. Chem.* 26, 1155-1160.

Gregg B. A. (1996) *Chem. Phys. Lett.* 258, 376-380.

Grygar T., Marken F., Schröder U., Scholz F. (2002) *Collection of Czechoslovak Chemical Communications* 67, 163–208.

Guelev V., Lee J., Ward J., Sorey S., Hoffman D. W., Iverson B. L. (2001) *Chem. Biol.* 8, 415-425.

Guelev V., Sorey S., Hoffman D. W., Iverson B. L. (2002) *J. Am. Chem. Soc.* 124, 2864-2865.

Haga M., Ohta M., Machida H., Chikira M., Tonegawa N. (2006) *Thin Solid Films* 499, 201-206.

Han H. Y., Bennett R. J., Hurley L. H. (2000) *Biochemistry* 39, 9311-9316.

Hayes R.T., Wasielewski M.R., Gosztola D. (2000) *J. Am. Chem. Soc.* 122, 5563.

Hermes M., Lovric M., Hartl M., Retter U., Scholz F. (2001) *J. Electroanal. Chem.* 501, 193-204.

Herrickhuyzen Jv., Syamakumari A., Schenning A. P. H. J., Meijer E. W. (2004) *J. Am. Chem. Soc.* 126, 10021-10027.

Hirahara T., Nakamura T., Aoyama Y., Maeda S. (1993) *Mitsubishi Kasei Corp. EP* 263,705-B1.

Hoch H., Jelinish L. W., Craighead H. G. (1996) *Nanofabrication and biosystems, integrated material science, engineering and biology*, Cambridge University Press, Cambridge.

Hopkins H. P., Stevenson K. A., Wilson W. D. (1986) *J. Solution Chem.* 15, 563-579.

Horne W. S., Ashkenasy N., Ghadiri M. R. (2005) *Chem. Eur. J.* 11, 1137-1144.

Hunter C. H., Sanders J. K. M., Beddard G. S., Evans S. (1989) *J. Chem. Soc. Chem. Commun.*, 1765–1767.

Icil H., Arslan E. (2001) *Spectrosc. Lett.* 34, 355-363.

Icil H., Icli S. (1995) *Spectrosc. Lett.* 28, 595-601.

Icil H., Uzun D., Arslan E. (2001) *Spectrosc. Lett.* 34, 605-614.

Icli S., Icil H. (1996) *Spectrosc. Lett.* 29, 1253-1257.

Irie M. (1994) *Photoreactive Materials for Ultrahigh Density Optical Memory*, Elsevier, Amsterdam.

Jazwinski J., Blacker A. J., Lehn J-M., Cesario M., Guilhem J., Pascard C. (1987) *Tetrahedron Lett.* 28, 6057–6060.

Kahlert H., Retter U., Lohse H., Siegler K., Scholz F. (1998) *J. Phys. Chem. B* 102, 8757–8765.

Komatsu M., Nojima T., Takenaka S. (2006) *Electrochemistry* 74, 65-67.

Krauß S., Lysetska M., Würthner F. (2005) *Lett. Org. Chem.* 2, 349-353.

Kudo T., Kimuna M., Hanabusa K., Shinai H. (1998) *J. Porphyr. Phtalocya.* 2, 231-235.

Kuhn W., Knopf E. Z. (1930) *Phys. Chem. B* 7, 292–310.

Langhals H. (1995) *Heterocycles* 40, 477-500.

Langhals H., Blanke P (2003) *Dyes and Pigments* 59, 109-116.

Langhals H., Gold J. (1997) *Liebigs Ann.* 1997, 1151-1153.

Langhals H., Ismael R., Yürük O. (2000) *Tetrahedron* 56, 5435-5441.

Langhals H., Jaschke H (2006) *Chem. Eur. J.* 12, 2815-2824.

Langhals H., Krotz O. (2006) *Angew. Chem. Int. Edit.* 45, 4444-4447.

- Langhals H., Schonmann G., Feiler L. (1995) *Tetrahedron Lett.* 36, 6423-6424.
- Lee J., Guelev V., Sorey S., Hoffman D. W., Iverson B. L. (2004) *J. Am. Chem. Soc.* 126, 14036-14042.
- Lewis F. D., Letsinger R. L., Wasielewski M. R. (2001) *Acc. Chem. Res.* 34, 159-170.
- Lewis F. D., Wasielewski M. R. (2004) *Top. Curr. Chem.* 236, 45-65.
- Lewis F. D., Zhang L., Kelley R. F., McCamant D., Wasielewski M. R. (2007) *Tetrahedron* 63, 3457-3464.
- Li A. D. Q., Wang W., Wang L. (2003) *Chem. Eur. J.* 9, 4594-4601.
- Lokey R. S., Kwok Y., Guelev V., Pursell C. J., Hurley L. H., Iverson B. L. (1997) *J. Am. Chem. Soc.* 119, 7202-7210.
- Lovric M., Hermes M., Scholz F. (2000) *J. Solid State Electr.* 4, 394-401.
- Lovric M., Scholz F. (1999) *J. Solid State Electr.* 3, 172-175.
- Lu W., Gao J. P., Wang Z. Y. (1999) *Macromolecules* 32, 8880-8885.
- Lukas A. S., Miller S. E., Wasielewski M. R. (2000) *J. Phys. Chem. B* 104, 931-940.

Mackinnon S. M., Wong Z. Y. (2000) *J. Polym. Sci. Pol. Chem.* 38, 3467-3475.

Masu H., Mizutani I., Kato T., Azumaya I., Yamaguchi K., Kishikawa K., Kohmoto S. (2006) *J. Org. Chem.* 71, 8037-8044.

Matsugo S., Yan L. J., Han D., Packer L. (1995) *Biochem. Biophys. Res. Commun.* 206, 138-145.

Menikh A., Bounaoui A. (1997) *J. Mol. Struct.* 403, 189-197.

Michel J., Bathany K., Schmitter J. M., Monti J. P., Moreau S. (2002) *Tetrahedron* 58, 7975-7982.

Miller L. L., Duan R. G., Tully D. C., Tomalia D. A. (1997) *J. Am. Chem. Soc.* 119, 1005-1010.

Mislow K. (2002) *Chirality* 14, 126-134.

Mokhir A., Zohm B., Fuessl A., Kraemer R. (2003) *Bioorg. Med. Chem. Lett.* 13, 2489-2492.

Murr M. M., Harting M. T., Guelev V., Ren J. S., Chaires J. B., Iverson B. L. (2001) *Bioorg. Med. Chem.* 9, 1141-1148.

Nagao Y. (1997) *Progress in Organic Coatings* 31, 43-49.

Nagata T. (1991) *Bull. Chem. Soc. Jpn.* 64, 3005–3016.

Nakajima M., Takeuchi T., Ogino K., Morimoto K. (2002) *Jpn. J. Cancer Res.* 93, 247-252.

Nakajima S., Akiyama K., Kawai K., Takada T., Ikoma T., Majima T., Tero-Kubota S. (2007) *Chemphyschem* 8, 507-509.

Nunez M. E., Noyes K. T., Gianolio D. A., McLaughlin L. W., Barton J. K. (2000) *Biochemistry* 39, 6190-6199.

O'Neil M.P., Niemczyk M.P., Svec W.A., Gosztola D., Gaines III G.L., Wasielewski M.R. (1992) *Science* 257, 63.

Okamoto A., Nakamura T., Yoshida K., Nakatani K., Saito I. (2000) *Org. Lett.* 2, 3249-3251.

Osswald P., Reichert M., Bringmann G., Würthner F. (2007) *J. Org. Chem.* 72, 3403-3411.

Osuka A., Marumo S., Wada Y., Yamazaki I., Yamazaki T., Shirakawa Y., Nishimura Y. (1995) *Bull. Chem. Soc. Jpn.* 68, 2909–2915.

Pasaogullari N., Icil H., Demuth M. (2006) *Dyes and Pigments* 69, 118-127.

Pasteur L. (1901) On the asymmetry of naturally occurring organic compounds. In: *The Foundation of Stereochemistry: Memoirs by Pasteur, Van't Hoff, Le Bel and Wislicenus*, American Book Co., New York.

Pasteur L. (1948) *Researches on the Molecular Asymmetry of Natural Organic Products*, Alembic Club Reprints, No. 14, reissue edition. F. and S. Livingstone, Edinburgh.

Peng Z., Bao Z., Galvin M. E. (1998) *Chem. Mater.* 10, 2086–2090.

Pösch P., Thelakkat M., Schmidt H. W. (1999) *Syn. Met.* 102, 1110-1112.

Qu J., Kohl C., Pottek M., Müllen K. (2004) *Angew. Chem. Int. Ed.* 43, 1528-1531.

Rahe N., Rinn C., Carell T. (2003) *Chem. Commun.*, 2120-2121.

Rahe N., Rinn C., Carell T. (2003) *Chem. Commun.* 17, 2120-2121.

Rogers J.E., Weiss S.J., Kelly L.A. (2000) *J. Am. Chem. Soc.* 122, 427-436.

Rudiono, Kaneko F., Takeuchi M. (1999) *Appl. Surf. Sci.* 142, 598-602.

Sato S., Fujii S., Yamashita K., Takagi M., Kondo H., Takenaka S. (2001) *J. Organometal. Chem.* 637, 476-483.

Sato S., Kondo H., Nojima T., Takenaka S. (2005) *Anal. Chem.* 77, 7304-7309.

Schenning A. P. H. J., Herrikhuyzen Jv., Jonkheijm P., Chen Z., Würthner F., Meijer E. W. (2002) *J. Am. Chem. Soc.* 124, 10252-10253.

Schlichting P., Rohr U., Mullen K. (1997) *Liebigs Ann. Recl.* 395-407.

Schröder U., Scholz F. (2000) *Inorg. Chem.* 39, 1006-1015.

Sessler J. L., Brown C. T., O'Connor D., Springs S. L., Wang R., Sathiosatham M., Hirose T. (1998) *J. Org. Chem.* 63, 7370-7374.

Shaller A. D., Wang W., Gan H., Li A. D. Q (2008) *Angew. Chem.* 120, 7819-7823.

Shchepinov M. S., Korshun V. A., Egeland R. D., Southern E. M. (2000) *Tetrahedron Letters* 41, 4943-4948.

Shim J. J., Lee C. W., Gong S. M. (2001) *Synthetic Met.* 124, 435-441.

- Shimizu K. D., Dewey T. M., Rebek J. (1994) *J. Am. Chem. Soc.* 116, 5145–5149.
- Sterzel M., Pilch M., Pawlikowski M. T., Gawroński J. (2003) *Chemical Physics* 291, 251-260.
- Steullet V., Dixon D. W. (1999) *Bioorg. Med. Chem. Lett.* 9, 2935-2940.
- Steullet V., Dixon D. W. (1999) *J. Chem. Soc. Perkin Trans. 2*, 1547-1558.
- Sübmeier F., Langhals H. (2001) *Eur. J. Org. Chem.*, 607-610.
- Sun R., Xue C., Owak M., Peetz R. M., Jin S. (2007) *Tetrahedron Lett.* 48, 6696-6699.
- Takenaka S., Uto Y., Saita H., Yokoyama M., Kondo H., Wilson W. D. (1998) *J. Chem. Soc. Chem. Commun.*, 1111–1112.
- Takenaka S., Yamashita K., Uto Y., Takagi M., Kondo H. (1998) *Denki Kagaku* 66, 1329-1334.
- Takenaka S., Yokoyama M., Kondo H. (1997) *Chem. Commun.*, 115-116.
- Tamizhmani G., Dodelet J. P. (1991) *Chem. Mater.* 3, 1046-1053.
- Tansil N. C., Xie H., Xie F., Gao Z. Q. (2005) *Anal. Chem.* 77, 126-134.

Thalacker C., Würthner F. (2002) *Adv. Funct. Mater.* 12, 209-218.

Thelakkat M., Posch P., Schmidt W. (2001) *Macromolecules* 34, 7441-7447.

Tian H., Liu P., Zhu W., Gao E., Wu D., Cai S. (2000) *J. Mater. Chem.* 10, 2708-2715.

Todd E. K., Wang S., Wan X., Wang Z. Y. (2005) *Tetrahedron Lett.* 46, 587-590.

Tok J. B. H., Fenker J. (2001) *Bioorg. Med. Chem. Lett.* 11, 2987-2991.

Tomasulo M., Naistat D. M., White A. J. P., Williams D. J., Raymo F. M. (2005)
Tetrahedron Lett. 46, 5695-5698.

Tomizaki K., Loewe R. S., Kirmaier C., Schwartz J. K., Retsek J. L., Bocian D. F.,
Holten D., Lindsey J. S. (2002) *J. Org. Chem.* 67, 6519-6534.

Turro N. J. (1965) *Molecular Photochemistry*, W. A. Benjamin, Inc, New York, p. 4-48.

Uzun D., Ozser M. E., Yuney K., Icil H. Demuth M. (2003) *J. Photochem. Photobiol., A*
156, 45-54.

Vicic D. A., Odom D. T., Nunez M. E., Gianolio D. A., McLaughlin L. W., Barton J. K.
(2000) *J. Am. Chem. Soc.* 122, 8603-8611.

Wainer L W. (1993) HPLC chiral stationary phases for the stereochemical resolution of enantiomeric compounds. In: Drug Stereochemistry, Analytical Methods and Pharmacology, 2nd edn., Marcel Dekker, New York.

Wang W., Zhou H., Niu S., Li A. D. Q. (2003) *J. Am. Chem. Soc.* 125, 5248-5249.

Widmann A., Kahlert H., Petrovic-Prelevic I., Wulff H., Yakhmi J. V., Bagkar N., Scholz F. (2002) *Inorg. Chem.* 41, 5706–5715.

Wiederrecht G. P., Niemczyk M. P., Svec W. A., Wasielewski M. R. (1996) *J. Am. Chem. Soc.* 118, 81–91.

Wiederrecht G. P., Svec W. A., Niemczyk M. P., Wasielewski M. R. (1995) *J. Phys. Chem.* 99, 8918–8926.

Williams M. E., Murray R. W. (1998) *Chem. Mater.* 10, 3603-3610.

Willner I., Rubin S. (1996) *Angew. Chem., Int. Ed. Engl.* 35, 367.

Wilson J. N., Gao J., Kool E. T. (2007) *Tetrahedron* 63, 3427-3433.

Würthner F. (2004) *Chem. Commun.*, 1564-1579.

Würthner F., Chen Z., Hoeben F. J. M., Osswald P., You C. C., Jonkheijm P., Herrikhuizen J. v., Schenning A. P. H. J., Schoot P. P. A. M. v. d., Meijer E. W., Beckers E. H. A., Meskers, S. C. J., Janssen R. A. J. (2004) *J. Am. Chem. Soc.* 126, 10611-10618.

Xue C., Chen M., Jin S. (2008) *Polymer* 49, 5314-5321.

Yang L. Y., Shi M. M., Wang M., Chen H. Z. (2008) *Chinese Chemical Letters* 19, 1260-1263.

Yashima E. & Okamoto Y. (1997) Chiral discrimination mechanism of polysaccharides chiral stationary phases. In: *The Impact of Stereochemistry on Drug Development and Use*, John Wiley & Sons, New York.

Zandonella G., Haalck L., Spener F., Faber K., Paltauf F., Hermetter A. (1996) *Chirality* 8, 481-489.

Zhang J., Albelda M. T., Liu Y., Canary J. W. (2005) *Chirality* 17, 404-420.

Zhou Y., Zhang D., Zhang Y., Tang Y., Zhu D. J. (2005) *Journal of Organic Chemistry* 70, 6164-6170.

Zsom R. L. J., Schroff L. G., Bakker C. J., Verhoeven J. W., de Boer T. J., Wright J. D., Kuroda H. (1978) *Tetrahedron* 34, 3225-3232.

CURRICULUM VITAE

Personal Information

Name	Süleyman
Surname	Aşır
Address	No:16 Salamis Yolu Famagusta - TRNC Mersin 10 Turkey
Phone	Office:+90 0392 630 10 26 / Mobile: 0533 860 88 21
e-mail	suleyman.asir@emu.edu.tr
Date of Birth	03/09/1980
Citizenship	TRNC
Marital Status	Married

Education

1985-1991	Alasya Primary School
1991-1997	Gazi Magusa Turk Maarif College
1997-1998	Gazi University Faculty of Art & Science Department of Chemistry
1998-2002	Hacettepe University Faculty of Science Department of Chemistry (BS)
2002-2004	Hacettepe University Faculty of Science Department of Chemistry Biochemistry (MS)
2004-present	Eastern Mediterranean University Faculty of Art & Science Department of Chemistry Organic Chemistry (PhD)

Training

TURKISH PETROLEUM RAFINERIES CORPORATION, KIRIKKALE RAFINERY

Quality Control Laboratory, Chemistry Laboratory, Physics Laboratory, Gas Chromatography Laboratory.

Work Experience

2002-2004

GST MEDIKAL SAGLIK URUNLERI VE BILGISAYAR

SAN. TIC. LTD. STI. (Responsible for the tenders and sales about Cardiovascular Surgery)

2004- present

EASTERN MEDITERRANEAN UNIVERSITY,

Department of Chemistry (Research Assistant)

Research Experience

- BS-2002** Preparation of Affinity Membranes for Cholesterol Removal
from Human Plasma
Hacettepe University, Ankara, Turkey
Supervisor: Prof. Dr. Adil Denizli
- MS-2004** Preparation of Ion-Selective Imprinted Polymeric Monolith
for Cadmium Detoxification from Human Plasma
Hacettepe University, Ankara, Turkey
Supervisor: Prof. Dr. Adil Denizli

Research Projects

- 1- 2005-2006, DPT-YUUP “**Synthetic Technology of Chiral Drug Materials within Health Biotechnology**”, (Scientific Researcher)

Organizations

- 1- XXIInd National Chemistry Congress, 6-10 October 2008, Eastern Mediterranean University, Magusa, TRNC, Congress Secretary
- 2- 11. International Biomedical Science and Technology Days , BIOMED 2004, 6-10 September 2004, Hacettepe University, Ankara, Turkey, Organizing Committee of Bioaffinity Section

Publications

- 1- S.Aşır, Ayhan S. Demir, H. İcil **“The synthesis of novel, unsymmetrically substituted, chiral naphthalene and perylene diimides: Photophysical, electrochemical, chiroptical and intramolecular charge transfer properties”**, Dyes and Pigments, 84: 1-13, 2009.
- 2- S. Aşır, L. Uzun, D. Türkmen, R. Say and A. Denizli, **“Ion-selective imprinted superporous monolith for cadmium removal from human plasma”**, Separation Science and Technology, 40:3167-3185, 2005.
- 3- M.Sc. Thesis on: **“Preparation of Ion-Selective Imprinted Polymeric Monolith for Cadmium Detoxification from Human Plasma”**, at Hacettepe University, Ankara, Turkey, 2004.

Conferences

- 1- S. Aşır, Ö. Akbaşak, H. İcil **“Fluorescent Chiral Perylene Dyes and Energy Transfer Studies”**, XXII. National Chemistry Congress, Mağusa, North Cyprus, October 2008.
- 2- S. Aşır, H. İcil **“Building Blocks for the Future Devices: The Synthesis of Chiral Perylene and Naphthalene Diimides”**, XXII. National Chemistry Congress, Mağusa, North Cyprus, October 2008.
- 3- D. Özdal, S. Aşır, H. İcil **“Fluorescence-Based Ligand Conjugated Biopolymer”**, XXII. National Chemistry Congress, Mağusa, North Cyprus, October 2008.
- 4- S. Aşır, Ö. Akbaşak, H. İcil **“Fluorescence Resonance Energy Transfer with Chiral and Achiral Imides”**, ‘EPA-08’ HRSMC Summer School – Photochemistry 2008: Fundamentals and Applications, Maastrich, The Netherlands, June 2008.
- 5- S. Aşır, H. İcil **“Synthesis of a rigid-flexible-rigid structure: A new bichromophoric perylene derivative”**, International Conference on Organic Chemistry, Erzurum, Turkey, June 2007.
- 6- S.Aşır, A. S. Demir and H.İcil **“Novel Chiral Perylene and Naphthalene Diimides as Potential Chiroptical Switches: Syntheses and Spectral Properties”**, 1st European Chemistry Congress, Budapest-Hungary, August 2006.
- 7- S.Aşır and H.İcil **“Kiroptikal Anahtar Olabilecek Nitelikte Yeni Kiral Diimidler: Sentezler ve Kiroptikal Özellikler”**, XX. National Chemistry Congress, Kayseri-Turkey, September 2006.

- 8- S.Aşır, A. S. Demir and H.İcil “**Antisimetrik Kiral Perilen ve Naftalendiimid Sentezi**”, XIX. National Chemistry Congress, Kuşadası-Turkey, October 2005.
- 9- S. Aşır, D. Türkmen, A. M. Andaç, L. Uzun and A. Denizli “**İnsan plazmasından Kadmiyum Detoksifikasyonu için İyon Seçici Baskılanmış Polimerik Monolitlerin Hazırlanması**”, I. National Affinity Techniques Congress, Ankara-Turkey, June 2005.
- 10- S. Aşır, D. Türkmen, A. M. Andaç, L. Uzun and A. Denizli “**Ion-Selective Imprinted Polymeric Rods for Cadmium Detoxification**” Biomed , Ankara-Turkey, 2004.